Faculty of Science and Technology

Millennial-scale variability of Atlantic water inflow in the northern Nordic Seas and the northwestern Barents Sea

Relationship to abrupt climate oscillations, cryosphere and methane seepage from the seafloor

Naima El bani Altuna

A dissertation for the degree of Philosophiae Doctor   June 2021

Millennial-scale variability of Atlantic water inflow in the northern Nordic Seas and the northwestern Barents Sea
Relationship to abrupt climate oscillations, cryosphere and methane seepage from the seafloor

Naima El bani Altuna

A dissertation for the degree of Philosophiae Doctor

UiT The Arctic University of Norway

Faculty of Science and Technology

Department of Geosciences

June 2021

Supervisors:

Professor Tine L. Rasmussen
CAGE – Centre for Arctic Gas Hydrate, Environment and Climate
Department of Geosciences,
UiT The Arctic University of Norway, Tromsø, Norway

Dr. Mohamed M. Ezat
CAGE – Centre for Arctic Gas Hydrate, Environment and Climate
Department of Geosciences
UiT The Arctic University of Norway, Tromsø, Norway
Department of Geology
Faculty of Science
Beni-Suef University, Beni-Suef, Egypt

Front page image: Sea ice covering the Arctic Ocean at 82°N in a morning sunset in October 2018
(Photo: Naima El bani Altuna)

Acknowledgments

First and foremost, I want to thank my supervisors Tine L. Rasmussen and Mohamed M. Ezat for giving me the unique opportunity to start this PhD journey and for all the opportunities that came along with it (cruises to the Arctic, international conferences and all the learning experiences, among other). I would lie if I said that this journey has always been easy, but your unvaluable guidance and persistent support motivated me to overcome the challenges and continue this PhD; without your encouragement I would have never reached this stage. Mange tak! شكراً!

I would like to thank the coauthors of the scientific papers presented in this thesis, specially Tine and Mohamed for being always so readily available to guide and give scientific advice, Mervyn Greaves for your patience and guidance with the ICP-OES in Cambridge and Sunil Vadakkepuliyambatta for being of great support and help with our second manuscript. Thanks to my supervisors, Pierre-Antoine Dessandier and Carmen Braun for (proof)reading my thesis, and Ana Galarraga for reading through the summary of the thesis in Basque.

I think I can safely say that I have spent at least two thirds of my PhD in the lab and it would not have been the same positive experience if it was not because of Trine Dahl, Karina Monsen, Ingvild Hald and Matteus Lindgren. Thank you also to the engineers, specially Steinar Iversen and Fabio Sarti. Both to the lab staff and the engineers, I am immensely thankful for your patience (even when I come with one question after the other), readiness to help and being so effective solving our issues. You have made my lab time very enjoyable and cruise preparation much easier than expected.

I am thankful to have had great officemates and office neighbors in the old building (Mariana, Emmelie and Calvin, and Arunima and Pierre-Antoine), and in the new building (Przemek, Fatih, Lina, Kasia, Christine and the others), as well as other early careers at the department with whom I can chat and vent about work, mental health and how to survive the PhD journey (during and after it). Siri, I am very thankful you were the 'more experienced PhD' in our group that I could look at and follow, thank you for being always there to celebrate the good moments and support in the difficult ones. Pierre-Antoine and Martin, I spent my first year locked in the microscope room with you both and thanks to you, your generally good mood (not in the morning for Martin) and jokes, the transition from Bordeaux to Tromsø became very smooth; merci beaucoup. Griselda and Marina, you showed up in Tromsø when I was already

I

half-way through my PhD and suddenly you became part of my life here; tías, qué suerte que aparecisteis. Sofia and Lis, I am very happy to have you two as frolleagues (i.e., friends and colleagues) that I can count on for age-depth modelling discussions, but also for life. Jack, Sunil, Louise, Ellery, Carmen, Amicia, people in Strikk og Drikk, everyone that came and went and for a few months became an important piece of life in Tromsø, you made these past years so nice and entertaining! To the early career researchers JEDI discussion group; you gave me hope for academia to become a better, fairer and more diverse place.

Magnus, thank you for your contagious joy, for believing in me and support me even when I am stressed and unbearable. I would like to thank my sister Aixa, my family and friends back at home. No matter how far I move, you make me feel that home is where you all are. And last, but certainly not least, I am thankful to my mom, for the unconditional encouragement and endless support. Ama zuri gustatzen zaizun bezala, zuretzako bertso txiki bat zure doinu eta neurri gogokoenean:

Duela hiru urte t'erdi hasi nuen PhDa	*Three years ago I started my PhD*
Artikora mugitu eta hasi bizitza berria	*Moved to the Arctic and start a new life*
Gorabehera asko eta hamaika esperientzia	*Up and downs and thousand new experiences*
Aurrera ateratzea ez da izan gauza txikia	*It has not been an easy job to get it done*
Faltan ditut etxekoak, lagunak eta familia	*I miss home, my friends and family*
Hemen aurkitu baitere pertsona izugarriak	*I have found as well amazing people here*
Baina bati bereziki eskaintzen diot tesia	*There's one person I dedicate this thesis*
Nire eredu, ameslari, amatxo zientzialaria	*(to) my role model, dreamer, and scientist mom*

Thank you all so much! Tusen takk alle sammen! Mila esker danoi!

Naima El bani Altuna
June 2021

II

Preface

This dissertation is the result of three and a half years (starting in January 2018) of doctoral education under the supervision of Prof. Tine L. Rasmussen and Dr. Mohamed M. Ezat at the Centre for Arctic Gas Hydrate, Environment and Climate (CAGE) in the Department of Geosciences at the Arctic University of Norway in Tromsø (UiT). The project was funded by the Research Council of Norway and supported by the Research Council of Norway Centers of Excellence funding scheme grant no. 223259.

The main objective of this PhD project is to study the evolution of Atlantic water inflow into the northern Nordic Seas and for that purpose the principal tool has been the benthic foraminiferal Mg/Ca thermometer. In the absence of adequate premises for elemental ratio analyses of foraminiferal tests at UiT, I spent a total of four and a half months at the Godwin Laboratory for Paleoclimate Research at the Department of Earth Sciences at the University of Cambridge (England). This research stay was financially supported by the UiT travel grant for PhD candidates.

In order to fulfill the educational requirements of the PhD program, I attended courses on benthic foraminifera (at the 11th International School on Foraminifera, Urbino, Italy), geochronology (GEO-8136 at UiT), science communication (GEN-8010 at UiT), research ethics (SVF-8600 at UiT) and scientific writing and proposal writing. I also took part in the Arctic Marine Geology and Geophysics (AMGG) educational scientific cruise and workshop in 2018 (GEO-8144 and GEO-8145 at UiT). During this period, I was affiliated and actively participating in the trainee school Geoscience Research Academy of Tromsø (GReAT; previous AMGG) and in the Norwegian Research School on Changing Climates in the coupled Earth System (CHESS). Furthermore, I have been a student representative in the GReAT steering committee since November 2019.

I participated in the following scientific cruises related to my PhD project and to other projects: CAGE18-3 (July 2018), Arven etter Nansen paleocruise (September-October 2018), GEO-3111 and GEO-3122 teaching cruises (October 2019 and October 2020). In the teaching cruises, I undertook the role of teaching assistant. I have also co-supervised and mentored three master students on their master projects related to paleoceanography.

In the course of the PhD education, I attended and presented preliminary results related to this work in the following national and international conferences: AMGG/GReAT Annual Meeting in 2018, 2019 and 2020 in Tromsø; CAGE winter meeting 2019 in Tromsø; CHESS Annual Meeting in 2018, 2019 and 2020, in Tromsø, Oslo and Tromsø/online, respectively; the International Symposium on Foraminifera FORAMS2018 in 2018 in Edinburgh (Scotland); 20th International Union of Quaternary Research INQUA Congress in 2019 in Dublin (Ireland); 14th International Conference on Paleoceanography ICP in 2019 in Sydney (Australia); 34th Nordic Geological Winter Meeting in 2020 in Oslo (Norway); American Geoscience Union AGU Fall Meeting in 2020 online; 2nd International PaleoArc Conference in 2021 online. Additionally, I also took part on dissemination activities on social media (Twitter), Basque audiovisual and written media, and in-person activities such as Geologiens Dag 2020 in Tromsø.

In this work we generated two bottom water temperature records in the northwestern Barents Sea and the northern Nordic Seas, where we have also reconstructed the evolution of sea ice conditions, spanning the last (de)glacial period that are useful to understand natural ocean-cryosphere interactions and the implications of warming oceans in sub-seafloor gas hydrate systems.

This thesis consists of an introduction to the following research articles:

- **Paper I.** El bani Altuna, N., Ezat, M.M., Greaves, M., Rasmussen, T.L., 2021. **Millennial-scale changes in bottom water temperature and water mass exchange through the Fram Strait 79°N, 63–13 ka.** *Paleoceanography and Paleoclimatology,* https://doi.org/10.1029/2020PA004061

    Data related to this paper: https://doi.org/10.1594/PANGAEA.925428

- **Paper II.** El bani Altuna, N., Rasmussen, T.L., Ezat, M.M., Vadakkepuliyambatta, S., Groeneveld, J., Greaves, M. **Deglacial bottom water warming intensified Arctic methane seepage, Northwestern Barents Sea**. In review in *Communications Earth and Environment* (minor revision requested).

    Data related to this paper: https://doi.org/10.18710/XFYDFL

- **Paper III.** El bani Altuna, N., Ezat, M.M., Smik, L., Muschitiello, F., Belt, S.T., Knies, J., Rasmussen, T.L. **Sea ice and Atlantic water coupling during Heinrich Stadials in the northern Nordic Seas during the last glacial period 63-13 ka.** In preparation for submission to *Science Advances*.

    Data related to this paper will be submitted to the UiT Open Research Data repository.

Contents

SECTION I   Synthesis

1 Introduction

Over last two decades, the global air temperature has increased due to anthropogenic greenhouse emissions (IPCC, 2014). In the Arctic region, the air temperature has warmed more than two times faster than the global average (Najafi et al., 2015; Meredith et al., 2019). This phenomenon is known as 'Arctic amplification', and is the result of positive feedback mechanisms such as the reduction of the albedo effect due to the loss sea ice and subsequent changes in the northward transport of heat (Serreze & Barry, 2011).

Enhanced heat flux via the increased inflow of Atlantic water (AW) into polar oceans and the reduction of sea-ice cover are particularly pronounced in the Barents Sea and the Eurasian Basin (Årthun et al., 2012; Polyakov et al., 2017). The sediments of the Arctic seafloor bear vast amounts of gas hydrates, which are ice-like compounds formed by water and gas that are stable under high pressure and low temperature (Sloan & Koh, 2007). Perturbing the conditions in which hydrates are stable can cause the dissociation of gas hydrates and the release of gas from the sediments to the water column. Warm ocean waters reaching the seafloor have, therefore, the potential to trigger the dissociation of gas hydrates and further contribute to current climate change (e.g., Westbrook et al., 2009; Maslin et al., 2010; Biastoch et al., 2011; Kretschmer et al., 2015; Ruppel & Kessler, 2017).

Future projections anticipate a further increasing warming in the Arctic (Overland et al., 2019), but uncertainties still remain large (e.g., Notz, 2015). Generating and improving long-term past records (i.e., improving our knowledge on past climatic states of the Earth) is needed to test, evaluate and validate Earth system models and decrease the uncertainty of future model predictions (Tierney et al., 2020).

Greenland ice core records show past periods with warming rates in the Arctic regions that are similar to, or larger than modern warming rates (Jansen et al., 2020). These abrupt atmospheric warmings occurred during the last glacial period, when the climate of the North Atlantic oscillated between glacial-like stable climatic periods (stadials) to warm and shorter periods (interstadials) at sub-millennial timescales (Dansgaard et al., 1982; S. O. Rasmussen et al., 2014). The transition from a stadial to an interstadial is characterized by the abrupt rise of atmospheric temperatures by 5°C to 16.5°C in a few decades (Kindler et al., 2014). The potential trigger(s) for such an abrupt warming remains unclear, even if the general consensus

highlights the important role played by sea-ice cover and reorganizations in oceanic circulation patterns in the North Atlantic (Broecker et al., 1985; Ganopolski & Rahmstorf, 2001; Rahmstorf, 2002; Gildor & Tziperman, 2003; Knutti et al., 2004; T. L. Rasmussen & Thomsen, 2004; Li et al., 2010; Petersen et al., 2013; Sadatzki et al., 2019; Jansen et al., 2020).

The interest of this thesis stems from the need to understand paleoceanographic changes at millennial timescales in relation to methane seepage history in the Arctic. The focus of the thesis lies on understanding the evolution of the inflow of AW by measuring bottom water temperatures (BWT) in the Nordic Seas and the Barents Sea for the last glacial period. To investigate this, we applied a similar approach in two key study areas: (a) Vestnesa Ridge, a deep-water gas hydrate system in Fram Strait west of Svalbard, where we studied the role of AW inflow and the evolution of sea-ice conditions and their interaction at millennial timescales in the last glacial period (**Papers I** and **III**), and (b) Storfjordrenna, a relatively shallow continental shelf area in the northwestern Barents Sea, where we investigated the implications of AW-induced sub-seafloor gas hydrate dissociation through the reconstruction of the gas hydrate stability zone since the beginning of the deglaciation (**Paper II**) (Figure 1).

1.1 Background

Ocean circulation in the Nordic Seas plays a crucial role in controlling the strength of the Atlantic Meridional Overturning Circulation (AMOC) (Chafik & Rossby, 2019). The AMOC is a system of ocean currents in the Atlantic Ocean, responsible for transporting heat on its upper limb northwards from the subpolar North Atlantic to the Nordic Seas and the Arctic Ocean. The climate of the Northern Hemisphere is therefore directly linked to the strength of the AMOC, with periods of weaker circulation associated with cooler climate periods and vice versa.

Out of 18.4 ± 3.4 Sverdrups (Sv) south of the Greenland-Scotland Ridge, about half (8.84 ± 0.9 Sv) of warm and salty AW crosses the Greenland Scotland Ridge and flows into the Nordic Seas (consisting of the Iceland-, Norwegian- and the Greenland Seas) (Chafik & Rossby, 2019) (Figure 1). In the Nordic Seas, the AW continues its poleward flow at the surface as the Norwegian Atlantic Current (NwAtC), progressively losing heat and gaining density, until it sinks to contribute to the formation of the deep- and intermediate water in the central Nordic Seas (Isachsen et al., 2007) (Figure 1). The newly formed deep-water is cooler and
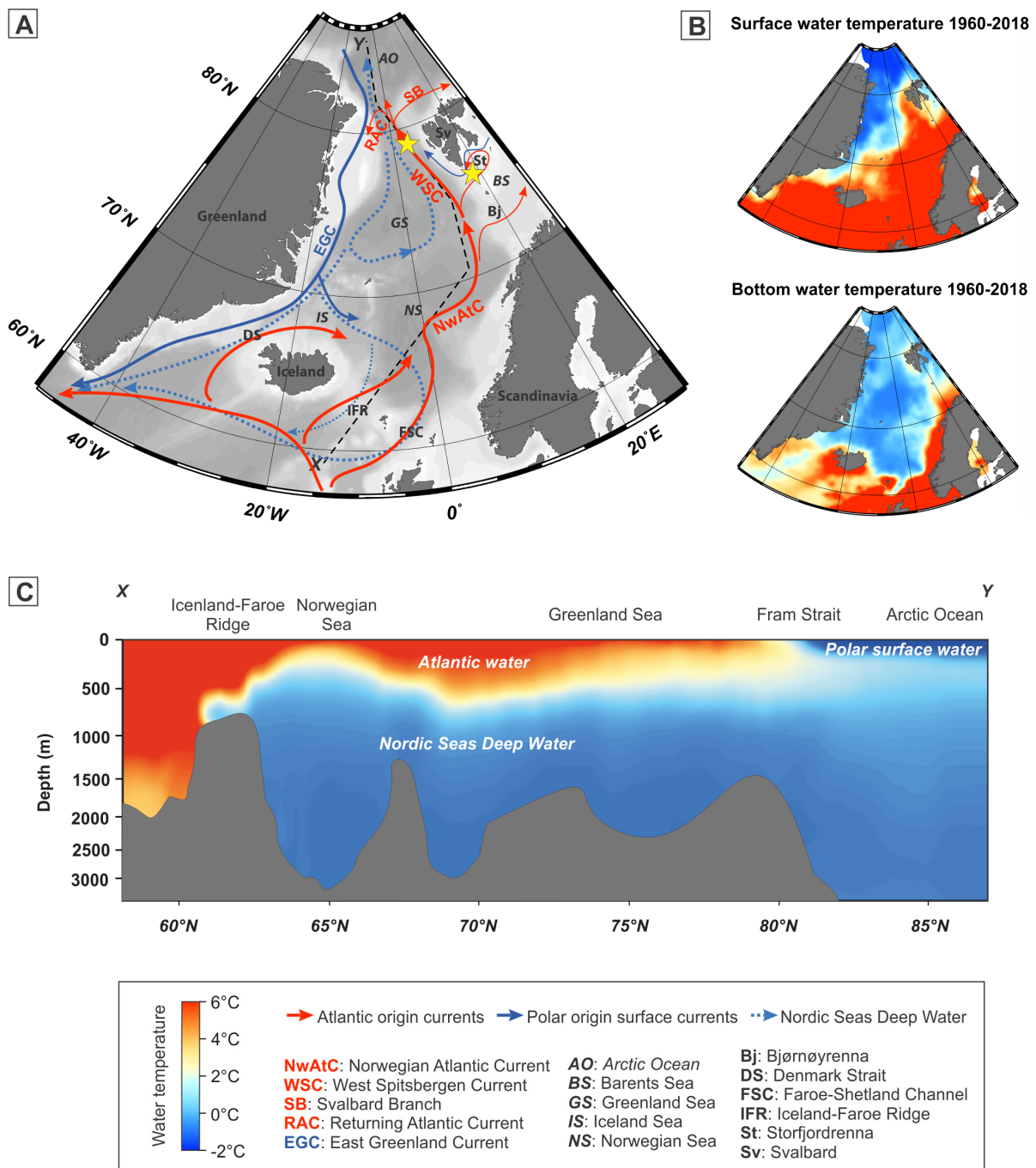
Figure 1. Modern oceanographic setting of the Nordic Seas. (**A**) Map of the North Atlantic and Nordic Seas showing major ocean currents (in blue and red) and locations of the two study areas in the western Svalbard margin and in Storfjordrenna (yellow stars). Black dotted line marks transect X-Y from the southern Nordic Seas to the Arctic Ocean shown in (**C**). The two maps in (**B**) show surface (uppermost) and bottom (lowermost) water temperatures for the period 1960-2018 obtained from high resolution CTD data (Boyer et al., 2018). The bathymetry of transect X-Y (**C**) is simplified. The figures were created with Ocean Data View (Schlitzer, 2001).

saltier than the surrounding water masses and flows back over the Greenland-Scotland Ridge to mid-latitudes in the North Atlantic (Østerhus et al., 2019) contributing to the North Atlantic Deep Water (Dickson & Brown, 1994).

Part of the NwAtC enters the Barents Sea mainly through Bjørnøyrenna, between Norway and Bjørnøya in the southwestern Barents Sea (Skagseth et al., 2008) (Figure 1). In the northern Barents Sea, the AW mixes with waters of polar origin, loses heat to the atmosphere and becomes fresher (Smedsrud et al., 2010). The southern Barents Sea is therefore permanently ice free, whereas the northern Barents Sea is seasonally sea-ice covered (Rudels et al., 2015). In Storfjordrenna (**Paper II**) in the northwestern Barents Sea (ca. 380 m water depth), dense water is created seasonally as a result of a polynya created by strong northwesterly winds and by the formation of sea ice and brine rejection (Skogseth et al., 2005). Here, the AW enters and leaves the Barents Sea in a cyclonic way following the bathymetry and flowing beneath a fresher surface layer (Fer et al., 2003) (Figure 1). Arctic water in the northwestern Barents Sea flows along the coast of Spitsbergen southwards as the East Spitsbergen Current (Loeng, 1991).

A large portion of the NwAtC continues northwards along the western Svalbard margin in the eastern Fram Strait as the West Spitsbergen Current (WSC), carrying Atlantic heat and salt into the Arctic Ocean (Aagaard et al., 1987; Rudels et al., 2015) (Figure 1). Vestnesa Ridge (**Paper I** and **III**), at a water depth of ca. 1,200 m, is located in this corridor of warm AW flowing northwards and is today affected by the cold Nordic Seas intermediate water. The Fram Strait is the only deep passage connecting the Atlantic and the Arctic Oceans and when the WSC reaches the Yermak Plateau, it splits into three branches (Quadfasel et al., 1987) (Figure 1). One of the branches recirculates back into the Nordic Seas (Returning Atlantic Water) and joins polar surface waters flowing southwards in the western Fram Strait east of Greenland as the East Greenland Current (Bourke et al., 1988). The second branch flows eastward along the shelf edge north of Svalbard (Svalbard Branch) and the third branch crosses the Yermak Plateau (Yermak Branch) (Quadfasel et al., 1987; Gascard et al., 1995) (Figure 1). When the AW encounters the sea ice north of Svalbard in the Arctic Ocean, the upper part of AW is mixed with fresh and cold Polar Surface Water, whereas the lower part subducts beneath the freshwater layer and becomes isolated from the atmosphere (Rudels, 2015) (Figure 1).

The novelty of this thesis lays on the reconstruction of BWT in two key areas in the Arctic. Changes in BWT are used as an indirect indicator of the strength of deep water formation and characteristics of water masses reaching the seafloor at the study sites, with warmer temperatures (site specific but generally >1°C; see **Paper I** and **II**) indicating an enhanced inflow (**Paper II**, shelf site) or deepening of AW, and therefore weaker AMOC and reduced deep-water formation in the Nordic Seas (**Paper I**). So far records of BWT in the Nordic Seas and the Barents Sea are scarce and reconstructions of absolute temperatures are needed to better understand the interactions between oceanographic changes, rapid sea-ice and climatic oscillations in the past and their links to the stability of the gas hydrate systems.

1.1.1 The role of the ocean at millennial-scale climate oscillations

The climate record of the Quaternary (2.58 million years ago to present) has a distinctive saw-tooth shape defined by glacial (cold) and interglacial (warm) cycles when continental ice sheets would grow and subsequently decay, paced by orbital (Milankovitch) cycles (Hays et al., 1976). At a millennial timescale, rapid (decadal) well-marked atmospheric temperature increases followed by slower cooling phases occurred during the last glacial (115,000–11,000 years ago) (Johnsen et al., 1992; Dansgaard et al., 1993; S. O. Rasmussen et al., 2014) when North America, Greenland and Eurasia were covered by large continental ice sheets. These events, termed Dansgaard-Oeschger (DO) events, are globally expressed in marine, terrestrial and ice core records especially in the Northern Hemisphere (e.g., Voelker & workshop participants, 2002), but the best-defined records are found in ice-cores from Greenland (Dansgaard et al., 1982; North Greenland Ice Core Project members, 2004; S. O. Rasmussen et al., 2014) (Figure 2).

The $\delta^{18}O$ record from ice cores from Greenland records 25 DO fluctuations, stratigraphically identified as Greenland Interstadials (GI; warm phase) and Greenland Stadials (GS; cold phase) (Dansgaard et al., 1982, 1993; S. O. Rasmussen et al., 2014). These events have their counterparts in the Southern Hemisphere that are in partial antiphase, with warmings in Greenland coinciding with cooling periods in Antarctica (EPICA Community Members, 2006; Steig, 2006). Atmospheric temperatures in Greenland warmed between 5°C and 16.5°C abruptly at the transition from stadials to interstadials (Kindler et al., 2014) (Figure 2). Even if the cause(s) for these abrupt climate fluctuations remain elusive, most of the authors follow the

hypothesis that stadial-interstadial shifts are modulated by sudden changes in the strength of the AMOC (e.g., Broecker et al., 1985; Ganopolski & Rahmstorf, 2001; Rahmstorf, 2002; Knutti et al., 2004; T. L. Rasmussen & Thomsen, 2004). The premise is that the stronger the AMOC is, the more heat is transported poleward, warming the North (Rahmstorf, 2002). Feedback mechanisms among the different components of the Earth's climate system (atmosphere, hydrosphere, lithosphere, biosphere and cryosphere) probably contributed to amplify (positive feedback) the effects of the initial causes, so finding a single causal mechanism is unlikely. Indeed, the reorganization of the AMOC seems tightly related to rapid changes in the sea-ice cover (e.g., Gildor & Tziperman, 2003; Li et al., 2010; T. L. Rasmussen & Thomsen, 2004; Sadatzki et al., 2019; **Paper III**).

A typical interstadial-stadial cycle (DO-event) starts with an abrupt warming to a short-lasting warm peak, followed by progressively decreasing temperatures during the interstadial cooling phase and a rapid transition to a cold stadial. The duration of these events varies between ca. 1,100 to 8,600 years (Andersen et al., 2006). Sedimentary proxy records from the
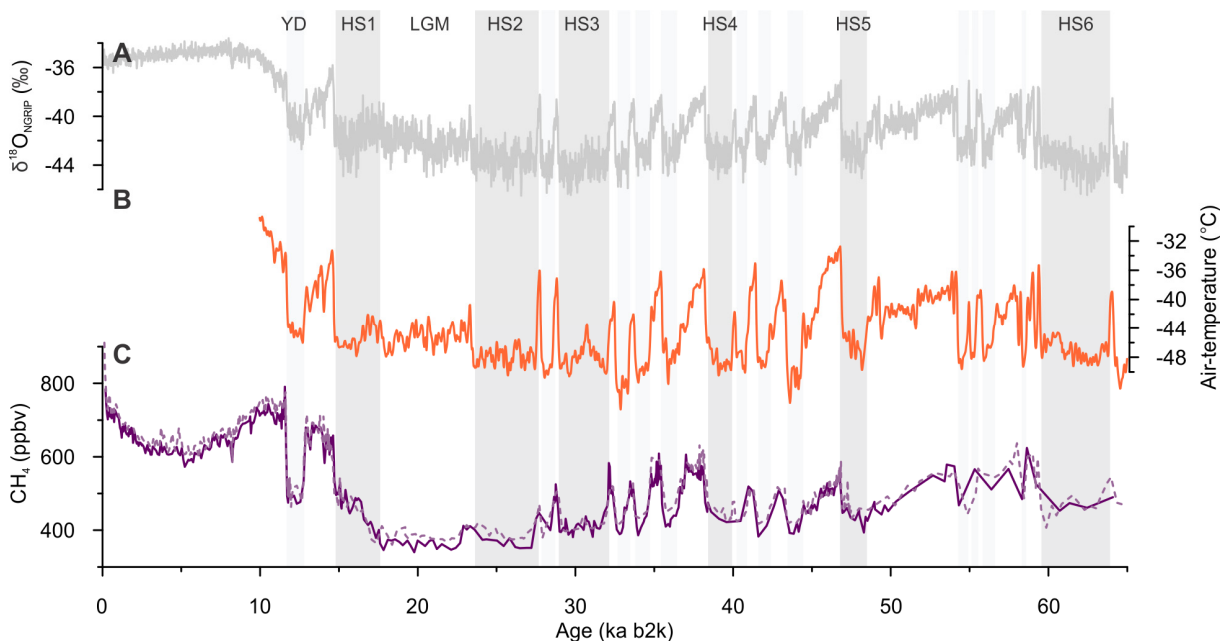
Figure 2. (**A**) Oxygen isotopic record of the North Greenland Ice Core (NGRIP) with (**B**) modelled air-temperature in Greenland (Kindler et al., 2014) and (**C**) reconstructed CH_4 in the GISP2 (dashed line) and GRIP (solid line) ice cores (see Seierstad et al., 2014 for references therein). The chronologies for the NGRIP, GISP2 and GRIP were synchronized in the GICC05modelext timescale by Seierstad et al. (2014). Heinrich stadials (HS) are marked with dark gray bars and other stadials are shown with light gray bars. Abbreviations: LGM=Last Glacial Maximum; YD: Younger Dryas.

northern hemisphere show that insterstadials (stadials) were warm (cold) and wet (dry) (Rahmstorf, 2002; Voelker & workshop participants, 2002).

Interstadials are associated with warmer surface ocean temperatures and less sea ice (Bond et al., 1993; T. L. Rasmussen & Thomsen, 2004; Hoff et al., 2016; Sadatzki et al., 2019). During interstadials, the ocean circulation of the North Atlantic is characterized by a relatively strong and deep AMOC in the Nordic Seas, similar to modern conditions (see Lynch-Stieglitz, 2017 for references therein). During stadials, the surface of the Nordic Seas was covered by sea ice as far south as the Greenland-Scotland Ridge (Hoff et al., 2016; Sadatzki et al., 2019, 2020; **Paper III**). In the North Atlantic and the Nordic Seas, proxy records show warm BWT, indicating an intermediate water warming, probably as a result of a reduced AMOC forming lees deep cold water and allowing the subduction of warm Atlantic water beneath the extended halocline (T. L. Rasmussen & Thomsen, 2004; Marcott et al., 2011; Ezat et al., 2014; Sessford et al., 2019; **Paper I**).

Some longer lasting stadials are associated with Heinrich events. These are expressed in sediment records from the mid-latitudes in the North Atlantic as accumulations of ice rafted detritus (IRD), the occurrence of polar planktic foraminiferal species *Neogloboquadrina pachyderma* and a large drop in planktic foraminiferal $\delta^{18}O$, probably as a result of surges of freshwater released from the discharge of melting icebergs (Bond et al., 1993; Hemming, 2004). The reason why some stadials are related to Heinrich events (hereafter Heinrich Stadial, HS) and others are not remains unclear, although some authors highlight a complete disruption of the AMOC leading to these anomalous 'extreme' stadials (see Lynch-Stieglitz, 2017 for references therein).

1.1.2 Environmental controls on Arctic gas hydrate systems

Gas in marine sediments can be found as free gas, gas dissolved in fluids or stored in a solid form as gas hydrates. Gas hydrates consist of a solid water lattice that enclose low molecular weight gases, mainly methane (Sloan & Koh, 2007). Gas hydrates are stable in the Gas Hydrate Stability Zone (GHSZ) over a range of high-pressure and low-temperature conditions and can therefore occur naturally in the sedimentary column in marine environments and polar areas (Collett et al., 2009). Other factors such as the composition of the gas, lithostatic pressure, geothermal gradients and pore water salinity also shape the GHSZ (e.g., Sloan & Koh, 2007).

1.1.2.1 Two gas hydrate systems: Vestnesa Ridge and Storfjordrenna

While both study areas (Vestnesa Ridge and Storfjordrenna) are relatively close, the dynamics of each gas hydrate system are rather different and therefore respond differently to environmental and geological controls.

Vestnesa Ridge is a 100-km long contourite drift stretching in a southeast to northwest direction at 79°N on the northwestern Svalbard margin at 1,200–1,300 m water depth. The ridge hosts an active gas hydrate system (Bünz et al., 2012). Here, gas seepage occurs both inside and outside the GHSZ, and the distribution of faults and fractures have revealed that the seepage from the seafloor to the water column in this area might be related to tectonic stress in the last 2.7 Ma (Bünz et al., 2012; Plaza-Faverola et al., 2015). Pressure changes associated with glacial-interglacial cycles (e.g., glacio-eustatic adjustments, glacial isostasy) might have played an additional role in reactivating fault systems and modulating seepage along Vestnesa Ridge (Plaza-Faverola et al., 2015; Plaza-Faverola & Keiding, 2019).

Storfjordrenna, a trough located in the northwestern Barents Sea at 76°N, hosts several gas hydrate related mounds (named 'pingos') at ca. 380 m water depth in a site informally called the 'Pingo area' (Serov et al., 2017). Here, the GHSZ is believed to have grown and stabilized gas hydrates during the last glacial period due to low basal temperature and high pressure under the Svalbard-Barents Sea Ice Sheet (SBIS). The GHSZ became thinner after the retreat of the ice sheet following the Last Glacial Maximum (Andreassen et al., 2017; Serov et al., 2017). Today the gas hydrate mounds are located inside the GHSZ, with a basal depth between 61 to 160 m below the seafloor (Waage et al., 2019) and methane is released in the area through faults in the Hornsund fault system (Mau et al., 2017; Waage et al., 2019). A relatively thin GHSZ in a shallow continental shelf *a priori* makes the gas hydrates here very sensitive to BWT changes (Biastoch et al., 2011).

1.1.2.2 Gas hydrates in a changing climate

Methane (CH_4) is a greenhouse gas 25 times more potent than carbon dioxide (CO_2) (Lelieveld et al., 1998). It therefore becomes necessary to advance knowledge on the fate of methane hydrates in a warming ocean, which could potentially trigger an increased dissociation and seepage from the seafloor with methane eventually reaching the atmosphere (e.g.,

Westbrook et al., 2009; Maslin et al., 2010; Biastoch et al., 2011; Kretschmer et al., 2015; Ruppel & Kessler, 2017).

The geological record contains examples of past seafloor methane release events associated with the dissociation of gas hydrates due to changing environmental factors. One of the most studied and extreme examples is the Paleocene-Eocene Thermal Maximum (PETM), which occurred ca. 55 million years ago, when a rapid global warming was probably triggered by the widespread dissociation of methane hydrates from the sub-seafloor due to increased BWT (e.g., Dickens et al., 1995; Dunkley Jones et al., 2013). During the late Quaternary, temperature variations and atmospheric CH_4 recorded in Greenland ice cores are strongly correlated (Brook et al., 1996; Huber et al., 2006) (Figure 2) and this opened the discussion about the potential sources of the methane. The 'Clathrate Gun Hypothesis' suggests that changes in BWT and sea-ice level resulted in episodic methane hydrate dissociations that, together with other feedback mechanisms, triggered the abrupt atmospheric warming at DO interstadials and longer-lasting warming events in the late Quaternary (Kennett et al., 2003). Isotopic evidence from the Greenland ice cores indicates that the initial warming at the onset of some interstadials (DO 7 and DO 8) was rather the consequence of methane emissions from wetlands (Bock et al., 2010). Other authors disagree with this interpretation and highlight the role of marine gas hydrates as the most probable source of atmospheric methane increase at the onset of interstadials (O'Hara, 2008). Modern studies show that methane released from the shallow seafloor off Prins Karls Forland west of Svalbard does not reach the atmosphere (Myhre et al., 2016) and therefore barely contributes to atmospheric warming. In the water column, methane is 'filtered' (i.e. consumed) by microbial activity, but dissolved methane still has the potential to increase the effects of ocean acidification and enhance oxygen depletion in the water column (Biastoch et al., 2011). The hypothesis supporting sub-seafloor hydrate dissociation triggering DO interstadials (at least as a major control) remains therefore minoritarian, except if the amount of dissociated hydrates was larger than it is today.

Today small (1 to 2°C) changes in BWT have an effect in methane seepage from the seafloor on the western Svalbard shelf at seasonal- (Berndt et al., 2014; Ferré et al., 2020) and longer human timescales (Ferré et al., 2012; Vadakkepuliyambatta et al., 2017). We hypothesize that BWT changes such as those observed in the Nordic Seas during HSs (see section 1.1.1.), with BWT up to 5°C higher than today, could trigger major hydrate dissociation events in the Arctic

(**Paper II**). In addition to changes in BWT, several environmental controls have been called on to explain changes in the thickness of the GHSZ, the dissociation of gas hydrates and the release of methane in the Arctic during the late Quaternary, such as sea level changes (Portnov et al., 2016), local sedimentation changes (Karstens et al., 2018) and ice-sheet dynamics (Crémière et al., 2016; Portnov et al., 2016; Andreassen et al., 2017; Wallmann et al., 2018; Dessandier et al., 2021).

To study the effect of BWT in methane seeping areas, both paleo-BWT conditions in areas close to seeping sites (see section 2.3.) and past seepage events must be reconstructed. Investigating methane seepage history using proxy data from sedimentary records remains a complex task (see Table 3 in Yao et al., 2020 for a summary of the most commonly used proxies for the reconstruction of methane seepage) since methane-affected sediment records can be highly disturbed. However, several studies have attempted to reconstruct the late Quaternary seepage history in the western Barents Sea (Yao et al., 2020) and Vestnesa Ridge (Consolaro et al., 2015; Sztybor & Rasmussen, 2017a; Schneider et al., 2018; Himmler et al., 2019; Thomsen et al., 2019; Dessandier et al., 2021). Another way to investigate the dynamics of gas hydrates in the past involves modelling the variability in thickness of the GHSZ (Portnov et al., 2016; Plaza-Faverola et al., 2017; Serov et al., 2017; Vadakkepuliyambatta et al., 2017). These models consider different reconstructed parameters, with BWT being a key parameter. Pre-industrial records of BWT are so far non-existent in the Barents Sea and western Svalbard margin and therefore previous attempts to estimate BWT in postglacial GHSZ models have included the conversion of benthic foraminiferal $\delta^{18}O$ into BWT (see section 2.2.1. for challenges associated to this method) and/or assuming a linear BWT evolution for the studied period (Portnov et al., 2016; Serov et al., 2017). In **Paper I** and **II**, we present the first BWT records for Vestnesa Ridge and Storfjordrenna, respectively. These data can be used to improve the understanding of the sensitivity of the GHSZ in the studied areas and the potential gas hydrate dissociation risk associated with an increase of BWT from global warming and warming such as observed during HSs.

1.2 Research questions

The overall objectives of this research are:

- To investigate the variability of AW inflow in the eastern Fram Strait and the

Barents Sea at millennial timescales through the reconstruction of absolute BWT using Mg/Ca measured in benthic foraminifera (**Paper I** and **II**)

- To understand the effects of BWT on shallow gas hydrate systems since the Last Glacial Maximum in the northwestern Barents Sea (**Paper II**)
- To characterize the relationship between AW inflow and sea-ice variability in the Nordic Seas in order to better understand the abrupt climate transitions during DO-events (**Paper III**)

In **Paper I** we presented the variability of AW, through the reconstruction of BWT. **Paper III** builds on the knowledge generated in **Paper I**, completing the paleoceanographic picture for the last glacial period (63–13 ka and 18–0 ka) and providing a broader understanding of the (causal?) linkages between sea ice development and variations in BWT during DO-events. Although the reconstruction of BWT is used to evaluate the impact of Atlantic water inflow in a shallow gas hydrate system in **Paper II**, this deglacial BWT record also overlaps with the BWT record from the northern Nordic Seas, thereby connecting the two study sites. Overall, the results of this thesis are used to better understand cryosphere-ocean circulation-carbon cycle-climate interactions in the northern Nordic Seas.
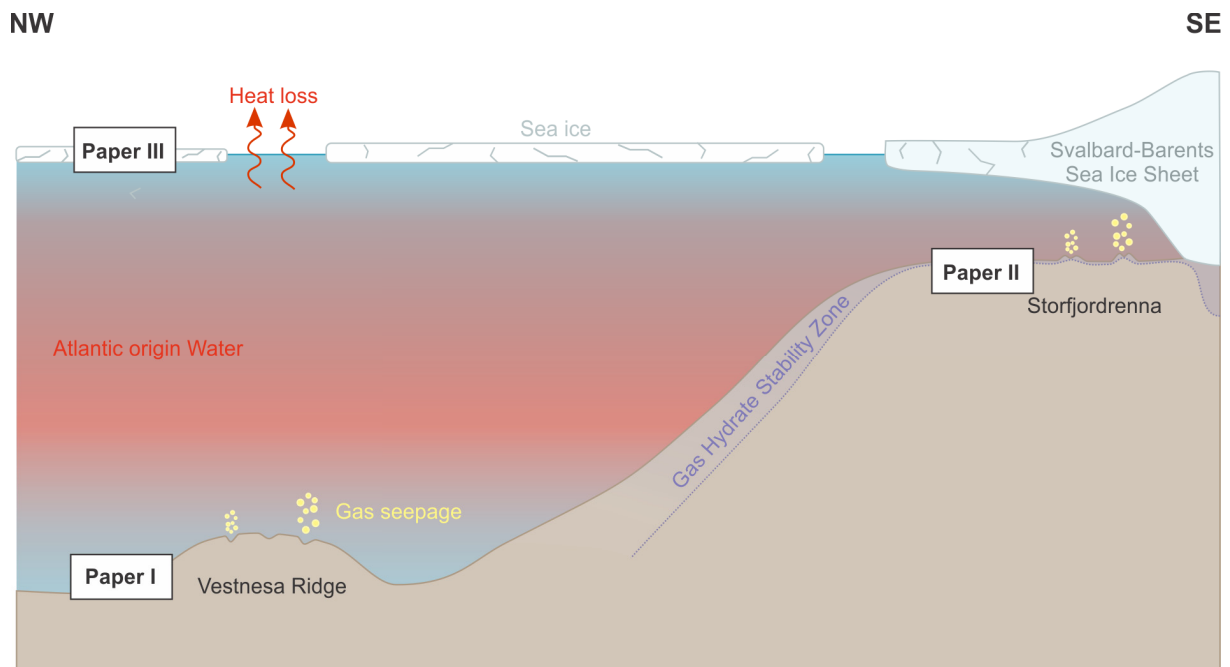
Figure 3. Overview of the goals of the research papers presented in this thesis.
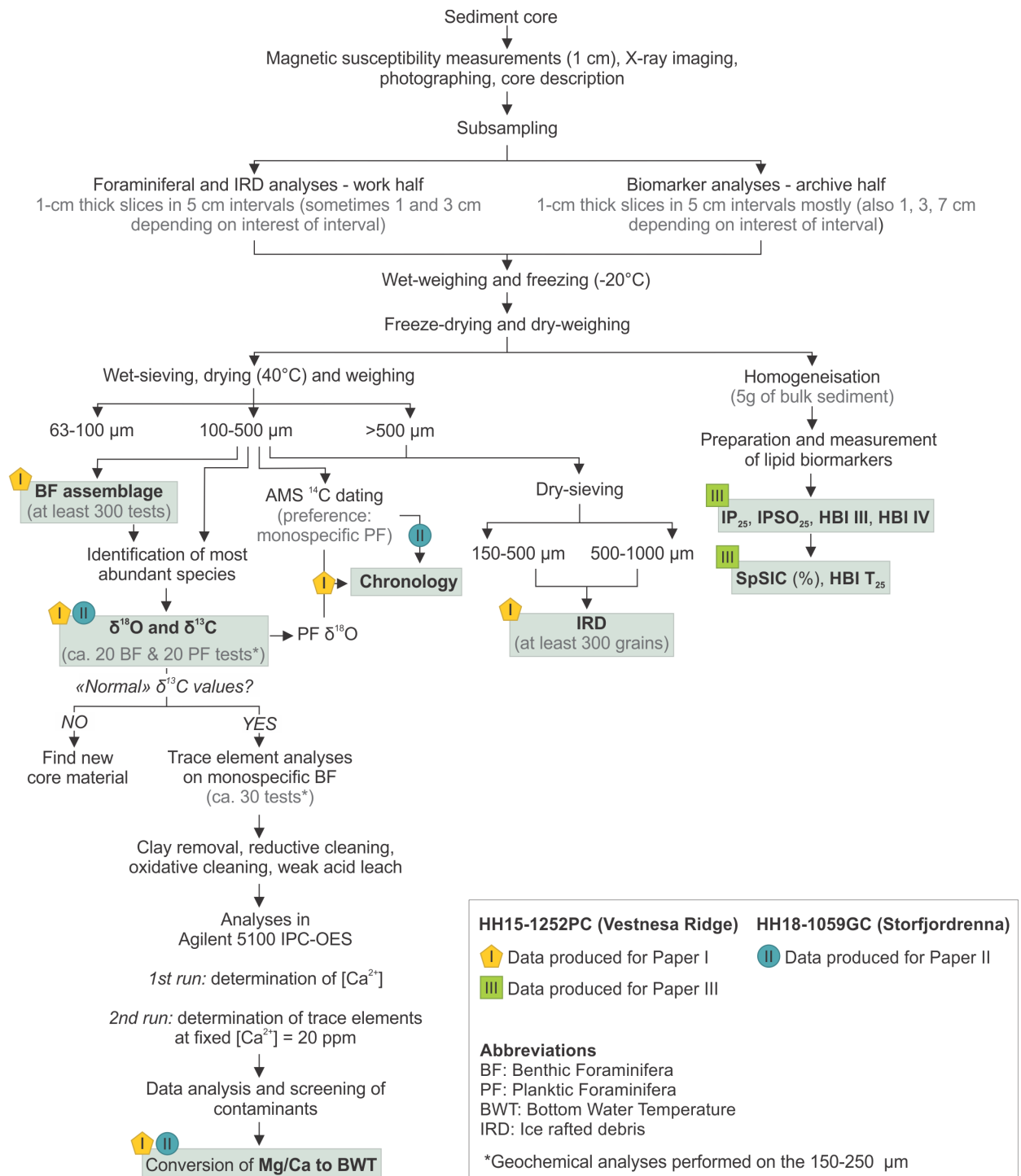
2 Scientific approach

Two sediment cores were investigated on this thesis: piston core HH15-1252PC from Vestnesa Ridge (1,273 m water depth; 79.04°N, 6.88°E; **Paper I** and **III**) and gravity core HH18-1059GC from Storfjordrenna (382 m water depth; 76.06°N, 15.58°E; **Paper II**) (Figure 1). Both cores were collected onboard the RV Helmer Hansen and processed onboard and at the Department of Geosciences at UiT The Arctic University of Norway (see Papers for further details). Figure 4 outlines the methodology used in this thesis.

In this section, I discuss the background and challenges of the main methodological approaches used during this work based mainly on the ecological and geochemical analysis of benthic foraminifera, and biomarker-based sea-ice reconstructions, as well as the approaches used for the construction of the age-depth models.

2.1 Foraminifera

Foraminifera are protists that can live in a wide range of marine environments. The majority build their test (shell) from calcite precipitated from the ambient sea water. Planktic foraminifera live in the water column close to the surface, and benthic foraminifera can live at the seafloor (as epifaunal species), or a few centimeters below (infaunal species) the water-sediment interface. Due to their small size and high abundance, their sensitivity to specific environmental conditions and generally good preservation, they are widely used in paleoceanographic investigations to trace variations in past currents, sea-level changes, nutrient export from surface to the bottom (benthic-planktic coupling), oxygen availability and salinity and temperature of the surrounding waters, among others (see Jones, 2014 for references therein). However, their occurrence and abundance in the fossil record depends on both the environmental conditions at the time of calcification and the post-mortem taphonomic processes that might affect their preservation and geochemistry of their tests (Jones, 2014).

These marine organisms can be studied in the fossil record both by the identification and quantification of key species (i.e., species that provide an array of environmental information by their presence/absence and relative abundance in the assemblage; e.g., Jones, 2014; T. L. Rasmussen & Thomsen, 2017), and by the chemical composition of their calcium carbonate ($CaCO_3$) test that, theoretically, reflect the elemental and isotopic composition of the ocean at

Sediment core

Magnetic susceptibility measurements (1 cm), X-ray imaging, photographing, core description

Subsampling

Foraminiferal and IRD analyses - work half
1-cm thick slices in 5 cm intervals (sometimes 1 and 3 cm depending on interest of interval)

Biomarker analyses - archive half
1-cm thick slices in 5 cm intervals mostly (also 1, 3, 7 cm depending on interest of interval)

Wet-weighing and freezing (-20°C)

Freeze-drying and dry-weighing

Wet-sieving, drying (40°C) and weighing

Homogeneisation
(5g of bulk sediment)

Preparation and measurement of lipid biomarkers

63-100 µm   100-500 µm   >500 µm

BF assemblage
(at least 300 tests)

AMS ^{14}C dating
(preference: monospecific PF)

Dry-sieving

III **IP$_{25}$, IPSO$_{25}$, HBI III, HBI IV**

Identification of most abundant species

Chronology

150-500 µm   500-1000 µm

III **SpSIC (%), HBI T$_{25}$**

δ^{18}O and δ^{13}C
(ca. 20 BF & 20 PF tests*)

→ PF δ^{18}O

IRD
(at least 300 grains)

«Normal» δ^{13}C values?

NO   YES

Find new core material

Trace element analyses on monospecific BF
(ca. 30 tests*)

Clay removal, reductive cleaning, oxidative cleaning, weak acid leach

Analyses in Agilent 5100 IPC-OES

1st run: determination of [Ca^{2+}]

2nd run: determination of trace elements at fixed [Ca^{2+}] = 20 ppm

Data analysis and screening of contaminants

Conversion of **Mg/Ca to BWT**

HH15-1252PC (Vestnesa Ridge)   **HH18-1059GC (Storfjordrenna)**

I Data produced for Paper I   II Data produced for Paper II

III Data produced for Paper III

Abbreviations
BF: Benthic Foraminifera
PF: Planktic Foraminifera
BWT: Bottom Water Temperature
IRD: Ice rafted debris

*Geochemical analyses performed on the 150-250 µm

Figure 4. Overview of the methodological approach followed in this thesis. Colored boxes show the type of data produced from the different analyses.

16

the time of calcification (e.g., Zachos et al., 2001; Skinner et al., 2003; Kristjánsdóttir et al., 2007; Elderfield et al., 2012; Ezat et al., 2014; see section 2.2.).

Arctic waters are quasi-exclusively dominated by the planktic foraminiferal species *Neogloboquadrina pachyderma* (e.g., Carstens et al., 1997; Volkmann, 2000)*,* whereas benthic foraminiferal faunas are more diverse, with *Cassidulina neoteretis* and *Melonis barleenus* being amongst the most abundant species at intermediate water depths (e.g., Wollenburg & Mackensen, 1998; Sejrup et al., 2004). In **Paper I** we used the composition of the benthic foraminiferal assemblages to trace the evolution of bottom water conditions.

2.2 Geochemical analyses

Geochemical analyses on foraminiferal tests constitute a great tool to study the chemical and physical properties of past oceans. Stable isotopes of selected species of both benthic and planktic foraminifera and trace element analyses on benthic foraminiferal tests were used as seawater proxies in **Paper I** and **II**.

2.2.1 Stable isotopes: δ¹⁸O and δ¹³C as seawater proxies and validation tools

Stable oxygen isotopes ($\delta^{18}O$) measured in foraminiferal tests have been widely used as a paleotemperature/paleosalinity proxy. Paleothermometry techniques based on the isotopic composition of foraminiferal calcite began in the early 1950s (e.g., Urey et al., 1951; Epstein et al., 1953; Emiliani, 1955), and even if the preliminary values overestimated the glacial-interglacial temperatures, the benthic foraminiferal $\delta^{18}O$ were used to define for the first time Marine Isotope Stages (MIS) and to support Milankovitch cycles (Hays et al., 1976). Ever since this technique was described, benthic foraminiferal $\delta^{18}O$ has been widely applied in paleoclimatology and paleoceanography to reconstruct the long-term history of Earth's climate during the Cenozoic (e.g., Zachos et al., 2001) and Pleistocene glacial-interglacial variations in ocean dynamics (e.g., Shackleton, 1967; Elderfield et al., 2012).

This widely used technique is accompanied by several uncertainties, which must be accounted for. Ideally, foraminiferal $\delta^{18}O$ values reflect seawater properties at the time that the shell calcifies, so they do not only depend only on temperature, but also on seawater $\delta^{18}O$,

which is in turn related to global ice volume and local $\delta^{18}O$ variations linked to salinity (see Ravelo & Hillaire-Marcel, 2007 for references therein). In addition, some species do not calcify in equilibrium with the surrounding waters (the so-called 'vital effect'), and this phenomenon might cause important differences in the oxygen and carbon isotope records between different foraminiferal species (e.g., Duplessy et al., 1970, 1980). The 'vital effect' can be corrected using known correction factors, but in order to reduce uncertainties, it is preferable to select a single species that is abundant down-core. In the case of planktic foraminifera the $\delta^{18}O$ of some species is size-dependent and it is therefore recommended to analyze specific size fractions (Hillaire-Marcel et al., 2004; El bani Altuna et al., 2018). Parallel $\delta^{18}O$ and independent paleotemperature proxies, such as Mg/Ca, can be used to discriminate the temperature component from the seawater $\delta^{18}O$ component of the $\delta^{18}O$ in foraminiferal tests (e.g., Skinner et al., 2003; **Paper II**).

The stable carbon isotope ratio ($\delta^{13}C$) in foraminifera is primarily a function of the $\delta^{13}C$ of the dissolved inorganic carbon (DIC) in the seawater. The $\delta^{13}C$ of epifaunal benthic foraminifera is used as a nutrient-proxy and therefore utilized for reconstructing the water mass geometry (e.g., Curry et al., 1988; Sarnthein et al., 1994; Curry & Oppo, 2005; Lynch-Stieglitz et al., 2007) and ventilation history (e.g., Thornalley et al., 2015). Infaunal benthic foraminiferal species calcify within the sediment and their $\delta^{13}C$ might be reflecting seawater $\delta^{13}C$ and/or pore water $\delta^{13}C$ (McCorkle et al., 1990; Mackensen et al., 2000). The former differs from seawater $\delta^{13}C$ due to the fact that the decomposition of organic matter lowers the pore water $\delta^{13}C$ signal.

In methane seep sites, the origin (thermogenic or biogenic) and the oxidation of the methane will further lower the $\delta^{13}C$ of the DIC in the sediment pore water (e.g., Whiticar & Faber, 1986; Whiticar, 1999). The low $\delta^{13}C$ of the DIC in the pore water can be recorded in the foraminiferal tests during the calcification or after their death as a result of overgrowth of authigenic calcite (e.g., Schneider et al., 2017; Sztybor & Rasmussen, 2017b).

While 'normal' values of $\delta^{13}C$ in benthic and planktic foraminifera do not exceed -4‰ and -2‰ respectively (this can also be species specific; McCorkle et al., 1990; Mackensen & Schmiedl, 2019), foraminifera affected by methane-seepage can record anomalously low $\delta^{13}C$ values (Torres et al., 2003; Hill et al., 2004; Sztybor & Rasmussen, 2017b). It is still debated whether or not foraminiferal $\delta^{18}O$ is affected by overgrowth of authigenic calcite (Sztybor & Rasmussen, 2017b; Dessandier et al., 2020).

18

One of the main purposes of this thesis is to reconstruct past BWT in the vicinity of methane seep sites, and for that purpose we performed Mg/Ca analyses on benthic foraminifera (see section 2.2.2.). This technique relies on measuring the primary (i.e. 'original') foraminiferal calcite. Authigenic carbonates can be rich in Mg and the tests of foraminifera affected by authigenic calcite overgrowth can, therefore, have a high Mg/Ca, yielding unrealistically high BWT (Torres et al., 2003; Detlef et al., 2020; T. L. Rasmussen & Groeneveld, unpublished data). In order to prevent this, we used foraminiferal $\delta^{13}C$ as a preliminary tool to evaluate the foraminiferal material (i.e., if samples were affected by methane-related authigenic overgrowth) and to decide whether or not Mg/Ca analyses should be performed on the selected samples.

2.2.2 Trace elements: Mg/Ca as oceanic temperature proxy

At the time of calcification foraminifera can incorporate trace elements from the seawater into their calcite tests depending on the physical and chemical properties of the water, as well as on species ecology and physiology. This makes foraminiferal tests a great tool for paleoceanographers to study past oceanic conditions (see Lea, 2002 for a review).

The incorporation of magnesium (Mg) into the foraminiferal test is primarily controlled by temperature (Nürnberg et al., 1996; Toyofuku et al., 2000). The Mg/Ca of benthic foraminifera has been widely used to reconstruct BWT (e.g., Skinner et al., 2003; Kristjánsdóttir et al., 2007; Marcott et al., 2011; Elderfield et al., 2012; Ezat et al., 2014; Thornalley et al., 2015; Sessford et al., 2018, 2019; **Paper I**; **Paper II**), and that of planktic foraminifera to reconstruct sea (sub)surface temperatures (e.g., Barker et al., 2005; Thornalley et al., 2009, 2011; Aagaard-Sørensen et al., 2014; Ezat et al., 2016). It is important to note that other factors at the time of calcification, such as salinity and carbonate chemistry (e.g., Nürnberg et al., 1996; Ferguson et al., 2008; Hönisch et al., 2013; Barrientos et al., 2018), and post-mortem calcite-pore water physicochemical interactions (e.g., Boyle, 1981, 1983; Dekens et al., 2002; Pena et al., 2005; Hasenfratz et al., 2017) may also influence the resulting Mg/Ca.

Given that this method relies on measuring the chemical composition of the primary calcite of the foraminiferal test, rigorous cleaning protocols need to be performed (Boyle & Keigwin, 1985; Martin & Lea, 2002; Barker et al., 2003, 2005; Ezat et al., 2016). In this work we applied the 'reductive-oxidative cleaning' method including the following steps: (1) clay removal, (2)

reductive cleaning with hydrous hydrazine to eliminate diagenetic Mn and Fe rich oxides, (3) oxidative cleaning to remove the adhered organic matter and (4) weak acid leach to reduce the effect of any remaining contaminants (Boyle & Keigwin, 1985; Pena et al., 2005; Ezat et al., 2016). The reductive cleaning step might cause the partial dissolution of the foraminiferal tests (Yu et al., 2007), but the 'full cleaning' approach is more efficient to eliminate the different contaminants than the 'Mg cleaning' (see Ezat et al., 2016).

Arctic foraminifera are usually smaller than their subpolar counterparts and often the material is scarce. This is why, the $[Ca^{2+}]$ concentration of all the samples was first measured in an ICP-OES to avoid the 'matrix effect' and then the solutions were diluted to correspond to 20 ppm $[Ca^{2+}]$ during the final round of analysis due to the small size of the samples (de Villiers et al., 2002). Other elemental ratios such as Al/Ca, Mn/Ca and Fe/Ca, were measured in parallel to Mg/Ca to evaluate the reliability of the cleaning method and to evaluate whether or not a sample was contaminated (Barker et al., 2003). The final Mg/Ca results were converted to BWT using existing Mg/Ca-BWT calibrations. In **Paper I** and **Paper II** we applied the calibration of Kristjánsdóttir et al (2007) for *C. neoteretis* and *M. barleeanus* (see further details in papers).

2.3 Sea-ice proxies

The evolution of sea ice in the Arctic has traditionally been studied using micropaleontological (key species and assemblage composition of dinoflagellate, diatom and benthic foraminifera; e.g., de Vernal et al. (2013), Seidenkrantz (2013)) and sedimentological (abundance of characteristic IRD; e.g., Dowdeswell & Dowdeswell (1989), Jessen & Rasmussen (2019)) approaches. In 2007, Belt et al. (2007) introduced IP25, a new sea-ice proxy based on a lipid compound produced by a few Arctic sea-ice diatoms that live in interstitial channels in, or at the base of the sea ice (Brown et al., 2011; Belt & Müller, 2013).

IP25 is a mono-unsaturated highly branched isoprenoid (HBI) lipid with 25 carbons (Belt et al., 2007). This lipid has been found in abundance in modern sediments from the Arctic region with seasonal sea ice, whereas it is absent in regions with perennial sea ice cover and in locations with open ocean conditions (Belt et al., 2007; see Belt & Müller, 2013 for references therein; Xiao et al., 2015). The absence of IP25 may therefore be indicative of two opposing scenarios, one with extensive sea ice conditions and the other one with no sea ice. Increased IP25 is, therefore, a very useful proxy for seasonal sea ice, but low IP25 must be interpreted with

caution. In an attempt to overcome the duality of IP_{25}, Müller et al. (2011) established the PIP_{25} index, based on the relation between IP_{25} and a phytoplankton marker indicative of phytoplankton production and open-water conditions. The two phytoplankton markers generally used in the PIP_{25} index are brassicasterol (produced primarily by diatoms but also coccolithophorids) or dinosterol (produced by dinoflagellates) (Volkman et al., 1998; Müller et al., 2011; Belt & Müller, 2013). This index varies between 0 and 1, representing a gradient from sea-ice free conditions to extensive sea ice cover (Müller et al., 2011). The original PIP_{25} equation included a balance factor c to compensate for the overall higher concentrations of the phytoplankton marker (brassicasterol and dinosterol) over IP_{25} and it is calculated as the ratio between the average IP_{25} and average phytoplankton marker (Müller et al., 2011).

A third kind of useful phytoplankton marker are tri-unsaturated HBI lipids (HBI III), thought to be indicative of neighboring sea ice and/or a marginal ice zone (Belt et al., 2015). The absolute abundance of HBI III in the sediments is closer to IP_{25} and it might be more suitable for PIP_{25} calculations because one could omit the c factor, therefore avoiding the biases related to its calculation (Belt et al., 2015; Smik et al., 2016). The resulting $P_{III}IP_{25}$ (using IP_{25} and HBI III) better reflects the relative concentration of spring sea ice (SpSIC) than using the PIP_{25} index with brassicasterol as the phytoplankton marker (Smik et al., 2016). These promising results allowed the creation of a calibration for the estimation of SpSIC in paleorecords. This calibration was obtained from a correlation between the $P_{III}IP_{25}$ in surface sediments from the Barents Sea and the SpSIC measured from instrumental sea-ice data (Smik et al., 2016). Recently an additional sea-ice index has been developed that allows the measurement of phytoplankton blooms: HBI T_{25} (Belt et al., 2019).

In **Paper I,** we speculated about periods where sea ice may have been present using indirect sea ice indicators such as benthic foraminiferal species feeding on phytodetritus and an IRD grain-size ratio that is useful to trace the origin (i.e., sea ice or iceberg transported) of the IRD (Jessen & Rasmussen, 2019). The trends observed in **Paper I** were later confirmed and improved in **Paper III** where we used IP_{25}, HBI III, SpSIC and HBI T_{25} to quantify the evolution of the sea ice in the northern Nordic Seas.

2.4 Chronology

Obtaining reliable estimates of the timing of past events is particularly important in paleoclimatology, especially when the aim of the study is to investigate the synchroneity of events (e.g. the chronological relationship between BWT, abrupt climate oscillations and release of methane). In the works presented in this dissertation, two different approaches to build the age-depth models were used to best fulfill the objectives and suit the type of material used for each study.

2.4.1 Radiocarbon dating

Radiocarbon (also referred to as carbon-14 or ^{14}C) dating is one of the most widely developed and used dating technique for late Quaternary sediments. In short, this method consists on determining the radioactive decay of ^{14}C in a dead organism that assimilated this isotope through their lifetime. Carbon-14 is constantly being produced in the upper atmosphere and enters the carbon cycle via plant photosynthesis and the food chain. Once an organism dies, the exchange of carbon with the atmosphere stops and the radioactive decay of ^{14}C can then be measured. There are two main techniques for radiocarbon dating: beta counting (also known as 'conventional radiocarbon dating' or 'radiometric dating') and Accelerator Mass Spectrometer (AMS) dating. The former consists on calculating the time passed since the death of the organisms using the known half-life of ^{14}C (Libby, 1970). The later has been used since the late 70s and consists of quantifying the amount of ^{14}C and ^{12}C (^{12}C being the most abundant carbon isotope in nature). This method requires less material than conventional radiocarbon dating and can be used to date approximately the last 55,000 years of Earth's history (Heaton et al., 2020; Reimer et al., 2020).

This ideal technique is accompanied by some limitations, one of them being the assumption that the production of atmospheric ^{14}C has not varied over time (de Vries, 1958). However, there are temporal variations in the rate of the production of ^{14}C in the atmosphere caused by changes in the Earth's magnetic field, so the measured ^{14}C age must be converted into calibrated calendar ages (i.e., the 'real' age) using calibration curves (Figure 5). The date calculated from measured ^{14}C is referred to as '^{14}C age before present (BP)', whereas the calibrated age is referred to as 'calibrated age BP' or 'ka' (where 'k' stands for kilo or thousand and 'a' for years). The most updated Northern Hemisphere radiocarbon calibration curves are IntCal20
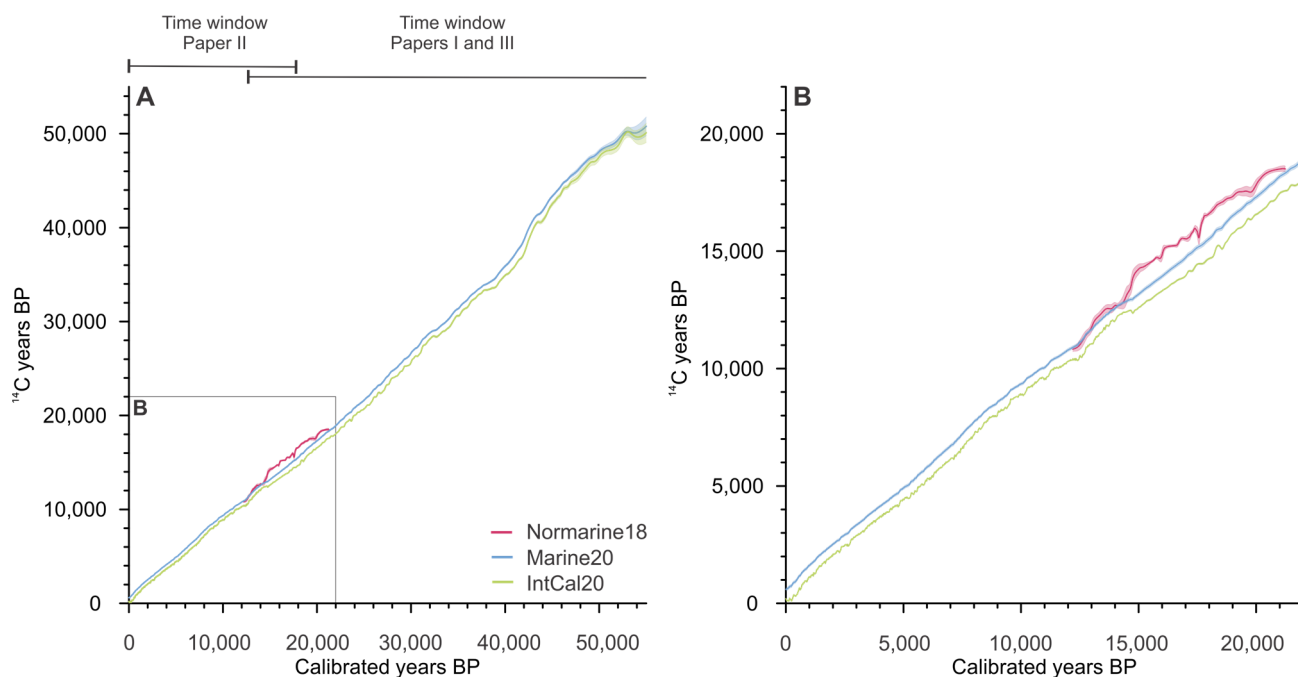
Figure 5. Plot of 14C years and calibrated (cal) yeas before present (BP) in Marine20 (Heaton et al., 2020), IntCal20 (Reimer et al., 2020) and Normarine18 (Brendryen et al., 2020) for the 0–55,000 cal years BP period (**A**) and 0–22,000 cal years BP (**B**).

(Reimer et al., 2020) for terrestrial samples, and Marine20 (Heaton et al., 2020) for marine samples.

Radiocarbon dating in marine materials comes with an additional problem: the reservoir age (R). The marine reservoir age is the offset between the ^{14}C content in the ocean and the atmosphere. This occurs due to a delay in the incorporation of atmospheric carbon into the ocean caused by slower mixing, and is further amplified in the deep ocean where old carbon is stored (e.g., Heaton et al., 2020). Ocean circulation (e.g. ventilation of the ocean, mixing of water masses) and the carbon cycle therefore have an effect on the marine reservoir effect (e.g., Skinner et al., 2019). By consequence, marine radiocarbon samples appear to be older than their terrestrial counterparts, and to be able to be compared, they need to be corrected using R estimates. Today, the marine reservoir age is on average between 400 and 500 ^{14}C years (Reimer et al., 2013), but this number can differ regionally; regional differences are expressed as ΔR.

At high latitudes, changes in ocean ventilation arise mostly from changes in sea-ice cover, wind strength, influence of polar meltwater, additions of 'old' carbon from decaying ice sheets among other factors, and may lead to a larger R offset (larger ΔR). The apparent ageing of polar

waters in comparison to the atmosphere was larger during glacial periods and stadials, when the sea-ice cover was more extensive and the strength of the AMOC was reduced, with ^{14}C ages over 1,000 years older in the North Atlantic and up to 10,000 years in the Nordic Seas (e.g., Stern & Lisiecki, 2013; Thornalley et al., 2015; Ezat et al., 2017; Telesiński et al., 2021). Hence, it is recommended to not use the Marine20 curve in polar areas (Heaton et al., 2020). Brendryen et al. (2020) built the Normarine18 calibration curve, the first calibration curve for the eastern Nordic Seas. This curve calibrates the age interval from 12,000 to 21,240 ^{14}C (whereas Marine20 calibrates from 0 to 50,788 ^{14}C years) with a ΔR that varies over time (ranging from 1,620 to 420 ^{14}C years) (Brendryen et al., 2020). As mentioned above, other studies found larger variations in ΔR, however, in the absence of a more comprehensive regional calibration curve, Normarine18 seems to be the best option for studies focusing on the deglaciation in our study areas. Radiocarbon ages in **Paper I** were thus calibrated using Marine20 due to the temporal window investigated in core HH15-1252PC (Figure 5). In **Paper II**, ^{14}C ages were calibrated using Marine20 and Normarine18 for the Holocene and the deglaciation, respectively (see details in Paper).

Last, it is important to bear in mind that different organisms incorporate carbon isotopes in different ways, and that their ecological preferences (e.g., preferred water depth and feeding mode) influence the radiocarbon age they record (e.g., Mangerud et al., 2006; Ezat et al., 2017). Planktic foraminifera reflect the ^{14}C of the subsurface of the ocean and are in a relatively good equilibrium with the atmosphere and in accordance with the global R. Benthic foraminifera record the ^{14}C of the bottom waters and might therefore seem older than fossil planktic foraminifera from the same time interval. Other benthic organisms, including different groups of Mollusca, are also widely used for dating purposes. However, the feeding mode of the different species can lead to very large uncertainties and deposit feeding mollusks (those that can digest old carbon particles) should be avoided (e.g., Forman & Polyak, 1997). Material sampled for radiocarbon dating was selected based on the following order of preference and depended strongly on the availability of the material: (1) (mono-specific) planktic foraminifera, (2) (mono-specific) benthic foraminifera, (3) mixed benthic and planktic foraminifera, (4) bivalves.

Table 1 shows all the material dated during this thesis and calibrations with different calibration curves.

Table 1. Radiocarbon ages obtained from the two cores studied in this thesis. Calibrated dates are presented with the different calibration curves. Dates in italics correspond to the calibrated dates originally used in the papers. PF = Planktic Foraminifera. [1]Heaton et al., 2020; [2]Brendryen et al., 2020.

	Lab code	Depth in core (cm)	Material	^{14}C age (years ± 1σ)	Marine20[1] calibrated age (years ± 1σ)	Normarine18[2] calibrated age (years ± 1σ)
HH15-1252PC Vestnesa Ridge	UBA-38275	140	Scaphopod	13,378 ± 49	*15,264 ± 120*	14,565 ± 310
	UBA-38276	145	*N. pachyderma* (PF)	14,806 ± 61	*17,100 ± 125*	15,859 ± 350
	UBA-38822	220	*N. pachyderma* (PF)	18,195 ± 90	*21,052 ± 165*	20,455 ± 736
	UBA-38823	315	*N. pachyderma* (PF)	23,420 ± 129	*26,843 ± 196*	-
	UBA-38824	460	Bivalve	33,662 ± 362	*37,540 ± 537*	-
	UBA-42495	495	*N. pachyderma* (PF)	26,360 ± 269	*29,728 ± 284*	-
	UBA-41568	590	*N. pachyderma* (PF)	36,514 ± 1206	*40,508 ± 868*	-
HH18-1059GC Storfjordrenna	UBA-42727	36	Bivalve	1,821 ± 25	*1,209 ± 176*	-
	UBA-42728	73	Bivalve	4,190 ± 33	*4,079 ± 253*	-
	UBA-42481	130	*N. pachyderma* (PF)	8,537 ± 36	*8,951 ± 272*	-
	UBA-43810	228	*Astarte* sp. (Bivalve)	10,776 ± 40	*12,016 ± 356*	-
	UBA-42482	291	*N. pachyderma* (PF)	12,436 ± 66	13,817 ± 310	*13,790 ± 869*
	UBA-42483	365	*N. pachyderma* (PF)	14,595 ± 64	16,826 ± 364	*15,528 ± 711*
	UBA-42484	378	*N. pachyderma* (PF)	15,956 ± 59	18,437 ± 318	*17,454 ± 347*
	UBA-42485	381	*N. pachyderma* (PF)	16,281 ± 72	18,799± 321	*17,655 ± 397*
	UBA-42486	384	*N. pachyderma* (PF)	16,458 ± 96	18,988 ± 406	*17,907 ± 368*

2.4.2 Alignment of ice-core-marine records

In order to study the interaction between the ocean and the atmosphere during DO-events, one must be able to compare marine archives to ice-core records (regarded as the best reference for such millennial-scale events; Svensson et al., 2008). Calibrated radiocarbon ages might be in line with ice-core records if ΔR is known for the entire record, however, due to the nature of Arctic waters, preservation issues of the fossil organisms and low sedimentation rates, obtaining a good, radiocarbon-based chronology is not always possible. Additionally, global calibration curves might not be useful in polar waters due to the large variability in the marine reservoir effect and ΔR (see section 2.3.1.). It is therefore necessary to build regional calibration curves accounting for local marine reservoir ages if ice-core and marine archives are correlated in the Arctic.

Event stratigraphy is a very useful tool to align both ice core and marine sedimentary records. It consists on focusing and identifying short-lived and distinct events (instant to thousand years of age), and using these events as a correlation tool to align two records (Rawson et al., 2002). In this case, the mid-point of rapid warming transitions from GS to GI are used to 'transfer' the ice core chronology to marine archives (see Shackleton et al., 2000; Austin & Hibbert, 2012). In marine records, the rapid atmospheric warmings would correspond to large meltwater episodes triggered by warming events and internal ice-sheet dynamics, and are reflected in rapid decreases of planktic foraminiferal $\delta^{18}O$. This method is associated with various sources of uncertainty, mainly related to the primary assumption that all changes are recorded in the paleoclimate archives (Austin & Hibbert, 2012). This might hamper the visual correlation as the record could have been affected by changes in the sedimentation rate and bioturbation. Other sources of uncertainty are related to the 'parent' ice chronology and the assumption that planktic foraminiferal $\delta^{18}O$ has a one-to-one relationship with salinity (see section 2.2.1.) (Austin & Hibbert, 2012).

In order to improve issues related to the alignment of ice core and marine records, several authors studying records from the southern Nordic Seas have used tephra horizons that are believed to have been deposited quasi-instantaneously from known and well-dated volcanic eruptions from Iceland and the Azores (e.g., Wastegård & Rasmussen, 2001, 2014; T.L. Rasmussen et al., 2003; Griggs et al., 2014;). In sedimentary records at higher latitudes, a pre-

Holocene tephra layer has been identified in a Svalbard lake at 79°N (van der Bilt & Lane, 2019), and a few tephra shards have been found in core JM04-25PC at the western Svalbard margin at 77°N (Abbott et al., 2018) and in the Fram Strait at 79°N (Zamelczyk et al., 2012). Unfortunately, no clear tephra horizons have yet been found in our study sites (T.L. Rasmussen, personal communication).

The age-depth model of **Paper I** and **III** is based on the alignment of core HH15-1252PC with the NGRIP ice core. Radiocarbon dates obtained from shell material (Table 1), as well as magnetic susceptibility tie-points obtained from the correlation to the western Svalbard magnetic susceptibility stack (Jessen et al., 2010), were then used as a tool to evaluate and validate the ice core-marine record 'tuning'. In the absence of better tools, the alignment of ice-core and marine records using the assumption of contemporaneous atmospheric warming and large freshwater releases from melting continental ice sheets is one of the best and most widely used tools one can use in the high north to study ocean-atmosphere interactions at DO-events. Therefore age-depth model construction must be regarded as a 'work in progress' that can be improved as chronostratigraphic tools and resources develop, and regional variations in ΔR are reconstructed.

3 Summary of research papers

3.1 Paper I

Bottom water temperature records from the southern Nordic Seas and North Atlantic show persistent intermediate water warmings during stadials, indicating reduced ocean convection during the cold phases of Dansgaard-Oeschger (DO) events (T. L. Rasmussen & Thomsen, 2004; Marcott et al., 2011; Ezat et al., 2014; T. L. Rasmussen et al., 2016; Sessford et al., 2019). Although benthic foraminiferal assemblage studies in the northern Nordic Seas pointed to a subsurface warming during the same periods, high resolution absolute BWT reconstructions were missing. In this work, we reconstructed BWT through the measurement of Mg/Ca of benthic foraminifera in core HH15-1252PC from north of Vestnesa Ridge in the northern Nordic Seas at 1,273 m water depth, in order to study its natural variability at millennial timescales during MIS 3 and 2 in the last glacial period (63–13 ka).

The reconstruction of BWT combined with benthic foraminiferal stable oxygen and carbon isotopes ($\delta^{18}O$ and $\delta^{13}C$, respectively), the composition of benthic foraminiferal faunas and IRD content, reveal at least two distinctive scenarios for 1) warm Greenland Interstadials and 2) cold Greenland Stadials. During stadials, BWT increased by up to 5±1°C, suggesting that deep water generation was reduced and therefore allowed the subsurface Atlantic water mass to both thicken and deepen to at least the core site depth, as has previously been suggested to have occurred in the southern Nordic Seas. Benthic foraminiferal faunas are dominated by *Cassidulina neoteretis*, a benthic foraminiferal species that has an affinity for Atlantic water (see Cage et al., 2021 for references therein). Heinrich Stadial 1 also shows a characteristic faunal assemblage composed of the so-called 'Atlantic species' group, which has affinity to warm bottom waters supporting our Mg/Ca-derived BWT, and their presence coincides with the highest recorded BWT in the core. The paleoceanographic context of this area during GIs was comparable to modern oceanographic settings, with benthic foraminiferal species that

respond rapidly to increased supply of phytodetritus, probably indicating the presence of highly productive surface waters, as in the Marginal Ice Zone or areas of seasonal sea-ice cover.

We also compiled previously published Mg/Ca-derived BWT results, BWT calculated from transfer functions and percentages of the 'Atlantic species' group from the literature covering the North Atlantic, Nordic Seas and Arctic Ocean during HSs. This compilation showed that a vast heat reservoir occupied the subsurface beneath a strong halocline during HS from the North Atlantic to the Arctic Ocean. We therefore hypothesized that the release of oceanic heat must have contributed to the large and abrupt atmospheric warmings at the start of Greenland Interstadials.

3.2 Paper II

El bani Altuna, N., Rasmussen, T.L., Ezat, M.M., Vadakkepuliyambatta, S., Groeneveld, J., Greaves, M. **Deglacial bottom water warming intensified Arctic methane seepage, Northwestern Barents Sea**. In review in *Communications Earth and Environment* (minor revision requested).

The Barents Sea is a shelf sea that connects the North Atlantic and the Arctic oceans. Release of methane at the seafloor is widespread in the area since the last deglaciation, and is closely linked to changing pressure (e.g., Andreassen et al., 2017; Serov et al., 2017). In order to understand the natural variability of the interactions between gas hydrate dissociation and BWT, we reconstructed BWT using Mg/Ca of benthic foraminifera in core HH18-1059GC, located in the gas hydrate 'Pingo area' in Storfjordrenna (northwestern Barents Sea) at 382 m water depth. The core spans the last deglaciation through to the Holocene and is situated in an area proximal to the former grounding zone of the Storfjorden ice stream from the SBIS.

We used our new BWT in a coupled ice sheet-hydrate stability model and aligned our record with other reference cores from the area, allowing comparisons between methane-influenced records (Yao et al., 2020) and our unaffected record. Our Mg/Ca results show BWTs varied by up to 6°C during the last deglaciation, and predictably reached a maximum during HS1. The BWT decreased and subsequently stabilized during the Holocene at ca. 3°C. Modelling of the GHSZ shows that the BWT shaped its thickness and caused its reduction and outcropping

following periods with anomalously high BWT. The correlation of cores demonstrates that this outcropping probably accelerated the dissociation of methane hydrates within the sediments, contributing to enhanced methane release from the seafloor during the deglaciation. The BWT reconstruction from this work is useful for studies targeting ice-sheet modelling in the western Barents Sea.

3.3 Paper III

El bani Altuna, N., Ezat, M.M., Smik, L., Muschitiello, F., Belt, S.T., Knies, J., Rasmussen, T.L. **Sea ice and Atlantic water coupling during Heinrich Stadials in the northern Nordic Seas during the last glacial period 63-13 ka.** In preparation for submission to *Science Advances*.

Although DO-events have been intensively studied, the mechanisms leading to the abrupt warming at the onset of interstadials is still debated (e.g., Gildor & Tziperman, 2003; Li et al., 2010; Li & Born, 2019). Arctic sea-ice variability is widely thought to be a key component of ocean-atmosphere feedbacks at the time of abrupt climate oscillations, but what drove changes in sea-ice cover is still poorly understood. Sea ice acts as a lid, limiting ocean-atmosphere exchanges, and is sensitive to changes in both the atmosphere and the ocean. The aim of this work was to investigate the millennial-scale relationship between BWT and variability in sea ice cover during MIS 3 and 2 on the western Svalbard slope (core HH15-1252PC), using benthic foraminiferal Mg/Ca (**Paper I**) and molecular biomarkers (IP$_{25}$, HBI III and calculated sea-ice indicators).

Our record shows generally open-ocean conditions during warm interstadials and extensive sea-ice cover during cold stadials. Previously reported bottom water warmings (up to 5°C) during stadials, specially during Heinrich Stadials, occur when extensive sea-ice layers covered the Nordic Seas, preventing the loss of heat from the warm subsurface Atlantic water layer. The stacking of sea-ice records and BWT during HS reveals a strong link between the new sea-ice biomarker distribution and BWT, with rapid reductions in the spring sea-ice cover and the retreat of sea ice or opening of the surface ocean (increase of HBI III) occurring synchronously with the decrease in BWT within stadials. This strong coupling highlights the role of BWT in controlling the sea-ice cover in the Nordic Seas at sub-millennial timescales, and likely in the dynamics of the GS-GI transitions.

3.4 Author contributions

The manuscripts presented in this thesis are the result of a collaborative work with colleagues from many national and international institutions. The roles of various contributors are summarized in Table 2.

Table 2. Author contributions to each manuscript is listed by the degree of involvement. The contributor roles have been defined following the CRediT criteria (https://casrai.org/credit/) and adapted for this table. *Supervision. [1]Early versions of the manuscript. FM=Francesco Muschitiello; HP=Henry Patton; JG=Jeroen Groeneveld; JK=Jochen Knies; LS=Lukas Smik; MME=Mohamed M. Ezat; MG=Mervyn Greaves; NEA=Naima El bani Altuna; SB=Simon Belt; SV=Sunil Vadakkepuliyambatta; TLR=Tine Lander Rasmussen.

	Paper I	Paper II	Paper III
Conceptualization	MME, TLR, NEA,	TLR, NEA, MME, SV, HP	NEA, MME, TLR, LS, SB
Funding acquisition	TLR, MME, NEA	TLR, MME	JK, SB, TLR, MME
Study design and methodology	NEA, MME, TLR	NEA, MME, TLR, SV, JG	NEA, LS, MME, SB, TLR
Data gathering	NEA, MME*, MG*, TLR*	NEA, MME*, MJ*, TLR*, SV	NEA, LS, MME*, SB*
Modelling/Statistical analysis	-	SV	FM, NEA
Interpretation	NEA, MME, TLR	NEA, MME, SV, TLR	NEA, MME, TLR, LS, FM
Visualization	NEA	NEA	NEA
Writing – original draft	NEA	NEA	NEA
Writing – review and editing	NEA, TLR, MME, MG	NEA, TLR, MME, SV, MG, JG, HP[1]	NEA, MME, TLR, FM, LS, SB, JK

4 Concluding remarks and future work

Prior to the completion of this thesis, no benthic foraminiferal Mg/Ca-derived BWT records existed at the high latitudes of our study sites and at a resolution that allowed resolving the temporal variability of AW inflow at the level of millennial-scale climate oscillations. The works presented in this PhD provide temperature reconstructions from two sites at shallow and intermediate water depths that are coherent with each other (both cores showing a considerable warming of up to 5°C during HS1; Figure 6) and with records previously published in the southern Nordic Seas (Ezat et al., 2014; Sessford et al., 2019). Our work demonstrates the
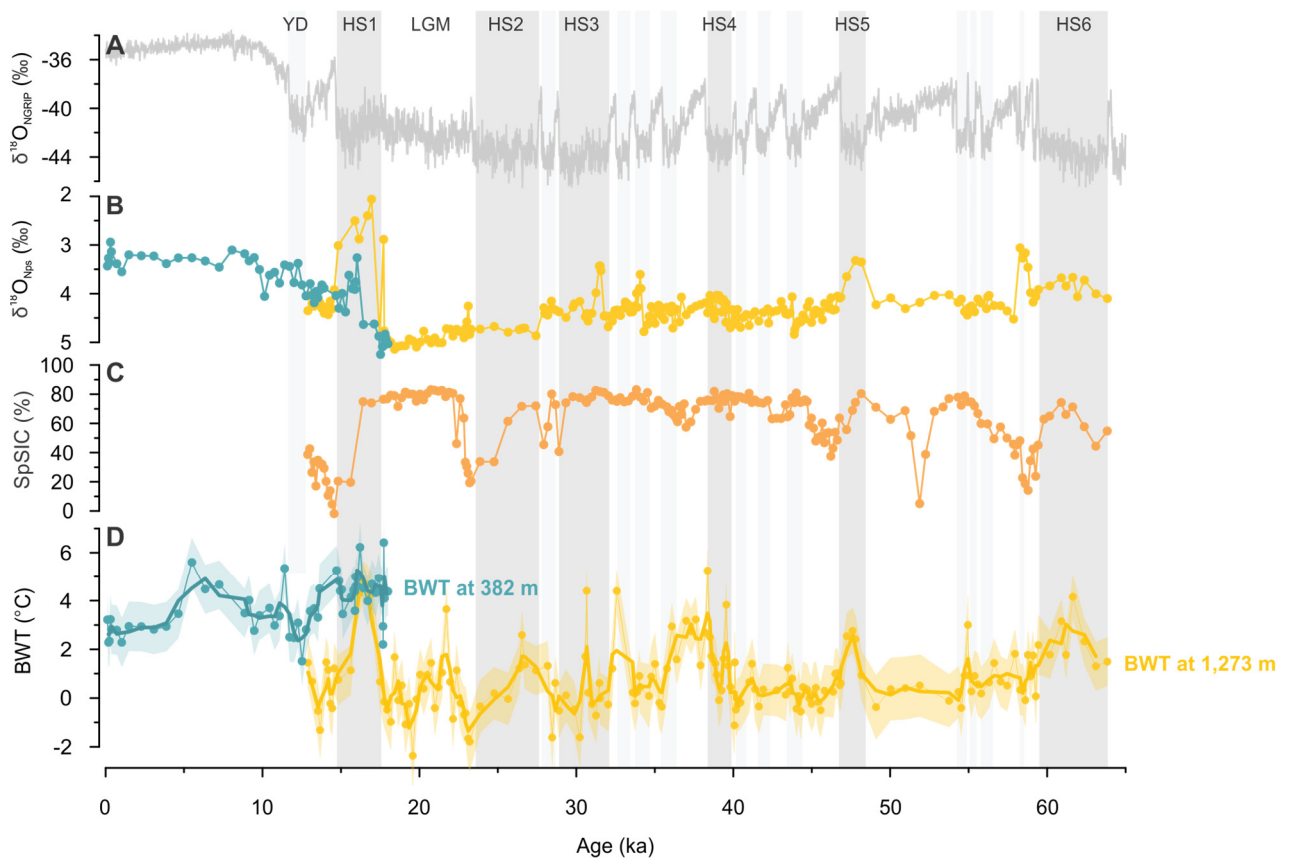
Figure 6. Evolution of bottom water temperature (BWT) in Vestnesa Ridge (yellow) and Storfjordrenna (blue) (**D**), relative spring sea-ice concentration (SpSIC) in Vestnesa Ridge (**C**) and planktic foraminifera *Neogloboquadrina pachyderma* (Nps) δ^{18}O (**B**) since 65 ka. The records are plotted with δ^{18}O record from the North Greenland Ice Project (NGRIP) ice core at the GICC05modelext timescale (**A**) (Svensson et al., 2008; Wolff et al., 2010; S. O. Rasmussen et al., 2014). Note that the age-depth models of core HH15-1252PC (yellow) and HH18-1059GC (blue) are not built using the same approach (see section 2.3. and further details in **Paper I** and **II**) and therefore the comparison of both records is not straightforward and needs to be done with caution. Heinrich stadials (HS) are marked with dark gray bars and other stadials are shown with light gray bars. Abbreviations: LGM=Last Glacial Maximum; YD=Younger Dryas.

inherent (causal?) linkage between sea ice and AW inflow (characterized by its temperature) during the last glacial period and potentially the important role of these two parameters shaping DO-events (**Paper I** and **III**). Furthermore, the results in the 'Pingo area' in Storfjordrenna reveal the key role of BWT modulating the dynamics of the GHSZ and dissociation of gas hydrates (**Paper II**). The promising results presented in this thesis highlight the importance of generating BWT records and studying its impacts on the carbon cycle (e.g., the effect of BWT in the release of sub-seafloor methane) and its paleoceanographic and paleoclimatic implications in the Arctic region.

4.1 Future work

4.1.1 Improvement of Mg/Ca and other bottom water temperature proxies

Mg/Ca-based temperature estimations are by far one of the best tools to reconstruct past oceanic temperatures. Nevertheless, elemental analysis techniques by dissolution of bulk foraminiferal samples require generally large amount of pristine foraminiferal tests, which can be challenging in Arctic sediments. In order to improve BWT reconstructions in cold Arctic waters further understanding of the local seawater chemistry could help assessing the non-thermal component (e.g., effect of salinity and the carbonate ion saturation effect) of benthic foraminiferal Mg/Ca.

In methane hydrate-bearing sediments, where reconstructing BWT is of major interest, diagenetic overprinting can impede temperature reconstructions using Mg/Ca of benthic foraminifera. Laser ablation ICP-MS techniques consist of measuring a spot in a foraminiferal test, which can help assess the intra-test trace element variability of single foraminifera. It can also be helpful in evaluating the diagenetic overprints of the primary calcite, allowing for the distinction between primary and authigenic calcite (Nairn, 2019; Detlef et al., 2020). This can be very useful when reconstructing BWT in methane-bearing sediments.

Another traditionally used paleo-BWT proxy is transfer functions using benthic foraminiferal faunal assemblage composition (e.g., T. L. Rasmussen et al., 2007, 2014, 2016; Chauhan et al., 2014, 2014; T. L. Rasmussen & Thomsen, 2017). In this method, a measured environmental variable is associated to the relative abundance of a given species in modern samples, and this dataset is then compared to the proportion of the same species in the

paleorecord to statistically quantify a given environmental parameter downcore; here BWT. This method is therefore highly dependent on the robustness on the modern dataset, the fossil record, and that the foraminiferal species in the assemblages respond to temperature before other factors.

Currently, Arctic benthic foraminiferal databases are restricted to the Barents Sea and Kara Sea (Sejrup et al., 2004; Saher et al., 2009), but do not cover intermediate and deep sites in the Nordic Seas, complicating the use of benthic foraminiferal transfer functions beyond the continental shelf. In order to improve and extend existing databases and generate a broad Arctic benthic foraminiferal database, joint collaborative efforts are needed to include modern foraminiferal samples from the entire Arctic region and to resolve taxonomic discrepancies of morphologically similar species that can be misidentified and grouped together as a single species. This new dataset should also include a broader set of environmental variables that would allow, for example, for the reconstruction of paleoproductivity in order to better understand past changes in the carbon cycle.

4.1.2 Bottom water temperature records in gas hydrate systems

The BWT record from the 'Pingo area' in Storfjordrenna, presented in **Paper II**, highlights the importance of generating long-term temperature records in areas with seafloor gas hydrate release in order to obtain a more comprehensive understanding of the dynamics of gas hydrate systems. We showed a sequence of events in a relatively shallow site where increased BWT triggered the outcropping of the GHSZ, causing the dissociation of gas hydrates and potential release of gas to the water column. This is of great interest for warming Arctic waters that host vast amounts of gas hydrates in the seafloor, and to improve our knowledge of the past carbon cycle.

The next natural step of this thesis would be to perform a similar 'model-data' investigation at Vestnesa Ridge, a gas hydrate system located at an intermediate water depth. This was not done in the present work as shallow gas hydrate systems (e.g. 'Pingo area' in Storfjordrenna) are recognized to be more sensitive than deeper locations to changes in BWT (Biastoch et al., 2011). Although pressure-related changes are thought to be the dominating factor controlling gas hydrate dissociation in Vestnesa Ridge (e.g., Plaza-Faverola et al., 2015), the BWT variations observed during HS in our record can cause changes to the base of the GHSZ

(Vadakkepuliyambatta et al., *in prep*) and, eventually, the subsequent release of gas to the water column (T.L. Rasmussen et al., *in prep*) also at this intermediate water depth site.

4.1.3   Ocean-cryosphere interactions

Interactions between the ocean and the cryosphere play a very important role in modern and past climate systems. This is highlighted by the results found in **Paper III**, where we observe a clear co-variability between subsurface warming and sea ice at times of abrupt climate change. Subsurface oceanic warming can trigger the retreat of sea ice, but has also potentially affected other components of the marine cryosphere, such as marine based ice sheets and marine terminating glaciers.

Today, subsurface warming is causing the retreat of ice sheets and marine terminating glaciers in specific sectors of the West Antarctic Ice Sheet (WAIS) (e.g., Khazendar et al., 2016) and in the Greenland Ice Sheet (e.g., Straneo & Heimbach, 2013). Periods with persistent subsurface warming can trigger the retreat of the grounding zone, affecting the stability of the ice sheet and accelerating its retreat (e.g., Bindschadler, 2006). The SBIS is a good analogue for the WAIS since both ice sheets are marine based (Andreassen & Winsborrow, 2009) and the western Barents Sea, where the grounding zone was located during the last glacial period, is a key area to study the relationship between the inflow of Atlantic water and the retreat of the BSIS. In this sense, our BWT is a great tool for ice sheet modelers.

Further paleo-BWT reconstructions in the western Barents Sea could potentially explain the dissimilarities in the timing of the retreat of the southwestern (Bjørnøyrenna) and northwestern (Storfjordrenna) sectors of the SBIS (Hughes et al., 2016). It has been postulated that subsurface warming controls the retreat of the west sector of the Greenland Ice Sheet since the last glacial period (Laberg et al., 2017), although this area is covered by only a few works. Foraminiferal studies and good chronological constraints from marine core records are needed to assess the impact of warm subsurface waters in the area.

Foraminiferal elemental analyses can help investigating other phenomena related to ocean-cryosphere interactions. Recent studies have suggested that salinity is the principal factor controlling the foraminiferal Na/Ca signal (Wit et al., 2013; Allen et al., 2016; Mezger et al., 2016; Bertlich et al., 2018). Although this seawater salinity proxy is still under development, if successful it can be a promising tool, in combination with benthic and planktic foraminiferal

Mg/Ca and $\delta^{18}O$, to trace large meltwater events associated with a the retreat of continental ice sheets and marine terminating glaciers.

5 References

Aagaard, K., Foldvik, A., & Hillman, S. R. (1987). The West Spitsbergen Current: Disposition and water mass transformation. *Journal of Geophysical Research*, *92*(C4), 3778–3784. https://doi.org/10.1029/JC092iC04p03778

Aagaard-Sørensen, S., Husum, K., Hald, M., Marchitto, T., & Godtliebsen, F. (2014). Sub sea surface temperatures in the Polar North Atlantic during the Holocene: Planktic foraminiferal Mg/Ca temperature reconstructions. *The Holocene*, *24*(1), 93–103. https://doi.org/10.1177/0959683613515730

Abbott, P. M., Griggs, A. J., Bourne, A. J., Chapman, M. R., & Davies, S. M. (2018). Tracing marine cryptotephras in the North Atlantic during the last glacial period: Improving the North Atlantic marine tephrostratigraphic framework. *Quaternary Science Reviews*, *189*, 169–186. https://doi.org/10.1016/j.quascirev.2018.03.023

Allen, K. A., Hönisch, B., Eggins, S. M., Haynes, L. L., Rosenthal, Y., & Yu, J. (2016). Trace element proxies for surface ocean conditions: A synthesis of culture calibrations with planktic foraminifera. *Geochimica et Cosmochimica Acta*, *193*, 197–221. https://doi.org/10.1016/j.gca.2016.08.015

Andersen, K. K., Svensson, A., Johnsen, S. J., Rasmussen, S. O., Bigler, M., Röthlisberger, R., Ruth, U., Siggaard-Andersen, M.-L., Peder Steffensen, J., & Dahl-Jensen, D. (2006). The Greenland Ice Core Chronology 2005, 15–42ka. Part 1: Constructing the time scale. *Quaternary Science Reviews*, *25*(23–24), 3246–3257. https://doi.org/10.1016/j.quascirev.2006.08.002

Andreassen, K., & Winsborrow, M. (2009). Signature of ice streaming in Bjørnøyrenna, Polar North Atlantic, through the Pleistocene and implications for ice-stream dynamics. *Annals of Glaciology*, *50*(52), 17–26. https://doi.org/10.3189/172756409789624238

Andreassen, K., Hubbard, A., Winsborrow, M., Patton, H., Vadakkepuliyambatta, S., Plaza-Faverola, A., Gudlaugsson, E., Serov, P., Deryabin, A., & Mattingsdal, R. (2017). Massive blow-out craters formed by hydrate-controlled methane expulsion from the Arctic seafloor. *Science*, *356*(6341), 948–953. https://doi.org/10.1126/science.aal4500

Årthun, M., Eldevik, T., Smedsrud, L. H., Skagseth, Ø., & Ingvaldsen, R. B. (2012). Quantifying the Influence of Atlantic Heat on Barents Sea Ice Variability and Retreat. *Journal of Climate*, *25*(13), 4736–4743. https://doi.org/10.1175/JCLI-D-11-00466.1

Austin, W. E. N., & Hibbert, F. D. (2012). Tracing time in the ocean: A brief review of chronological constraints (60–8 kyr) on North Atlantic marine event-based stratigraphies. *Quaternary Science Reviews*, *36*, 28–37. https://doi.org/10.1016/j.quascirev.2012.01.015

Barker, S., Cacho, I., Benway, H., & Tachikawa, K. (2005). Planktonic foraminiferal Mg/Ca as a proxy for past oceanic temperatures: A methodological overview and data compilation for the Last Glacial Maximum. *Quaternary Science Reviews*, *24*(7–9), 821–834. https://doi.org/10.1016/j.quascirev.2004.07.016

Barker, S., Greaves, M., & Elderfield, H. (2003). A study of cleaning procedures used for foraminiferal Mg/Ca paleothermometry. *Geochemistry, Geophysics, Geosystems*, *4*(9), 8407. https://doi.org/10.1029/2003GC000559

Barrientos, N., Lear, C. H., Jakobsson, M., Stranne, C., O'Regan, M., Cronin, T. M., Gukov, A. Y., & Coxall, H. K. (2018). Arctic Ocean benthic foraminifera Mg/Ca ratios and global Mg/Ca-temperature calibrations: New constraints at low temperatures. *Geochimica et Cosmochimica Acta*, *236*, 240–259. https://doi.org/10.1016/j.gca.2018.02.036

Belanger, P. E., & Streeter, S. S. (1980). Distribution and ecology of benthic foraminifera in the Norwegian-Greenland Sea. *Marine Micropaleontology*, *5*, 401–428. https://doi.org/10.1016/0377-8398(80)90020-1

Belt, S. T., Massé, G., Rowland, S. J., Poulin, M., Michel, C., & LeBlanc, B. (2007). A novel chemical fossil of palaeo sea ice: IP$_{25}$. *Organic Geochemistry*, *38*(1), 16–27. https://doi.org/10.1016/j.orggeochem.2006.09.013

Belt, S. T., & Müller, J. (2013). The Arctic sea ice biomarker IP$_{25}$: A review of current understanding, recommendations for future research and applications in palaeo sea ice reconstructions. *Quaternary Science Reviews*, *79*, 9–25. https://doi.org/10.1016/j.quascirev.2012.12.001

Belt, S. T., Cabedo-Sanz, P., Smik, L., Navarro-Rodriguez, A., Berben, S. M. P., Knies, J., & Husum, K. (2015). Identification of paleo Arctic winter sea ice limits and the marginal ice zone: Optimised biomarker-based reconstructions of late Quaternary Arctic sea ice. *Earth and Planetary Science Letters*, *431*, 127–139. https://doi.org/10.1016/j.epsl.2015.09.020

Belt, S. T., Smik, L., Köseoğlu, D., Knies, J., & Husum, K. (2019). A novel biomarker-based proxy for the spring phytoplankton bloom in Arctic and sub-arctic settings – HBI T$_{25}$. *Earth and Planetary Science Letters*, *523*, 115703. https://doi.org/10.1016/j.epsl.2019.06.038

Berndt, C., Feseker, T., Treude, T., Krastel, S., Liebetrau, V., Niemann, H., Bertics, V. J., Dumke, I., Dunnbier, K., Ferre, B., Graves, C., Gross, F., Hissmann, K., Huhnerbach, V., Krause, S., Lieser, K., Schauer, J., & Steinle, L. (2014). Temporal Constraints on Hydrate-Controlled Methane Seepage off Svalbard. *Science*, *343*(6168), 284–287. https://doi.org/10.1126/science.1246298

Bertlich, J., Nürnberg, D., Hathorne, E. C., de Nooijer, L. J., Mezger, E. M., Kienast, M., Nordhausen, S., Reichart, G.-J., Schönfeld, J., & Bijma, J. (2018). Salinity control on Na incorporation into calcite tests of the planktonic foraminifera *Trilobatus sacculifer* – Evidence from culture experiments and surface sediments. *Biogeosciences*, *15*, 5991–6018. https://doi.org/10.5194/bg-15-5991-2018

Biastoch, A., Treude, T., Rüpke, L. H., Riebesell, U., Roth, C., Burwicz, E. B., Park, W., Latif, M., Böning, C. W., Madec, G., & Wallmann, K. (2011). Rising Arctic Ocean temperatures cause gas hydrate destabilization and ocean acidification. *Geophysical Research Letters*, *38*(8). https://doi.org/10.1029/2011GL047222

Bindschadler, R. (2006). Hitting the Ice Sheets Where It Hurts. *Science*, *311*(5768), 1720–1721. https://doi.org/10.1126/science.1125226

Bock, M., Schmitt, J., Moller, L., Spahni, R., Blunier, T., & Fischer, H. (2010). Hydrogen Isotopes Preclude Marine Hydrate CH4 Emissions at the Onset of Dansgaard-Oeschger Events. *Science*, *328*(5986), 1686–1689. https://doi.org/10.1126/science.1187651

Bond, G., Broecker, W., Johnsen, S., McManus, J., Labeyrie, L., Jouzel, J., & Bonani, G. (1993). Correlations between climate records from North Atlantic sediments and Greenland ice. *Nature*, *365*(6442), 143–147. https://doi.org/10.1038/365143a0

Bourke, R. H., Weigel, A. M., & Paquette, R. G. (1988). The westward turning branch of the West Spitsbergen Current. *Journal of Geophysical Research*, *93*(C11), 14065–14077. https://doi.org/10.1029/JC093iC11p14065

Boyer, T. P., Baranova, O. K., Coleman, C., Garcia, H. E., Grodsky, A., Locarnini, R. A., Mishonov, A. V., Paver, C. R., Reagan, J. R., Seidov, D., Smolyar, I. V., Weathers, K. W., & Zweng, M. M. (2018). World Ocean Database 2018. *NOAA Atlas NESDIS 87*, 207.

Boyle, E. A. (1981). Cadmium, zinc, copper, and barium in foraminifera tests. *Earth and Planetary Science Letters*, *53*(1), 11–35. https://doi.org/10.1016/0012-821X(81)90022-4

Boyle, E. A. (1983). Manganese carbonate overgrowths on foraminifera tests. *Geochimica et Cosmochimica Acta*, *47*(10), 1815–1819. https://doi.org/10.1016/0016-7037(83)90029-7

Boyle, E. A., & Keigwin, L. D. (1985). Comparison of Atlantic and Pacific paleochemical records for the last 215,000 years: Changes in deep ocean circulation and chemical inventories. *Earth and Planetary Science Letters*, *76*(1–2), 135–150. https://doi.org/10.1016/0012-821X(85)90154-2

Brendryen, J., Haflidason, H., Yokoyama, Y., Haaga, K. A., & Hannisdal, B. (2020). Eurasian Ice Sheet collapse was a major source of Meltwater Pulse 1A 14,600 years ago. *Nature Geoscience*, *13*(5), 363–368. https://doi.org/10.1038/s41561-020-0567-4

Broecker, W. S., Peteet, D. M., & Rind, D. (1985). Does the ocean–atmosphere system have more than one stable mode of operation? *Nature*, *315*(6014), 21–26. https://doi.org/10.1038/315021a0

Brook, E. J., Sowers, T., & Orchardo, J. (1996). Rapid Variations in Atmospheric Methane Concentration During the Past 110,000 Years. *Science*, *273*(5278), 1087–1091. https://doi.org/10.1126/science.273.5278.1087

Brown, T. A., Belt, S. T., Philippe, B., Mundy, C. J., Massé, G., Poulin, M., & Gosselin, M. (2011). Temporal and vertical variations of lipid biomarkers during a bottom ice diatom bloom in the Canadian Beaufort Sea: Further evidence for the use of the IP_{25} biomarker as a proxy for spring Arctic sea ice. *Polar Biology*, *34*(12), 1857–1868. https://doi.org/10.1007/s00300-010-0942-5

Bünz, S., Polyanov, S., Vadakkepuliyambatta, S., Consolaro, C., & Mienert, J. (2012). Active gas venting through hydrate-bearing sediments on the Vestnesa Ridge, offshore W-

Svalbard. *Marine Geology*, *332–334*, 189–197. https://doi.org/10.1016/j.margeo.2012.09.012

Cage, A. G., Pieńkowski, A. J., Jennings, A., Knudsen, K. L., & Seidenkrantz, M.-S. (2021). Comparative analysis of six common foraminiferal species of the genera *Cassidulina*, *Paracassidulina* and *Islandiella* from the Arctic–North Atlantic domain. *Journal of Micropalaeontology*, *40*(1), 37–60. https://doi.org/10.5194/jm-40-37-2021

Carstens, J., Hebbeln, D., & Wefer, G. (1997). Distribution of planktic foraminifera at the ice margin in the Arctic (Fram Strait). *Marine Micropaleontology*, *29*(3–4), 257–269.

Chafik, L., & Rossby, T. (2019). Volume, Heat, and Freshwater Divergences in the Subpolar North Atlantic Suggest the Nordic Seas as Key to the State of the Meridional Overturning Circulation. *Geophysical Research Letters*, *46*, 4799–4808. https://doi.org/10.1029/ 2019GL082110

Chauhan, T., Rasmussen, T. L., Noormets, R., Jakobsson, M., & Hogan, K. A. (2014). Glacial history and paleoceanography of the southern Yermak Plateau since 132 ka BP. *Quaternary Science Reviews*, *92*, 155–169. https://doi.org/10.1016/j.quascirev.2013.10.023

Collett, T. S., Johnson, A. H., Knapp, C. C., & Boswell, R. (2009). Natural Gas Hydrates: A Review. In T. S. Collett, A. H. Johnson, C. C. Knapp, & R. Boswell (Eds.), *Natural gas hydrates—Energy resource potential and associated geologic hazards* (Vol. 89, pp. 146–219).

Consolaro, C., Rasmussen, T. L., Panieri, G., Mienert, J., Bünz, S., & Sztybor, K. (2015). Carbon isotope (δ^{13}C) excursions suggest times of major methane release during the last 14 kyr in Fram Strait, the deep-water gateway to the Arctic. *Climate of the Past*, *11*(4), 669–685. https://doi.org/10.5194/cp-11-669-2015

Crémière, A., Lepland, A., Chand, S., Sahy, D., Condon, D. J., Noble, S. R., Martma, T., Thorsnes, T., Sauer, S., & Brunstad, H. (2016). Timescales of methane seepage on the Norwegian margin following collapse of the Scandinavian Ice Sheet. *Nature Communications*, *7*, 11509. https://doi.org/10.1038/ncomms11509

Curry, W. B., Duplessy, J. C., Labeyrie, L. D., & Shackleton, N. J. (1988). Changes in the distribution of δ^{13}C of deep water ΣCO_2 between the Last Glaciation and the Holocene. *Paleoceanography*, *3*(3), 317–341. https://doi.org/10.1029/PA003i003p00317

Curry, W. B., & Oppo, D. W. (2005). Glacial water mass geometry and the distribution of δ^{13}C of ΣCO_2 in the western Atlantic Ocean. *Paleoceanography*, *20*(1), PA1017. https://doi.org/10.1029/2004PA001021

Dansgaard, W., Clausen, H. B., Gundestrup, N. S., Hammer, C. U., Johnsen, S. F., Kristinsdottir, P. M., & Reech, N. (1982). A New Greenland Deep Ice Core. *Science*, *218*(4579), 6. https://doi.org/10.1126/science.218.4579.1273

Dansgaard, W., Johnsen, S. J., Clausen, H. B., Dahl-Jensen, D., Gundestrup, N. S., Hammer, C. U., Hvidberg, C. S., Steffensen, J. P., Sveinbjörnsdottir, A. E., Jouzel, J., & Bond, G. (1993). Evidence for general instability of past climate from a 250-kyr ice-core record. *Nature*, *364*, 218–220.

de Vernal, A., Hillaire-Marcel, C., Rochon, A., Fréchette, B., Henry, M., Solignac, S., & Bonnet, S. (2013). Dinocyst-based reconstructions of sea ice cover concentration during the Holocene in the Arctic Ocean, the northern North Atlantic Ocean and its adjacent seas. *Quaternary Science Reviews*, *79*, 111–121. https://doi.org/10.1016/j.quascirev.2013.07.006

de Villiers, S., Greaves, M., & Elderfield, H. (2002). An intensity ratio calibration method for the accurate determination of Mg/Ca and Sr/Ca of marine carbonates by ICP-AES. *Geochemistry, Geophysics, Geosystems*, *3*(1). https://doi.org/10.1029/2001GC000169

de Vries, H. (1958). Variations in concentration of radiocarbon with time and location on Earth. *Koninklijke Nederlandse Akademie van Wetenschappen*, *61*, 94–102. https://doi.org/10.1017/S1061592X00020548

Dekens, P. S., Lea, D. W., Pak, D. K., & Spero, H. J. (2002). Core top calibration of Mg/Ca in tropical foraminifera: Refining paleotemperature estimation. *Geochemistry, Geophysics, Geosystems*, *3*(4), 1–29. https://doi.org/10.1029/2001GC000200

Dessandier, P.-A., Borrelli, C., Yao, H., Sauer, S., Hong, W.-L., & Panieri, G. (2020). Foraminiferal $\delta^{18}O$ reveals gas hydrate dissociation in Arctic and North Atlantic ocean sediments. *Geo-Marine Letters*, *40*, 507–523. https://doi.org/10.1007/s00367-019-00635-6

Dessandier, P.-A., Knies, J., Plaza-Faverola, A., Labrousse, C., Renoult, M., & Panieri, G. (2021). Ice-sheet melt drove methane emissions in the Arctic during the last two interglacials. *Geology*, *49*. https://doi.org/10.1130/G48580.1

Detlef, H., Sosdian, S. M., Kender, S., Lear, C. H., & Hall, I. R. (2020). Multi-elemental composition of authigenic carbonates in benthic foraminifera from the eastern Bering Sea continental margin (International Ocean Discovery Program Site U1343). *Geochimica et Cosmochimica Acta*, *268*, 1–21. https://doi.org/10.1016/j.gca.2019.09.025

Dickens, G. R., O'Neil, J. R., Rea, D. K., & Owen, R. M. (1995). Dissociation of oceanic methane hydrate as a cause of the carbon isotope excursion at the end of the Paleocene. *Paleoceanography*, *10*(6), 965–971. https://doi.org/10.1029/95PA02087

Dickson, R. R., & Brown, J. (1994). The production of North Atlantic Deep Water: Sources, rates, and pathways. *Journal of Geophysical Research*, *99*, 12319–12341. https://doi.org/10.1029/94JC00530

Dowdeswell, J. A., & Dowdeswell, E. K. (1989). Debris in Icebergs and Rates of Glaci-Marine Sedimentation: Observations from Spitsbergen and a Simple Model. *The Journal of Geology*, *97*(2), 221–231. https://doi.org/10.1086/629296

Dunkley Jones, T., Lunt, D. J., Schmidt, D. N., Ridgwell, A., Sluijs, A., Valdes, P. J., & Maslin, M. (2013). Climate model and proxy data constraints on ocean warming across the Paleocene–Eocene Thermal Maximum. *Earth-Science Reviews*, *125*, 123–145. https://doi.org/10.1016/j.earscirev.2013.07.004

Duplessy, J. C., Lalou, C., & Vinot, A. C. (1970). Differential Isotopic Fractionation in Benthic Foraminifera and Paleotemperatures Reassessed. *Science*, *168*(3928), 250–251. https://doi.org/10.1126/science.168.3928.250

Duplessy, J. C., Moyes, J., & Pujol, C. (1980). Deep water formation in the North Atlantic Ocean during the last ice age. *Nature*, *286*(5772), 479.

El bani Altuna, N., Pieńkowski, A. J., Eynaud, F., & Thiessen, R. (2018). The morphotypes of *Neogloboquadrina pachyderma*: Isotopic signature and distribution patterns in the Canadian Arctic Archipelago and adjacent regions. *Marine Micropaleontology*, *142*, 13–24. https://doi.org/10.1016/j.marmicro.2018.05.004

Elderfield, H., Ferretti, P., Greaves, M., Crowhurst, S., McCave, I. N., Hodell, D. A., & Piotrowski, A. M. (2012). Evolution of ocean temperature and ice volume through the mid-Pleistocene climate transition. *Science*, *337*(6095), 704–709. https://doi.org/10.1126/science.1221294

Emiliani, C. (1955). Pleistocene Temperatures. *The Journal of Geology*, *63*(6), 538–578. https://doi.org/10.2307/30080906

EPICA Community Members. (2006). One-to-one coupling of glacial climate variability in Greenland and Antarctica. *Nature*, *444*(7116), 195–198. https://doi.org/10.1038/nature05301

Epstein, S., Buchsbaum, R., Lowenstam, H. A., & Urey, H. C. (1953). Revised carbonate-water isotopic temperature scale. *Bulletin of the Geological Society of America*, *64*, 1315–1326. https://doi.org/10.1130/0016-7606(1953)64[1315:RCITS]2.0.CO;2

Ezat, M. M., Rasmussen, T. L., & Groeneveld, J. (2014). Persistent intermediate water warming during cold stadials in the southeastern Nordic seas during the past 65 k.y. *Geology*, *42*(8), 663–666. https://doi.org/10.1130/G35579.1

Ezat, M. M., Rasmussen, T. L., & Groeneveld, J. (2016). Reconstruction of hydrographic changes in the southern Norwegian Sea during the past 135 kyr and the impact of different foraminiferal Mg/Ca cleaning protocols. *Geochemistry, Geophysics, Geosystems*, *17*(8), 3420–3436. https://doi.org/10.1002/2016GC006325

Ezat, M. M., Rasmussen, T. L., Thornalley, D. J. R., Olsen, J., Skinner, L. C., Hönisch, B., & Groeneveld, J. (2017). Ventilation history of Nordic Seas overflows during the last (de)glacial period revealed by species-specific benthic foraminiferal ^{14}C dates: Glacial Circulation-Nordic Seas. *Paleoceanography*, *32*(2), 172–181. https://doi.org/10.1002/2016PA003053

Fer, I., Skogseth, R., Haugan, P. M., & Jaccard, P. (2003). Observations of the Storfjorden overflow. *Deep Sea Research Part I*, *50*, 1283–1303. https://doi.org/10.1016/S0967-0637(03)00124-9

Ferguson, J. E., Henderson, G. M., Kucera, M., & Rickaby, R. E. M. (2008). Systematic change of foraminiferal Mg/Ca ratios across a strong salinity gradient. *Earth and Planetary Science Letters*, *265*(1–2), 153–166. https://doi.org/10.1016/j.epsl.2007.10.011

Ferré, B., Mienert, J., & Feseker, T. (2012). Ocean temperature variability for the past 60 years on the Norwegian-Svalbard margin influences gas hydrate stability on human time scales. *Journal of Geophysical Research: Oceans*, *117*, C10017. https://doi.org/10.1029/2012JC008300

Ferré, B., Jansson, P. G., Moser, M., Serov, P., Portnov, A., Graves, C. A., Panieri, G., Gründger, F., Berndt, C., Lehmann, M. F., & Niemann, H. (2020). Reduced methane

seepage from Arctic sediments during cold bottom-water conditions. *Nature Geoscience*, *13*(2), 144–148. https://doi.org/10.1038/s41561-019-0515-3

Forman, S. L., & Polyak, L. (1997). Radiocarbon content of pre-bomb marine mollusks and variations in the [14]C Reservoir age for coastal areas of the Barents and Kara Seas, Russia. *Geophysical Research Letters*, *24*(8), 885–888. https://doi.org/10.1029/97GL00761

Ganopolski, A., & Rahmstorf, S. (2001). Rapid changes of glacial climate simulated in a coupled climate model. *Nature*, *409*(6817), 153–158. https://doi.org/10.1038/35051500

Gascard, J.-C., Richez, C., & Rouault, C. (1995). New insights on large-scale oceanography in Fram Strait: The West Spitsbergen Current. In W. O. Smith & J. M. Grebmeir (Eds.), *Coastal and Estuarine Studies* (Vol. 49, pp. 131–182). American Geophysical Union. https://doi.org/10.1029/CE049p0131

Gildor, H., & Tziperman, E. (2003). Sea-ice switches and abrupt climate change. *Philosophical Transactions of the Royal Society of London. Series A: Mathematical, Physical and Engineering Sciences*, *361*(1810), 1935–1944. https://doi.org/10.1098/rsta.2003.1244

Griggs, A. J., Davies, S. M., Abbott, P. M., Rasmussen, T. L., & Palmer, A. P. (2014). Optimising the use of marine tephrochronology in the North Atlantic: A detailed investigation of the Faroe Marine Ash Zones II, III and IV. *Quaternary Science Reviews*, *106*, 122–139. https://doi.org/10.1016/j.quascirev.2014.04.031

Hasenfratz, A. P., Martínez-García, A., Jaccard, S. L., Vance, D., Wälle, M., Greaves, M., & Haug, G. H. (2017). Determination of the Mg/Mn ratio in foraminiferal coatings: An approach to correct Mg/Ca temperatures for Mn-rich contaminant phases. *Earth and Planetary Science Letters*, *457*, 335–347. https://doi.org/10.1016/j.epsl.2016.10.004

Hays, J. D., Imbrie, J., & Shackleton, N. J. (1976). Variations in the Earth's Orbit: Pacemaker of the Ice Ages. *Science*, *194*(4270), 1121–1132. https://doi.org/10.1126/science.194.4270.1121

Heaton, T. J., Köhler, P., Butzin, M., Bard, E., Reimer, R. W., Austin, W. E. N., Bronk Ramsey, C., Grootes, P. M., Hughen, K. A., Kromer, B., Reimer, P. J., Adkins, J., Burke, A., Cook, M. S., Olsen, J., & Skinner, L. C. (2020). Marine20–The marine radiocarbon age calibration curve (0–55,000 cal BP). *Radiocarbon*, *62*(4), 779–820. https://doi.org/10.1017/RDC.2020.68

Hemming, S. R. (2004). Heinrich events: Massive late Pleistocene detritus layers of the North Atlantic and their global climate imprint. *Reviews of Geophysics*, *42*(1), RG1005. https://doi.org/10.1029/2003RG000128

Hill, T. M., Kennett, J. P., & Valentine, D. L. (2004). Isotopic evidence for the incorporation of methane-derived carbon into foraminifera from modern methane seeps, Hydrate Ridge, Northeast Pacific. *Geochimica et Cosmochimica Acta*, *68*(22), 4619–4627. https://doi.org/10.1016/j.gca.2004.07.012

Hillaire-Marcel, C., de Vernal, A., Polyak, L., & Darby, D. (2004). Size-dependent isotopic composition of planktic foraminifers from Chukchi Sea vs. NW Atlantic sediments—Implications for the Holocene paleoceanography of the western Arctic. *Quaternary Science Reviews*, *23*(3–4), 245–260. https://doi.org/10.1016/j.quascirev.2003.08.006

Himmler, T., Sahy, D., Martma, T., Bohrmann, G., Plaza-Faverola, A., Bünz, S., Condon, D. J., Knies, J., & Lepland, A. (2019). A 160,000-year-old history of tectonically controlled methane seepage in the Arctic. *Science Advances*, *5*(8), eaaw1450. https://doi.org/10.1126/sciadv.aaw1450

Hoff, U., Rasmussen, T. L., Stein, R., Ezat, M. M., & Fahl, K. (2016). Sea ice and millennial-scale climate variability in the Nordic seas 90 kyr ago to present. *Nature Communications*, *7*, 12247. https://doi.org/10.1038/ncomms12247

Hönisch, B., Allen, K. A., Lea, D. W., Spero, H. J., Eggins, S. M., Arbuszewski, J., deMenocal, P., Rosenthal, Y., Russell, A. D., & Elderfield, H. (2013). The influence of salinity on Mg/Ca in planktic foraminifers – Evidence from cultures, core-top sediments and complementary δ^{18}O. *Geochimica et Cosmochimica Acta*, *121*, 196–213. https://doi.org/10.1016/j.gca.2013.07.028

Huber, C., Leuenberger, M., Spahni, R., Flückiger, J., Schwander, J., Stocker, T. F., Johnsen, S., Landais, A., & Jouzel, J. (2006). Isotope calibrated Greenland temperature record over Marine Isotope Stage 3 and its relation to CH4. *Earth and Planetary Science Letters*, *243*(3–4), 504–519. https://doi.org/10.1016/j.epsl.2006.01.002

Hughes, A. L. C., Gyllencreutz, R., Lohne, Ø. S., Mangerud, J., & Svendsen, J. I. (2016). The last Eurasian ice sheets—A chronological database and time-slice reconstruction, DATED-1. *Boreas*, *45*(1), 1–45. https://doi.org/10.1111/bor.12142

IPCC (2014). *Climate change 2014: Synthesis report* (R. K. Pachauri, L. Mayer, & Intergovernmental Panel on Climate Change, Eds.). Intergovernmental Panel on Climate Change.

Isachsen, P. E., Mauritzen, C., & Svendsen, H. (2007). Dense water formation in the Nordic Seas diagnosed from sea surface buoyancy fluxes. *Deep Sea Research Part I: Oceanographic Research Papers*, *54*(1), 22–41. https://doi.org/10.1016/j.dsr.2006.09.008

Jansen, E., Christensen, J. H., Dokken, T., Nisancioglu, K. H., Vinther, B. M., Capron, E., Guo, C., Jensen, M. F., Langen, P. L., Pedersen, R. A., Yang, S., Bentsen, M., Kjær, H. A., Sadatzki, H., Sessford, E., & Stendel, M. (2020). Past perspectives on the present era of abrupt Arctic climate change. *Nature Climate Change*, *10*(8), 714–721. https://doi.org/10.1038/s41558-020-0860-7

Jessen, S. P., Rasmussen, T. L., Nielsen, T., & Solheim, A. (2010). A new Late Weichselian and Holocene marine chronology for the western Svalbard slope 30,000–0 cal years BP. *Quaternary Science Reviews*, *29*(9–10), 1301–1312. https://doi.org/10.1016/j.quascirev.2010.02.020

Jessen, S. P., & Rasmussen, T. L. (2019). Ice-rafting patterns on the western Svalbard slope 74-0 ka: Interplay between ice-sheet activity, climate and ocean circulation. *Boreas*, *48*(1), 236–256. https://doi.org/10.1111/bor.12358

Johnsen, S. J., Clausen, H. B., Dansgaard, W., Fuhrer, K., Gundestrup, N., Hammer, C. U., Iversen, P., Jouzel, J., Stauffer, B., & steffensen, J. P. (1992). Irregular glacial interstadials recorded in a new Greenland ice core. *Nature*, *359*(6393), 311–313. https://doi.org/10.1038/359311a0

Jones, R. W. (2014). *Foraminifera and their applications* (R. W. Jones, Ed.). Cambridge University Press.

Karstens, J., Haflidason, H., Becker, L. W. M., Berndt, C., Rüpke, L., Planke, S., Liebetrau, V., Schmidt, M., & Mienert, J. (2018). Glacigenic sedimentation pulses triggered post-glacial gas hydrate dissociation. *Nature Communications*, *9*(1), 635. https://doi.org/10.1038/s41467-018-03043-z

Kennett, J. P., Cannariato, K. G., Hendy, I. L., & Behl, R. J. (2003). *Methane hydrates in Quaternary climate change: The clathrate gun hypothesis* (J. P. Kennett, K. G. Cannariato, I. L. Hendy, & R. J. Behl, Eds.). American Geophysical Union.

Khazendar, A., Rignot, E., Schroeder, D. M., Seroussi, H., Schodlok, M. P., Scheuchl, B., Mouginot, J., Sutterley, T. C., & Velicogna, I. (2016). Rapid submarine ice melting in the grounding zones of ice shelves in West Antarctica. *Nature Communications*, *7*(1), 13243. https://doi.org/10.1038/ncomms13243

Kindler, P., Guillevic, M., Baumgartner, M., Schwander, J., Landais, A., & Leuenberger, M. (2014). Temperature reconstruction from 10 to 120 kyr b2k from the NGRIP ice core. *Climate of the Past*, *10*, 887–902. https://doi.org/10.5194/cp-10-887-2014

Knutti, R., Flückiger, J., Stocker, T. F., & Timmermann, A. (2004). Strong hemispheric coupling of glacial climate through freshwater discharge and ocean circulation. *Nature*, *430*(7002), 851–856. https://doi.org/10.1038/nature02786

Kretschmer, K., Biastoch, A., Rüpke, L., & Burwicz, E. (2015). Modeling the fate of methane hydrates under global warming. *Global Biogeochemical Cycles*, *29*(5), 610–625. https://doi.org/10.1002/2014GB005011

Kristjánsdóttir, G. B., Lea, D. W., Jennings, A. E., Pak, D. K., & Belanger, C. (2007). New spatial Mg/Ca-temperature calibrations for three Arctic, benthic foraminifera and reconstruction of north Iceland shelf temperature for the past 4000 years. *Geochemistry, Geophysics, Geosystems*, *8*(3), Q03P21. https://doi.org/10.1029/2006GC001425

Laberg, J. S., Forwick, M., & Husum, K. (2017). New geophysical evidence for a revised maximum position of part of the NE sector of the Greenland ice sheet during the last glacial maximum. *Arktos*, *3*(1), 3. https://doi.org/10.1007/s41063-017-0029-4

Lea, D. W. (2002). Trace elements in foraminiferal calcite. In B. K. Sen Gupta (Ed.), *Modern Foraminifera* (pp. 259–277). Kluwer Academic Publishers.

Lelieveld, J., Crutzen, P. J., & Dentener, F. J. (1998). Changing concentration, lifetime and climate forcing of atmospheric methane. *Tellus B*, *50*(2), 128–150. https://doi.org/10.1034/j.1600-0889.1998.t01-1-00002.x

Li, C., Battisti, D. S., & Bitz, C. M. (2010). Can North Atlantic Sea Ice Anomalies Account for Dansgaard–Oeschger Climate Signals?*. *Journal of Climate*, *23*(20), 5457–5475. https://doi.org/10.1175/2010JCLI3409.1

Li, C., & Born, A. (2019). Coupled atmosphere-ice-ocean dynamics in Dansgaard-Oeschger events. *Quaternary Science Reviews*, *203*, 1–20. https://doi.org/10.1016/j.quascirev.2018.10.031

Libby, W. F. (1970). Radiocarbon Dating. *Philosophical Transactions of the Royal Society of London*, *269*(1193), 1–10. https://doi.org/10.1098/rsta.1970.0079

Loeng, H. (1991). Features of the physical oceanographic conditions of the Barents Sea. *Polar Research*, *10*, 5–18. https://doi.org/10.3402/polar.v10i1.6723

Lynch-Stieglitz, J. (2017). The Atlantic Meridional Overturning Circulation and Abrupt Climate Change. *Annual Review of Marine Science*, *9*(1), 83–104. https://doi.org/10.1146/annurev-marine-010816-060415

Lynch-Stieglitz, J., Adkins, J. F., Curry, W. B., Dokken, T., Hall, I. R., Herguera, J. C., Hirschi, J. J.-M., Ivanova, E. V., Kissel, C., Marchal, O., Marchitto, T. M., McCave, I. N., McManus, J. F., Mulitza, S., Ninnemann, U., Peeters, F., Yu, E.-F., & Zahn, R. (2007). Atlantic Meridional Overturning Circulation During the Last Glacial Maximum. *Science*, *316*(5821), 66–69. https://doi.org/10.1126/science.1137127

Mackensen, A., & Hald, M. (1988). *Cassidulina teretis* Tappan and *C. laevigata* D'Orbigny: Their modern and late Quaternary distribution in the Northern Seas. *Journal of Foraminiferal Research*, *18*(1), 16–24. https://doi.org/10.2113/gsjfr.18.1.16

Mackensen, A., Schumacher, S., Radke, J., & Schmidt, D. N. (2000). Microhabitat preferences and stable carbon isotopes of endobenthic foraminifera: Clue to quantitative reconstruction of oceanic new production? *Marine Micropaleontology*, *40*(3), 233–258. https://doi.org/10.1016/S0377-8398(00)00040-2

Mackensen, A., & Schmiedl, G. (2019). Stable carbon isotopes in paleoceanography: Atmosphere, oceans, and sediments. *Earth-Science Reviews*, *197*, 102893. https://doi.org/10.1016/j.earscirev.2019.102893

Mangerud, J., Bondevik, S., Gulliksen, S., Karin Hufthammer, A., & Høisæter, T. (2006). Marine ^{14}C reservoir ages for 19th century whales and molluscs from the North Atlantic. *Quaternary Science Reviews*, *25*(23–24), 3228–3245. https://doi.org/10.1016/j.quascirev.2006.03.010

Marcott, S. A., Clark, P. U., Padman, L., Klinkhammer, G. P., Springer, S. R., Liu, Z., Otto-Bliesner, B. L., Carlson, A. E., Ungerer, A., Padman, J., He, F., Cheng, J., & Schmittner, A. (2011). Ice-shelf collapse from subsurface warming as a trigger for Heinrich events. *Proceedings of the National Academy of Sciences*, *108*(33), 13415–13419. https://doi.org/10.1073/pnas.1104772108

Martin, P. A., & Lea, D. W. (2002). A simple evaluation of cleaning procedures on fossil benthic foraminiferal Mg/Ca. *Geochemistry, Geophysics, Geosystems*, *3*(10), 1–8. https://doi.org/10.1029/2001GC000280

Maslin, M., Owen, M., Betts, R., Day, S., Dunkey Jones, T., & Ridgwell, A. (2010). Gas hydrates: Past and future geohazard? *Philosophical Transactions of the Royal Society of London*, *368*, 2369–2393. https://doi.org/10.1098/rsta.2010.0065

Mau, S., Römer, M., Torres, M. E., Bussmann, I., Pape, T., Damm, E., Geprägs, P., Wintersteller, P., Hsu, C.-W., Loher, M., & Bohrmann, G. (2017). Widespread methane seepage along the continental margin off Svalbard—From Bjørnøya to Kongsfjorden. *Scientific Reports*, *7*(1), 42997. https://doi.org/10.1038/srep42997

McCorkle, D. C., Keigwin, L. D., Corliss, B. H., & Emerson, S. R. (1990). The influence of microhabitats on the carbon isotopic composition of deep-sea benthic foraminifera. *Paleoceanography*, *5*(2), 161–185. https://doi.org/10.1029/PA005i002p00161

Meredith, M., Sommerkorn, M., Cassotta, S., Derksen, A., Ekaykin, A., Hollowed, A., Kofinas, G., Mackintosh, A., Melbourne-Thomas, J., Muelbert, M. M. C., Ottersen, G., Pritchard, H., & Schuur, E. A. G. (2019). Polar Regions. In H.-O. Pörtner, D. C. Roberts, V. Masson-Delmotte, P. Zhai, M. Tignor, E. Poloczanska, K. Mintenbeck, A. Alegría, M. Nicolai, A. Okem, J. Petzold, B. Rama, & N. M. Weyer (Eds.), *IPCC Special Report on the Ocean and Cryosphere in a Changing Climate*. In press.

Mezger, E. M., Nooijer, L. J., Boer, W., Brummer, G. J. A., & Reichart, G. J. (2016). Salinity controls on Na incorporation in Red Sea planktonic foraminifera. *Paleoceanography*, *31*(12), 1562–1582. https://doi.org/10.1002/2016PA003052

Müller, J., Wagner, A., Fahl, K., Stein, R., Prange, M., & Lohmann, G. (2011). Towards quantitative sea ice reconstructions in the northern North Atlantic: A combined biomarker and numerical modelling approach. *Earth and Planetary Science Letters*, *306*(3–4), 137–148. https://doi.org/10.1016/j.epsl.2011.04.011

Myhre, C. L., Ferré, B., Platt, S. M., Silyakova, A., Hermansen, O., Allen, G., Pisso, I., Schmidbauer, N., Stohl, A., Pitt, J., Jansson, P., Greinert, J., Percival, C., Fjaeraa, A. M., O'Shea, S. J., Gallagher, M., Le Breton, M., Bower, K. N., Bauguitte, S. J. B., … Mienert, J. (2016). Extensive release of methane from Arctic seabed west of Svalbard during summer 2014 does not influence the atmosphere: CH4 from Arctic Ocean to the atmosphere. *Geophysical Research Letters*, *43*(9), 4624–4631. https://doi.org/10.1002/2016GL068999

Nairn, M. G. (2019). *Mid-Late Miocene climate constrained by a new Laser Ablation ICP-MS set up* [PhD thesis]. Shcool of Earth and Ocean Sciences. Cardiff University.

Najafi, M. R., Zwiers, F. W., & Gillett, N. P. (2015). Attribution of Arctic temperature change to greenhouse-gas and aerosol influences. *Nature Climate Change*, *5*(3), 246–249. https://doi.org/10.1038/nclimate2524

North Greenland Ice Core Project members. (2004). High-resolution record of Northern Hemisphere climate extending into the last interglacial period. *Nature*, *431*(7005), 147–151. https://doi.org/10.1038/nature02805

Notz, D. (2015). How well must climate models agree with observations? *Philosophical Transactions of the Royal Society A: Mathematical, Physical and Engineering Sciences*, *373*(2052), 20140164. https://doi.org/10.1098/rsta.2014.0164

Nürnberg, D., Bijma, J., & Hemleben, C. (1996). Assessing the reliability of magnesium in foraminiferal calcite as a proxy for water mass temperatures. *Geochimica et Cosmochimica Acta*, *60*(5), 803–814. https://doi.org/10.1016/0016-7037(95)00446-7

O'Hara, K. D. (2008). A model for late Quaternary methane ice core signals: Wetlands versus a shallow marine source. *Geophysical Research Letters*, *35*(2), L02712. https://doi.org/10.1029/2007GL032317

Østerhus, S., Woodgate, R., Valdimarsson, H., Turrell, B., de Steur, L., Quadfasel, D., Olsen, S. M., Moritz, M., Lee, C. M., Larsen, K. M. H., Jónsson, S., Johnson, C., Jochumsen, K., Hansen, B., Curry, B., Cunningham, S., & Berx, B. (2019). Arctic Mediterranean exchanges: A consistent volume budget and trends in transports from two decades of observations. *Ocean Science*, *15*, 379–399. https://doi.org/10.5194/os-15-379-2019

Overland, J., Dunlea, E., Box, J. E., Corell, R., Forsius, M., Kattsov, V., Olsen, M. S., Pawlak, J., Reiersen, L.-O., & Wang, M. (2019). The urgency of Arctic change. *Polar Science*, *21*, 6–13. https://doi.org/10.1016/j.polar.2018.11.008

Pena, L. D., Calvo, E., Cacho, I., Eggins, S., & Pelejero, C. (2005). Identification and removal of Mn-Mg-rich contaminant phases on foraminiferal tests: Implications for Mg/Ca past temperature reconstructions. *Geochemistry, Geophysics, Geosystems*, *6*(9). https://doi.org/10.1029/2005GC000930

Petersen, S. V., Schrag, D. P., & Clark, P. U. (2013). A new mechanism for Dansgaard-Oeschger cycles. *Paleoceanography*, *28*, 24–30. https://doi.org/10.1029/2012PA002364

Plaza-Faverola, A., Bünz, S., Johnson, J. E., Chand, S., Knies, J., Mienert, J., & Franek, P. (2015). Role of tectonic stress in seepage evolution along the gas hydrate-charged Vestnesa Ridge, Fram Strait: Arctic seepage modulated by tectonics. *Geophysical Research Letters*, *42*(3), 733–742. https://doi.org/10.1002/2014GL062474

Plaza-Faverola, A., Vadakkepuliyambatta, S., Hong, W.-L., Mienert, J., Bünz, S., Chand, S., & Greinert, J. (2017). Bottom-simulating reflector dynamics at Arctic thermogenic gas provinces: An example from Vestnesa Ridge, offshore west Svalbard: Arctic Gas Hydrate Stability Dynamics. *Journal of Geophysical Research: Solid Earth*, *122*(6), 4089–4105. https://doi.org/10.1002/2016JB013761

Plaza-Faverola, A., & Keiding, M. (2019). Correlation between tectonic stress regimes and methane seepage on the western Svalbard margin. *Solid Earth*, *10*(1), 79–94. https://doi.org/10.5194/se-10-79-2019

Polyakov, I. V., Pnyushkov, A. V., Alkire, M. B., Ashik, I. M., Baumann, T. M., Carmack, E. C., Goszczko, I., Guthrie, J., Ivanov, V. V., Kanzow, T., Krishfield, R., Kwok, R., Sundfjord, A., Morison, J., Rember, R., & Yulin, A. (2017). Greater role for Atlantic inflows on sea-ice loss in the Eurasian Basin of the Arctic Ocean. *Science*, *356*(6335), 285–291. https://doi.org/10.1126/science.aai8204

Portnov, A., Vadakkepuliyambatta, S., Mienert, J., & Hubbard, A. (2016). Ice-sheet-driven methane storage and release in the Arctic. *Nature Communications*, *7*(1), 10314. https://doi.org/10.1038/ncomms10314

Quadfasel, D., Gascard, J.-C., & Koltermann, K.-P. (1987). Large-scale oceanography in Fram Strait during the 1984 Marginal Ice Zone Experiment. *Journal of Geophysical Research*, *92*(C7), 6719. https://doi.org/10.1029/JC092iC07p06719

Rahmstorf, S. (2002). Ocean circulation and climate during the past 120,000 years. *Nature*, *419*(6903), 207–214. https://doi.org/10.1038/nature01090

Rasmussen, S. O., Bigler, M., Blockley, S. P., Blunier, T., Buchardt, S. L., Clausen, H. B., Cvijanovic, I., Dahl-Jensen, D., Johnsen, S. J., Fischer, H., Gkinis, V., Guillevic, M., Hoek, W. Z., Lowe, J. J., Pedro, J. B., Popp, T., Seierstad, I. K., Steffensen, J. P., Svensson, A. M., … Winstrup, M. (2014). A stratigraphic framework for abrupt climatic changes during the Last Glacial period based on three synchronized Greenland ice-core records: Refining and extending the INTIMATE event stratigraphy. *Quaternary Science Reviews*, *106*, 14–28. https://doi.org/10.1016/j.quascirev.2014.09.007

Rasmussen, T. L., & Thomsen, E. (2004). The role of the North Atlantic Drift in the millennial timescale glacial climate fluctuations. *Palaeogeography, Palaeoclimatology, Palaeoecology*, *210*(1), 101–116. https://doi.org/10.1016/j.palaeo.2004.04.005

Rasmussen, T. L., & Thomsen, E. (2017). Ecology of deep-sea benthic foraminifera in the North Atlantic during the last glaciation: Food or temperature control. *Palaeogeography, Palaeoclimatology, Palaeoecology*, *472*, 15–32. https://doi.org/10.1016/j.palaeo.2017.02.012

Rasmussen, T. L., Wastegård, S., Kuijpers, A., van Weering, T. C. E., Heinemeier, J., & Thomsen, E. (2003). Stratigraphy and distribution of tephra layers in marine sediment cores from the Faeroe Islands, North Atlantic. *Marine Geology*, *199*(3–4), 263–277. https://doi.org/10.1016/S0025-3227(03)00219-6

Rasmussen, T. L., Thomsen, E., Ślubowska, M. A., Jessen, S., Solheim, A., & Koç, N. (2007). Paleoceanographic evolution of the SW Svalbard margin (76°N) since 20,000 ^{14}C yr BP. *Quaternary Research*, *67*(01), 100–114. https://doi.org/10.1016/j.yqres.2006.07.002

Rasmussen, T. L., Thomsen, E., Skirbekk, K., Ślubowska-Woldengen, M., Klitgaard Kristensen, D., & Koç, N. (2014). Spatial and temporal distribution of Holocene temperature maxima in the northern Nordic seas: Interplay of Atlantic-, Arctic- and polar water masses. *Quaternary Science Reviews*, *92*, 280–291. https://doi.org/10.1016/j.quascirev.2013.10.034

Rasmussen, T. L., Thomsen, E., & Moros, M. (2016). North Atlantic warming during Dansgaard-Oeschger events synchronous with Antarctic warming and out-of-phase with Greenland climate. *Scientific Reports*, *6*(1), 20535. https://doi.org/10.1038/srep20535

Ravelo, A. C., & Hillaire-Marcel, C. (2007). Chapter Eighteen: The Use of Oxygen and Carbon Isotopes of Foraminifera in Paleoceanography. In C. Hillaire-Marcel & A. C. Ravelo (Eds.), *Developments in Marine Geology* (Vol. 1, pp. 735–764). Elsevier. https://doi.org/10.1016/S1572-5480(07)01023-8

Rawson, P. F., Allen, P. M., Bevins, R. E., Brenchley, P. J., Cope, J. C. W., Evans, J. A., Gale, A. S., Gibbard, P. L., Gregory, F. J., Hesselbo, S. P., Marshall, J. E. A., Knox, R. W. O. B., Oates, M. J., Riley, N. J., Rushton, A. W. A., Smith, A. G., Trewin, N. H., & Zalasiewicz, J. A. (2002). *A guide to stratigraphical procedure*.

Reimer, P. J., Bard, E., Bayliss, A., Beck, J. W., Blackwell, P. G., Ramsey, C. B., Buck, C. E., Cheng, H., Edwards, R. L., Friedrich, M., Grootes, P. M., Guilderson, T. P., Haflidason, H., Hajdas, I., Hatté, C., Heaton, T. J., Hoffmann, D. L., Hogg, A. G., Hughen, K. A., … van der Plicht, J. (2013). IntCal13 and Marine13 Radiocarbon Age Calibration Curves 0–50,000 Years cal BP. *Radiocarbon*, *55*(4), 1869–1887. https://doi.org/10.2458/azu_js_rc.55.16947

Reimer, P. J., Austin, W. E. N., Bard, E., Bayliss, A., Blackwell, P. G., Bronk Ramsey, C., Butzin, M., Cheng, H., Edwards, R. L., Friedrich, M., Grootes, P. M., Guilderson, T. P., Hajdas, I., Heaton, T. J., Hogg, A. G., Hughen, K. A., Kromer, B., Manning, S. W., Muscheler, R., … Talamo, S. (2020). The IntCal20 Northern Hemisphere radiocarbon

age calibration curve (0-55 cal kBP). *Radiocarbon*, *62*(4), 725–757. https://doi.org/10.1017/RDC.2020.41

Rudels, B. (2015). Arctic Ocean circulation, processes and water masses: A description of observations and ideas with focus on the period prior to the International Polar Year 2007-2009. *Progress in Oceanography*, *132*, 22–67. https://doi.org/10.1016/j.pocean.2013.11.006

Rudels, B., Korhonen, M., Schauer, U., Pisarev, S., Rabe, B., & Wisotzki, A. (2015). Circulation and transformation of Atlantic water in the Eurasian Basin and the contribution of the Fram Strait inflow branch to the Arctic Ocean heat budget. *Progress in Oceanography*, *132*, 128–152. https://doi.org/10.1016/j.pocean.2014.04.003

Ruppel, C. D., & Kessler, J. D. (2017). The interaction of climate change and methane hydrates: Climate-Hydrates Interactions. *Reviews of Geophysics*, *55*(1), 126–168. https://doi.org/10.1002/2016RG000534

Sadatzki, H., Dokken, T. M., Berben, S. M. P., Muschitiello, F., Stein, R., Fahl, K., Menviel, L., Timmermann, A., & Jansen, E. (2019). Sea ice variability in the southern Norwegian Sea during glacial Dansgaard-Oeschger climate cycles. *Science Advances*, *5*(3), eaau6174. https://doi.org/10.1126/sciadv.aau6174

Sadatzki, H., Maffezzoli, N., Dokken, T. M., Simon, M. H., Berben, S. M. P., Fahl, K., Kjær, H. A., Spolaor, A., Stein, R., Vallelonga, P., Vinther, B. M., & Jansen, E. (2020). Rapid reductions and millennial-scale variability in Nordic Seas sea ice cover during abrupt glacial climate changes. *Proceedings of the National Academy of Sciences*, *117*(47), 29478–29486. https://doi.org/10.1073/pnas.2005849117

Saher, M., Kristensen, D. K., Hald, M., Korsun, S., & Jørgensen, L. (2009). Benthic foraminifera assemblages in the Central Barents Sea: An evaluation of the effect of combining live and total fauna studies in tracking environmental change. *Norwegian Journal of Geology*, *89*, 149–161.

Sarnthein, M., Winn, K., Jung, S. J. A., Duplessy, J.-C., Labeyrie, L., Erlenkeuser, H., & Ganssen, G. (1994). Changes in East Atlantic Deepwater Circulation over the last 30,000 years: Eight time slice reconstructions. *Paleoceanography*, *9*(2), 209–267. https://doi.org/10.1029/93PA03301

Schlitzer, R. (2001). *Ocean Data View*. http://www.awi-bremerhaven.de/GEO/ODV

Schneider, A., Crémière, A., Panieri, G., Lepland, A., & Knies, J. (2017). Diagenetic alteration of benthic foraminifera from a methane seep site on Vestnesa Ridge (NW Svalbard). *Deep Sea Research Part I: Oceanographic Research Papers*, *123*, 22–34. https://doi.org/10.1016/j.dsr.2017.03.001

Schneider, A., Panieri, G., Lepland, A., Consolaro, C., Crémière, A., Forwick, M., Johnson, J. E., Plaza-Faverola, A., Sauer, S., & Knies, J. (2018). Methane seepage at Vestnesa Ridge (NW Svalbard) since the Last Glacial Maximum. *Quaternary Science Reviews*, *193*, 98–117. https://doi.org/10.1016/j.quascirev.2018.06.006

Seidenkrantz, M.-S. (2013). Benthic foraminifera as palaeo sea-ice indicators in the subarctic realm – examples from the Labrador Sea–Baffin Bay region. *Quaternary Science Reviews*, *79*, 135–144. https://doi.org/10.1016/j.quascirev.2013.03.014

Seierstad, I. K., Abbott, P. M., Bigler, M., Blunier, T., Bourne, A. J., Brook, E., Buchardt, S. L., Buizert, C., Clausen, H. B., Cook, E., Dahl-Jensen, D., Davies, S. M., Guillevic, M., Johnsen, S. J., Pedersen, D. S., Popp, T. J., Rasmussen, S. O., Severinghaus, J. P., Svensson, A., & Vinther, B. M. (2014). Consistently dated records from the Greenland GRIP, GISP2 and NGRIP ice cores for the past 104 ka reveal regional millennial-scale δ^{18}O gradients with possible Heinrich event imprint. *Quaternary Science Reviews*, *106*, 29–46. https://doi.org/10.1016/j.quascirev.2014.10.032

Sejrup, H. P., Birks, H. J. B., Kristensen, D. K., & Madsen, H. (2004). Benthonic foraminiferal distributions and quantitative transfer functions for the northwest European continental margin. *Marine Micropaleontology*, *53*(1–2), 197–226. https://doi.org/10.1016/j.marmicro.2004.05.009

Serov, P., Vadakkepuliyambatta, S., Mienert, J., Patton, H., Portnov, A., Silyakova, A., Panieri, G., Carroll, M. L., Carroll, J., Andreassen, K., & Hubbard, A. (2017). Postglacial response of Arctic Ocean gas hydrates to climatic amelioration. *Proceedings of the National Academy of Sciences*, *114*(24), 6215–6220. https://doi.org/10.1073/pnas.1619288114

Serreze, M. C., & Barry, R. G. (2011). Processes and impacts of Arctic amplification: A research synthesis. *Global and Planetary Change*, *77*, 85–96. https://doi.org/10.1016/j.gloplacha.2011.03.004

Sessford, E. G., Tisserand, A. A., Risebrobakken, B., Andersson, C., Dokken, T., & Jansen, E. (2018). High-Resolution Benthic Mg/Ca Temperature Record of the Intermediate Water in the Denmark Strait Across D-O Stadial-Interstadial Cycles. *Paleoceanography and Paleoclimatology*, *33*(11), 1169–1185. https://doi.org/10.1029/2018PA003370

Sessford, E. G., Jensen, M. F., Tisserand, A. A., Muschitiello, F., Dokken, T., Nisancioglu, K. H., & Jansen, E. (2019). Consistent fluctuations in intermediate water temperature off the coast of Greenland and Norway during Dansgaard-Oeschger events. *Quaternary Science Reviews*, *223*, 105887. https://doi.org/10.1016/j.quascirev.2019.105887

Shackleton, N. J. (1967). Oxygen isotope analyses and Pleistocene temperatures re-assessed. *Nature*, *215*(5096), 15–17. https://doi.org/10.1038/215015a0

Shackleton, N. J., Hall, M. A., & Vincent, E. (2000). Phase relationships between millennial-scale events 64,000-24,000 years ago. *Paleoceanography*, *15*(6), 565–569. https://doi.org/10.1029/2000PA000513

Skagseth, Ø., Furevik, T., Ingvaldsen, R., Loeng, H., Mork, K. A., Orvik, K. A., & Ozhigin, V. (2008). Volume and Heat Transports to the Arctic Ocean Via the Norwegian and Barents Seas. In R. R. Dickson, J. Meincke, & P. Rhines (Eds.), *Arctic–Subarctic Ocean Fluxes: Defining the Role of the Northern Seas in Climate* (pp. 45–64). Springer Netherlands. https://doi.org/10.1007/978-1-4020-6774-7_3

Skinner, L. C., Shackleton, N. J., & Elderfield, H. (2003). Millennial-scale variability of deep-water temperature and $\delta^{18}O_{dw}$ indicating deep-water source variations in the Northeast Atlantic, 0-34 cal. Ka BP $^{18}O_{dw}$. *Geochemistry, Geophysics, Geosystems*, *4*(12). https://doi.org/10.1029/2003GC000585

Skinner, L. C., Muschitiello, F., & Scrivner, A. E. (2019). Marine reservoir age variability over the last deglaciation: Implications for marine carbon cycling and prospects for regional radiocarbon calibrations. *Paleoceanography and Paleoclimatology*, *34*(11), 1807–1815. https://doi.org/10.1029/2019PA003667

Skogseth, R., Haugan, P. M., & Jakobsson, M. (2005). Watermass transformations in Storfjorden. *Continental Shelf Research*, *25*(5–6), 667–695. https://doi.org/10.1016/j.csr.2004.10.005

Sloan, E. D., & Koh, C. (2007). *Clathrate Hydrates of Natural Gases, Third Edition* (Third). CRC Press.

Smedsrud, L. H., Ingvaldsen, R., Nilsen, J. E. Ø., & Skagseth, Ø. (2010). Heat in the Barents Sea: Transport, storage, and surface fluxes. *Ocean Science*, *6*, 219–234. https://doi.org/10.5194/os-6-219-2010

Smik, L., Cabedo-Sanz, P., & Belt, S. T. (2016). Semi-quantitative estimates of paleo Arctic sea ice concentration based on source-specific highly branched isoprenoid alkenes: A further development of the PIP_{25} index. *Organic Geochemistry*, *92*, 63–69. https://doi.org/10.1016/j.orggeochem.2015.12.007

Steig, E. J. (2006). The south-north connection. *Nature*, *444*, 152–153. https://doi.org/10.1038/444152a

Stern, J. V., & Lisiecki, L. E. (2013). North Atlantic circulation and reservoir age changes over the past 41,000 years. *Geophysical Research Letters*, *40*(14), 3693–3697. https://doi.org/10.1002/grl.50679

Straneo, F., & Heimbach, P. (2013). North Atlantic warming and the retreat of Greenland's outlet glaciers. *Nature*, *504*(7478), 36–43. https://doi.org/10.1038/nature12854

Svensson, A., Andersen, K. K., Bigler, M., Clausen, H. B., Dahl-Jensen, D., Davies, S. M., Johnsen, S. J., Muscheler, R., Parrenin, F., Rasmussen, S. O., Rothlisberger, R., Seierstad, I., Steffensen, J. P., & Vinther, B. M. (2008). A 60 000 year Greenland stratigraphic ice core chronology. *Climate of the Past*, *4*, 47–57. https://doi.org/10.5194/cp-4-47-2008

Sztybor, K., & Rasmussen, T. L. (2017a). Late glacial and deglacial palaeoceanographic changes at Vestnesa Ridge, Fram Strait: Methane seep versus non-seep environments. *Palaeogeography, Palaeoclimatology, Palaeoecology*, *476*, 77–89. https://doi.org/10.1016/j.palaeo.2017.04.001

Sztybor, K., & Rasmussen, T. L. (2017b). Diagenetic disturbances of marine sedimentary records from methane-influenced environments in the Fram Strait as indications of variation in seep intensity during the last 35 000 years. *Boreas*, *46*(2), 212–228. https://doi.org/10.1111/bor.12202

Telesiński, M. M., Ezat, M. M., Muschitiello, F., Bauch, H. A., & Spielhagen, R. F. (2021). Ventilation history of the Nordic Seas deduced from pelagic-benthic radiocarbon age offsets. *Geochemistry, Geophysics, Geosystems*, *22*, e2020GC009132. https://doi.org/10.1029/2020GC009132

Thomsen, E., Rasmussen, T. L., Sztybor, K., Hanken, N.-M., Tendal, O. S., & Uchman, A. (2019). Cold-seep fossil macrofaunal assemblages from Vestnesa Ridge, eastern Fram

Strait, during the past 45 000 years. *Polar Research*, *38*. https://doi.org/10.33265/polar.v38.3310

Thornalley, D. J. R., Elderfield, H., & McCave, I. N. (2009). Holocene oscillations in temperature and salinity of the surface subpolar North Atlantic. *Nature*, *457*(7230), 711–714. https://doi.org/10.1038/nature07717

Thornalley, D. J. R., Elderfield, H., & McCave, I. N. (2011). Reconstructing North Atlantic deglacial surface hydrography and its link to the Atlantic overturning circulation. *Global and Planetary Change*, *79*(3–4), 163–175. https://doi.org/10.1016/j.gloplacha.2010.06.003

Thornalley, D. J. R., Bauch, H. A., Gebbie, G., Guo, W., Ziegler, M., Bernasconi, S. M., Barker, S., Skinner, L. C., & Yu, J. (2015). A warm and poorly ventilated deep Arctic Mediterranean during the last glacial period. *Science*, *349*(6249), 706–710. https://doi.org/10.1126/science.aaa9554

Tierney, J. E., Poulsen, C. J., Montañez, I. P., Bhattacharya, T., Feng, R., Ford, H. L., Hönisch, B., Inglis, G. N., Petersen, S. V., Sagoo, N., Tabor, C. R., Thirumalai, K., Zhu, J., Burls, N. J., Foster, G. L., Goddéris, Y., Huber, B. T., Ivany, L. C., Turner, S. K., … Zhang, Y. G. (2020). Past climates inform our future. *Science*, *370*(eaay3701), 11. https://doi.org/10.1126/science.aay3701

Torres, M. E., Mix, A. C., Kinports, K., Haley, B., Klinkhammer, G. P., McManus, J., & de Angelis, M. A. (2003). Is methane venting at the seafloor recorded by δ^{13}C of benthic foraminifera shells? *Paleoceanography*, *18*, 1062. https://doi.org/10.1029/2002PA000824

Toyofuku, T., Kitazato, H., Kawahata, H., Tsuchiya, M., & Nohara, M. (2000). Evaluation of Mg/Ca thermometry in foraminifera: Comparison of experimental results and measurements in nature. *Paleoceanography*, *15*(4), 456–464. https://doi.org/10.1029/1999PA000460

Urey, H. C., Lowenstam, H. A., Epstein, S., & McKinney, C. R. (1951). Measurement of paleotemperatures and temperatures of the Upper Cretaceous of England, Denmark and the southeastern United States. *Bulletin of the Geological Society of America*, *62*(4), 399–416. https://doi.org/10.1130/0016-7606(1951)62[399:MOPATO]2.0.CO;2

Vadakkepuliyambatta, S., Chand, S., & Bünz, S. (2017). The history and future trends of ocean warming-induced gas hydrate dissociation in the SW Barents Sea. *Geophysical Research Letters*, *44*(2), 835–844. https://doi.org/10.1002/2016GL071841

van der Bilt, W. G. M., & Lane, C. S. (2019). Lake sediments with Azorean tephra reveal ice-free conditions on coastal northwest Spitsbergen during the Last Glacial Maximum. *Science Advances*, *5*(10), eaaw5980. https://doi.org/10.1126/sciadv.aaw5980

Voelker, A. H. L., & workshop participants. (2002). Global distribution of centennial-scale records for Marine Isotope Stage (MIS) 3: A database. *Quaternary Science Reviews*, *21*(10), 1185–1212. https://doi.org/10.1016/S0277-3791(01)00139-1

Volkman, J. K., Barrett, S. M., Blackburn, S. I., Mansour, M. P., Sikes, E. L., & Gelin, F. (1998). Microalgal biomarkers: A review of recent research developments. *Organic Geochemistry*, *29*(5–7), 1163–1179. https://doi.org/10.1016/S0146-6380(98)00062-X

Volkmann, R. (2000). Planktic foraminifer ecology and stable isotope geochemistry in the Arctic Ocean: Implications from water column and sediment surface studies for quantitative reconstructions of oceanic parameters (Ökologie planktischer Foraminiferen und stabile Isotope im Arktischen Ozean: Anwendbarkeit für die quantitative Rekonstruktion von ozeanischen Parametern). *Berichte Zur Polarforschung*, *361*. http://epic.awi.de/26541/1/BerPolarforsch2000361.pdf

Waage, M., Portnov, A., Serov, P., Bünz, S., Waghorn, K. A., Vadakkepuliyambatta, S., Mienert, J., & Andreassen, K. (2019). Geological controls on fluid flow and gas hydrate pingo development on the Barents Sea margin. *Geochemistry, Geophysics, Geosystems*, *20*(2), 630–650. https://doi.org/10.1029/2018GC007930

Wallmann, K., Riedel, M., Hong, W. L., Patton, H., Hubbard, A., Pape, T., Hsu, C. W., Schmidt, C., Johnson, J. E., Torres, M. E., Andreassen, K., Berndt, C., & Bohrmann, G. (2018). Gas hydrate dissociation off Svalbard induced by isostatic rebound rather than global warming. *Nature Communications*, *9*, 83. https://doi.org/10.1038/s41467-017-02550-9

Wastegård, S., & Rasmussen, T. L. (2001). New tephra horizons from Oxygen Isotope Stage 5 in the North Atlantic: Correlation potential for terrestrial, marine and ice-core archives. *Quaternary Science Reviews*, *20*(15), 1587–1593. https://doi.org/10.1016/S0277-3791(01)00055-5

Wastegård, S., & Rasmussen, T. L. (2014). Faroe Marine Ash Zone IV: A new MIS 3 ash zone on the Faroe Islands margin. *Geological Society, London, Special Publications*, *398*(1), 81–93. https://doi.org/10.1144/SP398.3

Westbrook, G. K., Thatcher, K. E., Rohling, E. J., Piotrowski, A. M., Pälike, H., Osborne, A. H., Nisbet, E. G., Minshull, T. A., Lanoisellé, M., James, R. H., Hühnerbach, V., Green, D., Fisher, R. E., Crocker, A. J., Chabert, A., Bolton, C., Beszczynska-Möller, A., Berndt, C., & Aquilina, A. (2009). Escape of methane gas from the seabed along the West Spitsbergen continental margin. *Geophysical Research Letters*, *36*(15), L15608. https://doi.org/10.1029/2009GL039191

Whiticar, M. J., & Faber, E. (1986). Methane oxidation in sediment and water column environments—Isotope evidence. *Organic Geochemistry*, *10*(4–6), 759–768. https://doi.org/10.1016/S0146-6380(86)80013-4

Whiticar, M. J. (1999). Carbon and hydrogen isotope systematics of bacterial formation and oxidation of methane. *Chemical Geology*, *161*(1–3), 291–314. https://doi.org/10.1016/S0009-2541(99)00092-3

Wit, J. C., de Nooijer, L. J., Wolthers, M., & Reichart, G. J. (2013). A novel salinity proxy based on Na incorporation into foraminiferal calcite. *Biogeosciences*, *10*(10), 6375–6387. https://doi.org/10.5194/bg-10-6375-2013

Wolff, E. W., Chappellaz, J., Blunier, T., Rasmussen, S. O., & Svensson, A. (2010). Millennial-scale variability during the last glacial: The ice core record. *Quaternary Science Reviews*, *29*(21–22), 2828–2838. https://doi.org/10.1016/j.quascirev.2009.10.013

Wollenburg, J. E., & Mackensen, A. (1998). Living benthic foraminifers from the central Arctic Ocean: Faunal composition, standing stock and diversity. *Marine Micropaleontology*, *34*(3), 153–185. https://doi.org/10.1016/S0377-8398(98)00007-3

Xiao, X., Fahl, K., Müller, J., & Stein, R. (2015). Sea-ice distribution in the modern Arctic Ocean: Biomarker records from trans-Arctic Ocean surface sediments. *Geochimica et Cosmochimica Acta*, *155*, 16–29. https://doi.org/10.1016/j.gca.2015.01.029

Yao, H., Niemann, H., & Panieri, G. (2020). Multi-proxy approach to unravel methane emission history of an Arctic cold seep. *Quaternary Science Reviews*, *244*, 106490. https://doi.org/10.1016/j.quascirev.2020.106490

Yu, J., Elderfield, H., Greaves, M., & Day, J. (2007). Preferential dissolution of benthic foraminiferal calcite during laboratory reductive cleaning. *Geochemistry, Geophysics, Geosystems*, *8*, Q06016. https://doi.org/10.1029/2006GC001571

Zachos, J., Pagani, M., Sloan, L., Thomas, E., & Billups, K. (2001). Trends, rhythms, and aberrations in global climate 65 Ma to present. *Science*, *292*(5517), 686. https://doi.org/10.1126/science.1059412

Zamelczyk, K., Rasmussen, T. L., Husum, K., Haflidason, H., de Vernal, A., Ravna, E. K., Hald, M., & Hillaire-Marcel, C. (2012). Paleoceanographic changes and calcium carbonate dissolution in the central Fram Strait during the last 20 ka. *Quaternary Research*, *78*(3), 405–416. https://doi.org/10.1016/j.yqres.2012.07.006

SECTION II   Research papers

Paper I

Key Points:

- Bottom water temperature in the Fram Strait increased up to 5°C during Heinrich Stadials (HSs) due to subsurface flow of Atlantic water
- During HSs, a strong halocline prevented heat loss from the Atlantic water, from 45°N in the North Atlantic to the Arctic Ocean >79°N
- Release of subsurface heat from this vast area contributed to the abrupt regional atmospheric warmings at the start of Greenland Interstadials

Supporting Information:

- Supporting Information S1

Correspondence to:

N. El bani Altuna,
naima.e.altuna@uit.no

Millennial-Scale Changes in Bottom Water Temperature and Water Mass Exchange Through the Fram Strait 79°N, 63-13 ka

N. El bani Altuna[1] ID, **M. M. Ezat[1,2]** ID, **M. Greaves[3]** ID, **and T. L. Rasmussen[1]** ID

[1]Department of Geology, CAGE - Centre for Arctic Gas Hydrate, Environment and Climate, UiT, Arctic University of Norway, Tromsø, Norway, [2]Department of Geology, Faculty of Science, Beni-Suef University, Beni-Suef, Egypt, [3]Department of Earth Sciences, Godwin Laboratory for Palaeoclimate Research, University of Cambridge, Cambridge, UK

Abstract The Svalbard margin, in the eastern Fram Strait with its high sediment accumulation, form a key area for the reconstruction of water mass and heat exchange between the North Atlantic and Arctic Ocean in relation to abrupt climate changes as seen in glacial Greenland Interstadial and Greenland Stadial (GI-GS) events. Here, we present a bottom water temperature (BWT) record from the northern Nordic Seas (79°N) at 1,273 m water depth based on benthic foraminiferal Mg/Ca. The BWT reconstructions, combined with benthic foraminiferal stable isotopes, benthic foraminiferal fauna compositions and ice-rafted debris (IRD), reveal at least two distinctive scenarios for the GI-GS events during the last glacial period (13–63 ka). During GIs, conditions were similar to modern with high productivity, low BWT and deep convection. During GS6, GS8, and GS15 and during Heinrich Stadials (HSs), BWT increased up to 5°C ± 1°C generally concomitant with low planktic and benthic δ^{18}O. Our results suggest, that during some GSs and HSs, deep water generation was reduced, allowing the subsurface Atlantic water (AW) to thicken and deepen down to at least the core site depth. A strong halocline during HSs and GSs prevented heat release from the subsurface AW, which we can now trace from 45°N in the North Atlantic to the Arctic Ocean >79°N. Surfacing of the salty Atlantic subsurface water preconditioned the Nordic seas for convection. Release of the subsurface heat from this vast reservoir must have contributed to the large and abrupt atmospheric warmings at the start of GIs.

Plain Language Summary The Fram Strait is an area where warm and salty Atlantic water (AW) enters the Arctic Ocean from the North Atlantic Ocean. As it flows northwards in the Nordic Seas, the AW mass releases heat to the atmosphere and sinks to form deep cold water, both moderating regional climate and driving deep ocean circulation. To better understand future changes in ocean circulation and interactions under ongoing climate change, it is necessary to study past oceanic changes in relation to climate change. We investigated benthic foraminifera (single-celled organisms with shells living at the sea floor) with the aim of reconstructing bottom water temperature variations during the last ice age during abrupt atmospheric warmings and coolings on millennial time scales. Our results show that during events of extremely low atmospheric temperature, the deep ocean from the northern North Atlantic to the Arctic Ocean was warmer than today. The ocean surface was cold and stratified due to the presence of polar meltwater. The accumulation of subsurface heat in this vast area toward the end of these periods and decrease of meltwater supply probably broke the stratification, and the subsequent heat release from the ocean to the atmosphere contributed to the abrupt atmospheric warming and onset of renewed convection and cold deep water formation.

1. Introduction

During the last glacial period, the climate of the northern hemisphere was affected by abrupt millennial-scale climate changes called Dansgaard-Oeschger (D-O) events (Dansgaard et al., 1982, 1993; Johnsen et al., 1992). Greenland ice cores record ~25 sudden atmospheric warmings in the order of 8°C–16°C from cold stadials (Greenland Stadials, GS) to warm interstadials (Greenland Interstadials, GI) occurring within a few decades (Dansgaard et al., 1993; Huber et al., 2006; Landais et al., 2006; S.O. Rasmussen et al., 2014a). In marine records from the Nordic Seas, GIs are generally short (from centuries to millennia) with variable

hydrographic conditions, whereas GSs are long-lasting (millennia) and characterized by generally more stable and stratified hydrographic conditions (e.g., T. L. Rasmussen & Thomsen, 2004). During some GS events, layers with large amounts of ice-rafted debris (IRD) and dominance of the polar planktic foraminifera *Neogloboquadrina pachyderma* have been found at mid-latitudes in the Northern Hemisphere. These layers were deposited during Heinrich events occurring during Heinrich Stadials (HSs) or Heinrich-like Stadials, depending on the origin of the IRD (e.g., Bond & Lotti, 1995; Elliot et al., 2001; Hemming, 2004). These events are characterized by massive freshwater supply from the melting of icebergs traversing the North Atlantic Ocean (Bond et al., 1993; Heinrich, 1988).

In the Nordic Seas, the development of GI-GS events have been studied combining (sub)surface and bottom water proxy tools (e.g., foraminiferal $\delta^{18}O$ and Mg/Ca, microfossil assemblages, sea-ice proxy IP_{25}) to reconstruct surface and bottom water conditions and sea-ice extent (e.g., Dokken & Hald, 1996; Ezat et al., 2016; Hoff et al., 2016; Jessen & Rasmussen, 2019; Müller & Stein, 2014; T. L. Rasmussen & Thomsen, 2004; T. L. Rasmussen et al., 1996a, 1996b, 2014a; Sadatzki et al., 2019; Sarnthein et al., 2001; Wary et al., 2017). Many previous studies propose scenarios with an active warm Atlantic water (AW) inflow to the Nordic Seas during GIs similar to modern ocean circulation. The inflow contributes to open ocean convection and formation of cold deep water in the Nordic Seas (Ezat et al., 2014; T. L. Rasmussen & Thomsen, 2004; T. L. Rasmussen et al., 1996a, 1996b).

During cold GS and HS events, proxy records from the Nordic Seas and the subpolar North Atlantic show that the Atlantic warm water was subducted beneath a strong halocline, occupying the intermediate depths in the absence of deep water formation under extensive sea-ice cover (e.g., Ezat et al., 2014, 2017, 2019; Hoff et al., 2016; Marcott et al., 2011; T. L. Rasmussen & Thomsen, 2004; T. L. Rasmussen et al., 1996a, 1996b, 2014b). This is in agreement with several modeling studies that simulated D-O-like events in response to freshwater forcing, that caused changes in deep convection and the northward transport of heat (e.g., Brady & Otto-Bliesner, 2011; Ganopolski & Rahmstorf, 2001; Knutti et al., 2004).

Bottom water temperature (BWT) has been investigated in the southern part of the Nordic Seas for the last 60 Kyr using Mg/Ca measured in tests of benthic foraminifera (Ezat et al., 2014). Sessford et al. (2018, 2019) investigated the evolution of BWT for a shorter ca. 8 ka time interval of four D-O events northwest of Iceland and in a nearby record to Ezat et al. (2014). The results show a consistent warming at intermediate depths during GSs, and particularly HSs, with temperatures reaching up to 5.5°C at depths between 1,200 and 1,500 m water depth indicating low or no convection in the Nordic Seas. In the central Arctic Ocean, temperature reconstructions for the intermediate depths (ca. 800–1,500 m water depth) also show millennial-scale changes (Cronin et al., 2012, 2017), but very low sedimentation rates prevented the study of BWT on detailed D-O time scales. The reconstruction of variations in BWT thus constitutes an indirect tool to study the changes in deep-water formation in the past and can be used to trace the circulation of the different water masses and the Atlantic-Arctic Ocean exchange through the Fram Strait.

Here, we present a benthic foraminiferal Mg/Ca record in order to quantify changes in BWT and trace the AW inflow to the Arctic Ocean in relation to millennial-scale climate change. The core site is located in the Fram Strait at 1,273 m water depth on the western Svalbard slope at 79°N. The BWT are compared with benthic foraminiferal assemblage composition, foraminiferal stable isotopes, grain-size distribution and IRD content in order to reconstruct the paleoceanographic development of this high-latitude area.

2. Regional Setting

2.1. Modern Oceanography

The Fram Strait constitutes the major pathway for the exchange of deep and intermediate water masses between the Atlantic and the Arctic Oceans (Aagaard & Coachman, 1968; Hopkins, 1991). In the eastern part of the Fram Strait, the West Spitsbergen Current (WSC) transports warm Atlantic surface water northwards along the western Svalbard slope (Figure 1a). The AW carries heat and salt into the Arctic Ocean and keeps the western Svalbard area free of sea ice today (Hopkins, 1991). In the northern part of the Fram Strait, the AW slightly cools and deepens to become the intermediate Atlantic layer that flows below the thick, cold, low salinity Polar Surface Water in the Arctic Ocean (Aagaard et al., 1981; Rudels, 1987).
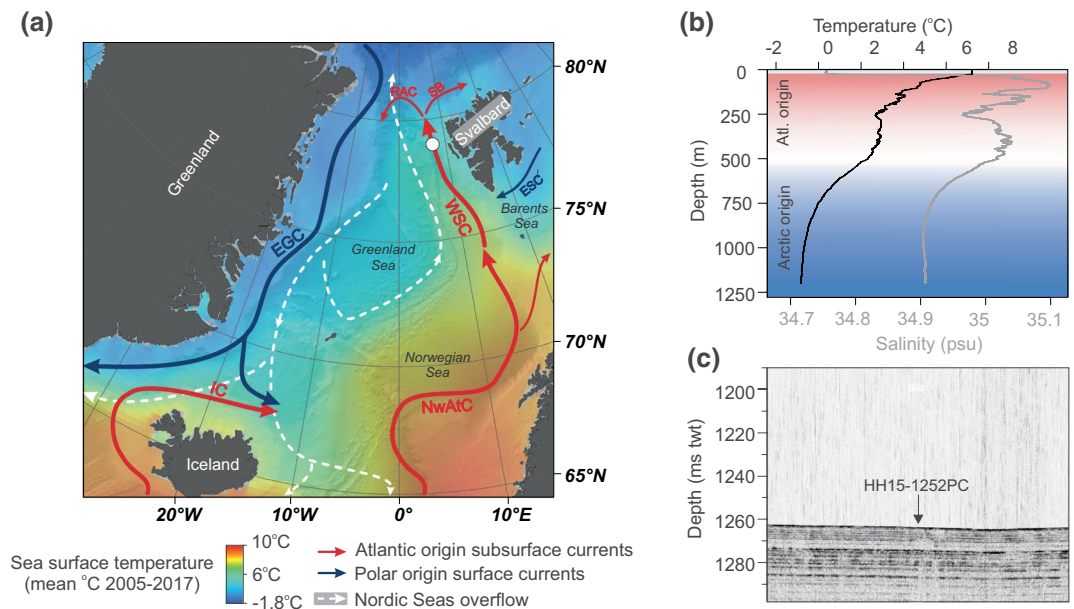
Figure 1. (a) Map of the Greenland Sea showing the position of piston core HH15-1252PC at Vestnesa Ridge (white circle). Main surface and deep currents and mean annual sea surface temperature for the 2005–2017 period (Locarnini et al., 2018) are also shown. The location of other cores from the literature used in the discussion are shown in Figure S1. (b) CTD (Conductivity-Temperature-Depth) data and (c) chirp image taken during core retrieval showing undisturbed, stratified sediments. Abbreviations: EGC, East Greenland Current; ESC, East Spitsbergen Current; IC, Irminger Current; NwAtC, Norwegian Atlantic Current; RAC, Return Atlantic Current; SB, Svalbard Branch; WSC, West Spitsbergen Current.

In the western part of the Fram Strait, the East Greenland Current (EGC) flows southwards along East Greenland and into the Atlantic Ocean (Figure 1a). The EGC carries cold and low saline polar surface water from the Transpolar Drift in the Arctic Ocean overlaying the warmer and saltier Return Atlantic Water (RAW), a branch of the WSC that diverges southward over the Yermak Plateau as an intermediate depth layer of AW. The Arctic Ocean Deep Water is found below RAW (Hopkins, 1991). The mixing and sinking of cold and saline surface waters in the Nordic Seas generate overflows across the Greenland-Scotland Ridge, which contributes to the formation of North Atlantic Deep Water (NADW).

A conductivity-temperature-depth taken close to the core location north of Vestnesa Ridge at the northwestern Svalbard margin in July 2015 shows that the water column here is characterized by a thin mixed surface water layer ($T = 7°C$, $S = 34.8$) generated by the mixing of meltwater and AW (Figure 1b). The main core of AW ($T = 1°C–4°C$, $S = 34.9–35$) occurs beneath the mixed surface layer in the upper 500–800 m of the water column. The bottom water at the core site is influenced by Greenland Sea Intermediate Water (GSIW), with an average temperature of $−0.8°C$ (Figure 1b). No seasonal changes in BWT in the area for the 1981–2010 period were recorded (Locarnini et al., 2018).

2.2. Geological Settings

The sediments along the western Svalbard margin date mainly from the Late Pliocene to Quaternary (Eidvin et al., 1993; Vorren et al., 1998). Vestnesa Ridge is a sediment drift located at 79°N in the eastern part of the Fram Strait (Eiken & Hinz, 1993; Howe et al., 2007) (Figure 1a). The shallow sedimentary evolution of this area is closely related to the strength of the bottom water contour currents and the ridge is flanked by thick contourite deposits (Eiken & Hinz, 1993; Howe et al., 2007; Ottesen et al., 2005). Methane release from the seafloor occurs from a series of pockmarks at the crest of Vestnesa Ridge (e.g., Bunz et al., 2012; Vogt et al., 1994). Bünz et al. (2012) reported at least six active venting pockmarks at 1,200 m water depth in the eastern part of Vestnesa Ridge.

Table 1
Radiocarbon Dates and Tie-Point Ages in Core HH15-1252PC

Core depth (cm)	Lab code/Tie-point (TP)	Dated material	^{14}C age (years ± 2σ)	Calibrated age (years ± 2σ)	Reference
65	TP5		12,400 ± 150	13,811 ± 412	Jessen et al., 2010
120	TP6		12,700 ± 150	14,289 ± 508	Jessen et al., 2010
140	UBA-38275	Scaphopod	13,378 ± 49	15,280 ± 237	This work
145	UBA-38276	*N. pachyderma* sx.	14,806 ± 61	17,101 ± 244	This work
220	UBA-38822	*N. pachyderma* sx.	18,195 ± 90	21,074 ± 319	This work
260	TP7		19,710 ± 130	22,785 ± 341	Jessen et al., 2010
291	TP8		20,140 ± 130	23,320 ± 356	Jessen et al., 2010
306	TP9		22,900 ± 200	26,320 ± 477	Jessen et al., 2010
315	UBA-38823	*N. pachyderma* sx.	23,420 ± 129	26,786 ± 351	This work
460	UBA-38824	Bivalve	33,662 ± 362	37,652 ± 1,023	This work
495	UBA-42495	*N. pachyderma* sx.	26,360 ± 269	29,693 ± 547	This work[a]
590	UBA-41568	*N. pachyderma* sx.	36,514 ± 1,206	40,519 ± 1,696	This work

[a]Not used due too low carbon content.

3. Material and Methods

Piston core HH15-1252PC (79.04°N; 6.89°E) was retrieved from undisturbed contourite deposits north of Vestnesa Ridge, where no modern methane seepage occurs (Figure 1c). The 9.35 m long core was taken during a cruise with RV *Helmer Hanssen* in July 2015 from a water depth of 1,273 m (Figures 1a and 1c).

3.1. Core Handling and Sampling

The core was cut into 1-m sections, capped and taped at both ends, and stored at 4°C. Prior to opening, magnetic susceptibility was measured with a Bartington MS2 loop sensor. Thereafter the core sections were split longitudinally and the archive halves were X-rayed with a GEOTEK Multi Sensor Core Logger and color imaged with a Jai L-107CC 3 CCD RGB line scan camera installed on an Avaatech XRF.

The core was sampled in 1-cm-thick slices at 1–5 cm intervals. Samples were weighed, freeze-dried, and weighed again. They were subsequently wet-sieved over mesh-sizes 63, 100, and 500 μm. The residues were dried at 40°C and weighed and weight percent of each grain size was calculated.

3.2. AMS ^{14}C Dating

Seven AMS-^{14}C dates were performed on monospecific planktic foraminiferal samples and mollusks at the Chrono Centre of Queen's University, Belfast, Northern Ireland, UK) (Table 1). The radiocarbon dates were calibrated using the Marine20 calibration curve (Heaton et al., 2020) using CLAM 2.3.2. package in R software (Blaauw, 2010; Table 1).

3.3. Stable Isotope Analyses

Oxygen and carbon isotopes were measured on pristine tests of the benthic foraminiferal species *Cassidulina neoteretis* or *Melonis barleeanus* (150–250 μm size fraction; 31 overlapping samples), and planktic foraminiferal species *Neogloboquadrina pachyderma* (100–500 μm size fraction). We picked specimens with 4-chambers and avoided the largest and smallest tests within the 100–500 μm range. Up to 20 specimens of each species were analyzed on a Thermo Scientific MAT253 IRMS and Gasbench II at the Department of Geosciences, UiT the Arctic University of Norway, Tromsø, Norway. The analytical precision of the instrument is 0.1‰ for carbon and oxygen isotopes. The results are reported against the Vienna Peedee Belemnite

in-house standard. The δ^{18}O values of *M. barleeanus* were corrected by +0.4‰ to adjust for vital effects (Duplessy et al., 1980).

3.4. Element/Ca Analyses

For elemental analyses 10 to 30 pristine tests of *C. neoteretis* (150–250 μm size fraction), or *M. barleeanus* (150–350 μm size fraction), were picked and carefully crushed between two glass slides. *C. neoteretis*, the dominant benthic species in the record was selected. In some intervals, due to low occurrence of *C. neoteretis*, the second most common species *M. barleeanus* was measured ensuring overlap when possible. The samples were cleaned following the oxidative-reductive approach (Boyle & Keigwin, 1985/1986; Pena et al., 2005). The cleaning steps included removal of clay, reductive cleaning with hydrous hydrazine, oxidative cleaning with an alkali-buffered solution of hydrogen peroxide, and finally weak acid leaching. The samples were subsequently dissolved in HNO$_3$ (0.1 M) and analyzed using an inductively coupled plasma-optical emission spectrometer (Agilent 5100 ICP-OES) at the Department of Earth Sciences at the University of Cambridge, UK, to measure the [Ca^{2+}]. Samples were analyzed again at fixed [Ca^{2+}] following the method of de Villiers et al. (2002), with concentrations ranging from 10 to 20 ppm of [Ca^{2+}] used because of the small amount of material available for these samples. Two samples fell outside this range (8.8 and 9.2 ppm), but were retained in this investigation due to their consistency with the rest of the data set. Repeated measurements of an in-house standard solution with Mg/Ca of 1.46 mmol/mol showed a precision of 1.16% when run at a calcium concentration of 20 ppm during the analysis period, in comparison with a long-term precision of 0.53% for the same standard when run at a calcium concentration of 100 ppm over the 2-year period from July 2017 to July 2019.

Elemental ratios Mn/Ca, Fe/Ca, Al/Ca, and Na/Ca were used in combination to evaluate potential contamination. Thirteen samples were excluded because of indication of potential contamination shown by anomalously high values of Mn/Ca, Fe/Ca, Al/Ca, and Na/Ca (Table S1). The remaining samples showed small correlation between Mn/Ca, Fe/Ca, and Mg/Ca ($r^2 = 0.02$ for *C. neoteretis* and $r^2 = 0.34$ for *M. barleeanus* Mn/Ca-Mg/Ca; $r^2 = 0.08$ for *C. neoteretis* and $r^2 = 0.37$ for *M. barleeanus* Fe/Ca-Mg/Ca; Figure S2). Aluminum concentrations were under detection limits in 90% of the samples.

In order to obtain BWT changes, the Mg/Ca values were converted into temperature values using the calibration formulas from the Iceland shelf published by Kristjánsdóttir et al. (2007):

$$\mathrm{Mg/Ca}_{C.neoteretis} = 0.864 \pm 0.07 \times \exp\left(0.082 \pm 0.020 \times \mathrm{BWT}\right)$$

$$\mathrm{Mg/Ca}_{M.barleeanus} = 0.658 \pm 0.07 \times \exp\left(0.137 \pm 0.020 \times \mathrm{BWT}\right)$$

The data set of Kristjánsdóttir et al. (2007) comprise 10 surface samples containing living *C. neoteretis* and 31 samples of *M. barleeanus* from the Iceland shelf at water depths ranging from 211 to 637 m. Their Mg/Ca values range from 0.93 to 1.38 mmol/mol and 0.64 to 2.21 for *C. neoteretis* and *M. barleeanus*, respectively. Their BWT cover a temperature range from 0.19°C to 6.99°C. The equation from Barrientos et al. (2018) includes the *C. neoteretis* samples from Kristjánsdóttir et al. (2007) with the addition of 15 new core-top samples from the central Arctic Ocean. However, the calculated BWT based on our Mg/Ca data and the calibration formula by Barrientos et al. (2018) gave physically unrealistic values (down to −8.31°C; Figure S3). The calibration equation presented by Hansefrantz et al. (2018) for *M. barleeanus* and the equation presented in Sessford et al. (2018) for *C. neoteretis* do not change the reconstructed relative changes (Figure S3).

For *C. neoteretis*, the calibration of our Mg/Ca values based on the equation of Kristjánsdóttir et al. (2007) gave results of BWT varying from −1.78°C to 5.26°C downcore (ranging from 0.75 to 1.33 mmol/mol). One sample reached −2.36°C due to its low Mg/Ca (0.71 mmol/mol), however, it falls within the error of estimate of ±0.62°C of the calibration. For *M. barleeanus*, calibration based on the equation from Kristjánsdóttir et al. (2007) resulted in BWT estimates from −1.09°C to 2.99°C (Mg/Ca values range from 0.57 to 0.99 mmol/mol). The standard error of the estimate is ±1.1°C (Kristjánsdóttir et al., 2007).

We used the analytical error (±0.036 mmol/mol as 2 times the mean standard deviation) and the calibration errors from Kristjánsdóttir et al. (2007) to calculate the propagation error (calculated as the squared root

of the sum of the squared errors). Accordingly, the average of the estimated errors in BWT are ±1.03°C and ± 1.27°C for *C. neoteretis* and *M. barleeanus*, respectively.

3.5. Benthic Foraminiferal Analysis

Whenever possible, a total of >300 benthic foraminifera were counted from the 100–1,000 μm size fraction (the >500 μm fraction was dry-sieved with a 1-mm mesh size sieve). A total of 174 samples were counted of which 150 samples contained >300 specimens. Samples containing less than 100 specimens are considered to be nonrepresentative (Fatela & Taborda, 2002), but presented here when >50 specimens were counted. The foraminifera were identified to species level and relative abundance (%) calculated. The concentration (no. of tests/gram dry weight sediment) was also calculated.

3.6. Ice-Rafted Debris

IRD was counted on the >500 μm and the 150–500 μm size fractions, and the concentration of IRD grains per sample (no. of IRD/gram dry weight sediment) was calculated. To count IRD in the 150–500 μm size fraction, the 100–500 μm fraction was dry sieved using a 150-μm mesh-size sieve. Here, at least 300 mineral grains per sample were counted and the concentration calculated.

In order to differentiate the origin between sea ice and iceberg transported IRD, the grain-size ratio was calculated using the equation from Jessen and Rasmussen (2019):

$$\frac{(\text{no. of IRD} > 500\,\mu m\, /\, \text{no. of IRD}\,150 - 500\,\mu m)_{\text{sample}}}{(\text{no. of IRD} > 500\,\mu m\, /\, \text{no. of IRD}\,150 - 500\,\mu m)_{\text{average}}}$$

Although sea ice can transport any size of sediment grains, sea ice is more likely to transport fine-grained sediments (150–500 μm) compared to icebergs that can transport generally coarser material (Dowdeswell & Dowdeswell, 1989; Jessen & Rasmussen, 2019). Therefore, a grain-size ratio <1 would indicate a higher proportion of sea-ice transported grains, whereas a ratio >1 would indicate that IRD was likely transported by icebergs (Jessen & Rasmussen, 2019).

4. Results

4.1. AMS [14]C Dates

The calibrated ^{14}C dates and re-calibrated magnetic susceptibility tie-point dates (see Section 4.4. below) show that the age of the core for the interval between 5.46 and 0.65 m ranges from 40.5 to 13.8 ka (Table 1). The age at 4.95 m is considered too young and was discarded (Table 1). This is probably because the sample size was too low, which led to a too low content of graphite, increasing the impact of potential contamination with modern carbon (e.g., Gottschalk et al., 2018; Ruff et al., 2010).

4.2. Bottom Water Temperatures and Oxygen Isotopes

Mg/Ca values vary from 0.71 to 1.33 mmol/mol for *C. neoteretis* and from 0.56 to 0.99 mmol/mol for *M. barleeanus*. Using the calibrations of Kristjánsdóttir et al. (2007) and combining the records, BWT varies from −2.36°C to 5.26°C, and is 0.8°C in average (Figures 3 and 4). Seven samples of Mg/Ca were measured in both species and show that the difference in BWT calculated from the two species is 0.72°C ± 0.17°C.

The $\delta^{18}O$ of *C. neoteretis* $\delta^{18}O$ vary from 5.85‰ to 4.03‰ and *M. barleeanus* varies from 5.7‰ to 4.76‰. The values for the two species are in accordance for the upper 6.5 m (between 12 and 44 ka; Figure 4). Below 6.5 m (before 44 ka), both species show divergent $\delta^{18}O$ values and *M. barleenus* $\delta^{18}O$ remains generally higher with values ranging from 5.82‰ to 4.24‰ (Figure 4). In the upper part, the difference of $\delta^{18}O$ between *M. barleeanus* (after correction) and *C. neoteretis* (i.e., $\delta^{18}O_{M.\ barleeanus}$ minus $\delta^{18}O_{C.\ neoteretis}$) is 0.16 ± 0.03‰ (*n* = 9) and in the lower (below 6.50 m) 0.58 ± 0.07‰ (*n* = 22).

4.3. Benthic Foraminifera

Over 60 benthic foraminiferal species were identified in core HH15-1252PC. Almost 10% of the investigated samples contained less than 50 benthic foraminiferal specimens. The most abundant species is *C. neoteretis* (43% on average throughout the record and present in all samples except one)*,* followed by *Cassidulina reniforme* and *M. barleeanus.* Other present species are *Astrononion gallowayi* and *Cibicides lobatulus* (presented together due to similar ecological preferences; Table 2), *Islandiella norcrossi, Elphidium* spp. (predominantly *E. excavatum*), *Nonionella* spp., and *Stainforthia* spp. Warm-water benthic species normally absent in the deep Nordic seas today include: *Bulimina costata*, *Sigmoilopsis schlumbergeri*, *Cibicidoides pachyderma*, *Gyroidina umbonata*, *Eggerella bradyi*, *Discospirina italica*, *Spirophthalmidium acutimargo*, *Sagraina subspinescens*, and *Anomalinoides minimus*. They have been grouped together as the "Atlantic species" group sensu (T. L. Rasmussen et al., 1996a). *Pyrgo serrata* has also been included in the group since it follows the distribution pattern of the other species. The group is restricted to a narrow horizon at 1.45–1.47 m (at ca. 17 ka) correlating with minimum $\delta^{18}O$ values (Figures 3 and 4). The ecological preferences of the most representative benthic foraminiferal species are given in Table 2.

4.4. Construction of the Age Model

The age-depth model of core HH15-1252PC was constructed using the planktic foraminiferal $\delta^{18}O$ record, supported by the magnetic susceptibility and the distribution of *C. neoteretis* (Figure 2). Marine isotope stage (MIS) 3 (from 9.1 m to 3.61 m depth in core) and MIS 2 (3.61 m to the top of the core) are identified by their characteristic planktic foraminiferal $\delta^{18}O$ (Figure 2). Additionally, the MIS 4/MIS 3 transition and early MIS 3 are characterized by high content of coarse IRD (Jessen et al., 2019) and the percentage of *C. neoteretis* exceeds 70% in MIS 2 (T. L. Rasmussen et al., 2014b; Sztybor & Rasmussen, 2017) and top MIS 4 (T. L. Rasmussen et al., 2014b) (Figure 3).

GI and GS events are recognized by correlating the planktic foraminiferal $\delta^{18}O$ to the $\delta^{18}O$ record in the North Greenland Ice Project (NGRIP) ice core with the GICC05modelext timescale b2k (= before 2 ka) (S.O. Rasmussen et al., 2014a; Svensson et al., 2008; Wolff et al., 2010). This relies on earlier results that show that low planktic $\delta^{18}O$ are caused by increased meltwater supply during GSs (e.g., Bond et al., 1993) (Figure 2). In addition, the distribution of the benthic foraminiferal species *C. neoteretis* follows the pattern of dominance of the polar planktic foraminiferal species *N. pachyderma* in modern settings (Lubinski et al., 2001; Polyak & Mikhailov, 1999). These species are most abundant in stadials in the North Atlantic and Nordic seas (e.g., Bond et al., 1993; T. L. Rasmussen & Thomsen, 2004). Therefore, the peaks of maximum percentages of *C. neoteretis* have been used here for further identification of stadial intervals (Figure 2). With this tuning to the ice core time scale, all ages are referring to b2k in the following.

The "24-ka event" (Jessen & Rasmussen, 2019) is a debris flow event followed by a pronounced deposition of IRD that occurred near-synchronously at the western Svalbard slope within a time interval of 500 years (Jessen et al., 2010). The lower boundary of the event at 2.92 m is coeval to the beginning of GI2/end of HS2. In order to reflect the rapid debris flow a tie-point was set 500 years earlier at the lower boundary of the event (22.84 ka at 2.65 m) (Figure 2).

The age model is also tested by the comparison of core HH15-1252PC to the magnetic susceptibility and planktic $\delta^{18}O$ of core JM11-19PC from the SE Norwegian Sea, which is independently tuned to the NGRIP ice core time scale (Ezat et al., 2014) (Figure 2). This core has been studied in great detail and includes well-described and well-dated tephra layers that can serve as direct tie-points to the NGRIP ice core (Davies et al., 2010, 2008; Ezat et al., 2014; Griggs et al., 2014; Wastegård & Rasmussen, 2014). The planktic $\delta^{18}O$ of both cores align and therefore strongly support our age-depth model (Figure S4).

In addition to AMS ^{14}C dates in core HH15-1252PC, magnetic susceptibility tie-points (TP5–TP9) are identified based on the reference magnetic susceptibility stack record for the western Svalbard slope (Jessen et al., 2010). The corresponding depths in the core and re-calibrated age for each tie-point are presented in Table 1. These dates are compared to the age-depth model in order to confirm the correlation between our sedimentary record and the ice core record. The age model curves are nearly parallel and the average difference between the estimated ages by the tuning to NGRIP and the calibrated ages is 509 ± 164 years (excluding the ^{14}C age at 4.95 m depth), which could be attributed to past changes in reservoir ages (Ezat

Table 2
Environmental Preference of Most Representative Benthic Foraminiferal Species in Core HH15-1252PC

Species	Environmental preference	Reference
Cassidulina neoteretis	Shallow infaunal. Cooled Atlantic origin waters with BWT from −1°C to 5.5°C (−1°C to 2°C in the slope). Found in organic-rich terrigenous fine-grained mud and responding to phytoplankton blooms. Present in seasonally ice-free sites and rare in permanently ice-covered areas.	Gooday & Lambshead, 1989; Jennings & Helgadottir, 1994; Kristjánsdóttir et al., 2007; Mackensen & Hald, 1988; Mackensen et al., 1985; Wollenburg & Kuhnt, 2000; Wollenburg & Mackensen, 1998
Melonis barleeanus	Deep to intermediate infaunal. Might migrate in the sediment column during times of food starvation. Feeds on altered organic detritus and it is related to high organic fluxes and stable primary productivity.	Caralp, 1989; Corliss, 1985; Linke & Lutze, 1993; Mackensen et al., 2000; Schönfeld, 2001; Wollenburg & Kuhnt, 2000
Cassidulina reniforme	Often in ice-distal glaciomarine environments. Prefers BWT <2°C and high food supply.	Hald & Korsun, 1997; Jernas et al., 2018; Mudie et al., 1984; Polyak et al., 2002; Steinsund, 1994
Astrononion gallowayi and Cibicidoides lobatulus	Occur in cold waters with coarse sediments and strong current activity.	Polyak et al., 2002; Sejrup et al., 1981; Steinsund, 1994; Wollenburg & Mackensen, 1998
Elphidium spp.	Sea-ice-edge related species. It can occur in varying and unstable conditions with low temperature and salinity and high turbidity.	Hald & Korsun, 1997; Korsun & Hald, 2000; Steinsund, 1994
Nonionella spp.	Indicator of high productivity areas. Feeds ion seasonally produced fresh phytodetritus, although it is capable of surviving prolonged starvation periods	Cedhagen, 1991; Gooday & Hughes, 2002; Korsun & Hald, 1998; Steinsund, 1994
Stainforthia spp.	Opportunistic species related to cold waters in high productivity areas covered seasonally by sea ice or areas where the sea ice margin is located. *S. fusiformis* and *S. feylingi* cope well with anoxic or low oxygen environments caused likely by high input of fresh food by algal blooms. *S. fusiformis* is also an indicator of rapidly changing environmental conditions	Alve, 1995, 2003; Hald & Korsun, 1997; Polyak et al., 2002; Seidenkrantz, 2013; Steinsund, 1994
"Atlantic species" group	Group consisting of species commonly found today at mid-latitudes in the North Atlantic and Mediterranean in BWT >2°C. Mainly phytodetritus species depending on pulsed food supply.	Rasmussen et al., 1996a, 1996b; Wollenburg & Mackensen, 1998; Wollenburg et al., 2004

et al., 2017b; Thornalley et al., 2015). This further validates our marine record-ice core synchronization (Figure 2). The sources of uncertainty in our age-depth model originate from (1) the uncertainties related to the identification of annual layers in NGRIP at GICC05modelext timescale (Svensson et al., 2016) and (2) the tuning between planktic foraminiferal $\delta^{18}O$ and the NGRIP $\delta^{18}O$. The core covers the end of MIS 4 to the end of MIS 2, from 63.8 to 12.9 ka.

5. Discussion

Together the planktic and benthic $\delta^{18}O$, IRD, BWT and benthic foraminiferal distribution patterns show clear millennial-scale variability (Figures 3 and 4). In general, low planktic and benthic $\delta^{18}O$ are linked to increases in BWT.

Benthic foraminiferal $\delta^{13}C$ have been widely used to track methane seepage from gas-influenced sediments by anomalously low $\delta^{13}C$ (e.g., Wefer et al., 1994). The $\delta^{13}C$ values of *C. neoteretis* and *M. barleeanus* range between −1.46‰ to −0.15‰ and −2.28‰ to −0.13‰ throughout the record, respectively. These values are within the range of "normal" carbon isotopes signatures for the species (Mackensen & Schmiedl, 2019; McCorkle et al., 1990) and therefore, the presence of methane affecting core HH15-1252PC can be excluded.
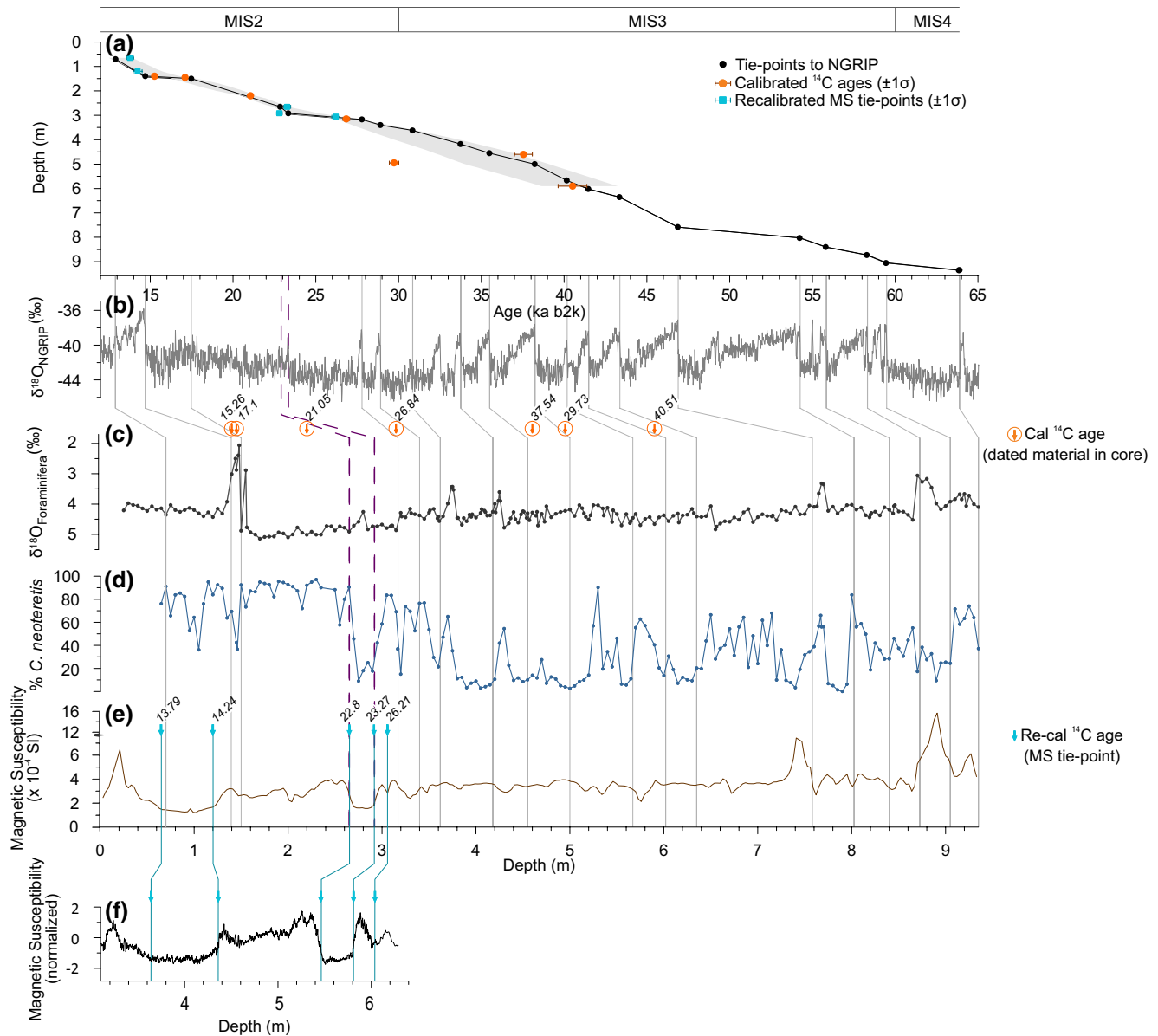
Figure 2. (a) Age-depth model of core HH15-1252PC constructed by correlating to (b) NGRIP ice-core with the GICC05modelext timescale (S.O. Rasmussen et al., 2014a; Svensson et al., 2008; Wolff et al., 2010). The shaded gray area in panel (a) shows the 95% confidence interval of the age-depth model with the calibrated radiocarbon ages. (c) δ¹⁸O measured in planktic foraminiferal species *Neogloboquadrina pachyderma*. (d) Relative abundance of *Cassidulina neoteretis*. (e) Magnetic susceptibility of HH15-1252PC. (f) Magnetic susceptibility stack for the western Svalbard margin (Jessen et al., 2010). (e) Blue lines show the correlation between the magnetic susceptibility of core HH15-1252PC and (f) the western Svalbard magnetic susceptibility stack. (c–e) Gray lines indicate the correlation between core HH15-1252PC. Dashed purple lines show the upper and lower boundaries of the "24 ka event". Tie-point (TP) dates (blue vertical arrows) and calibrated ¹⁴C dates performed in core HH15-1252PC (orange encircled vertical arrows) were used to confirm the tuning between our sediment core and NGRIP. Figure S4 shows the same data plotted against age.

5.1. Orbital Scale Changes

During the MIS 4/3 transition and early MIS 3 (64-55 ka), the content of coarse IRD deposited from icebergs increases (Figure 4). Benthic foraminiferal concentrations are generally low. *Cassidulina neoteretis* and *M. barleeanus* coexist in the interval, opposite to the rest of the record where they alternate in proportions, with *C. neoteretis* in general being the most abundant species of the two (Figure 3). In modern sediments at mid-depth on the slope of the Nordic Seas, *C. neoteretis* and *M. barleeanus* are some of the most common benthic foraminiferal species (Belanger & Streeter, 1980; Mackensen et al., 1985; Sejrup et al., 1981; Wollenburg &
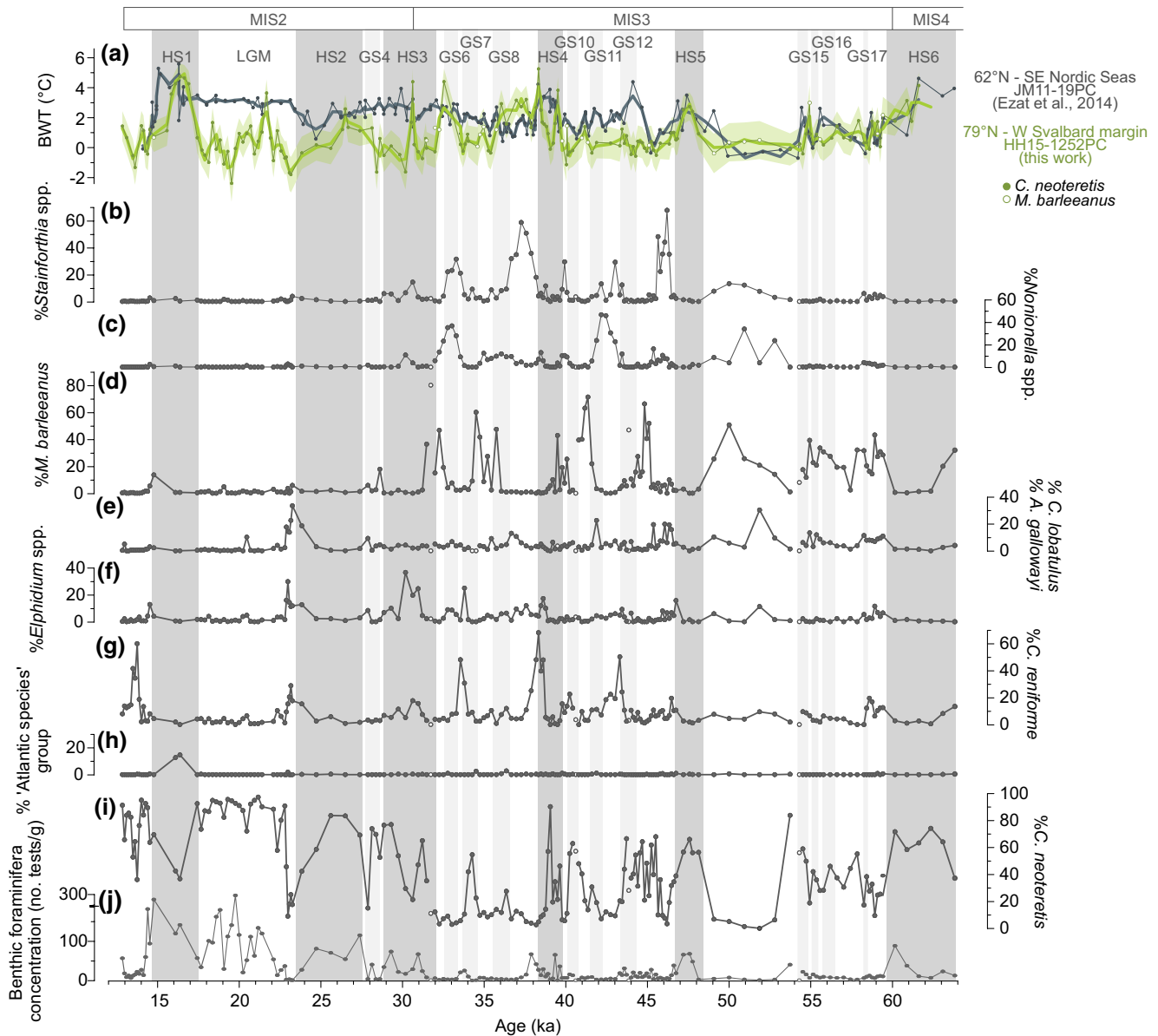
Figure 3. Records of core HH15-1252PC plotted versus GICC05modelext timescale (ka b2k; S.O. Rasmussen et al., 2014a; Svensson et al., 2008; Wolff et al., 2010). (a) Reconstructed bottom water temperature (BWT) from the northern Nordic Seas (core HH15-1252PC; this work) and southern Nordic Seas (JM11-19PC; Ezat et al., 2014). Light green shading indicates uncertainty interval calculated with error propagation in core HH15-1252PC. Thick line in both records shows smoothed records with Savitzky-Golay filtering. (b–i) Relative abundance of representative benthic foraminiferal species. (j) Concentration of benthic foraminiferal tests in number of specimens per g dry weight sediment. Open dots in (b–j) indicate samples with <50 benthic foraminifera per sample. Dark gray bands mark Heinrich Stadials (HS) and light gray bands Greenland Stadials (GS).

Mackensen, 1998). During early to mid MIS 3 (58-49 ka), the BWT remain relatively stable (except during GS and HS) with temperatures ca. 0.4°C for this period. The similarities between the benthic assemblage composition and the BWT with modern characteristics of the area indicate bottom water conditions similar to modern, with cold BWT implying deep convection (Figure 3). Planktic δ18O show an increasing trend during MIS 3 (Figure 4).

A reduced Svalbard-Barents Sea Ice Sheet (SBIS) has been proposed for MIS 3 (Batchelor et al., 2019; Hughes et al., 2016; Jessen & Rasmussen, 2019). This is in agreement with the low concentration or absence of coarse IRD from mid to late MIS 3 (Figure 4). The grain-size ratio (<1) instead points to a higher abundance of rafted debris coming from sea ice. This is in accordance with the presence of benthic foraminiferal spe-
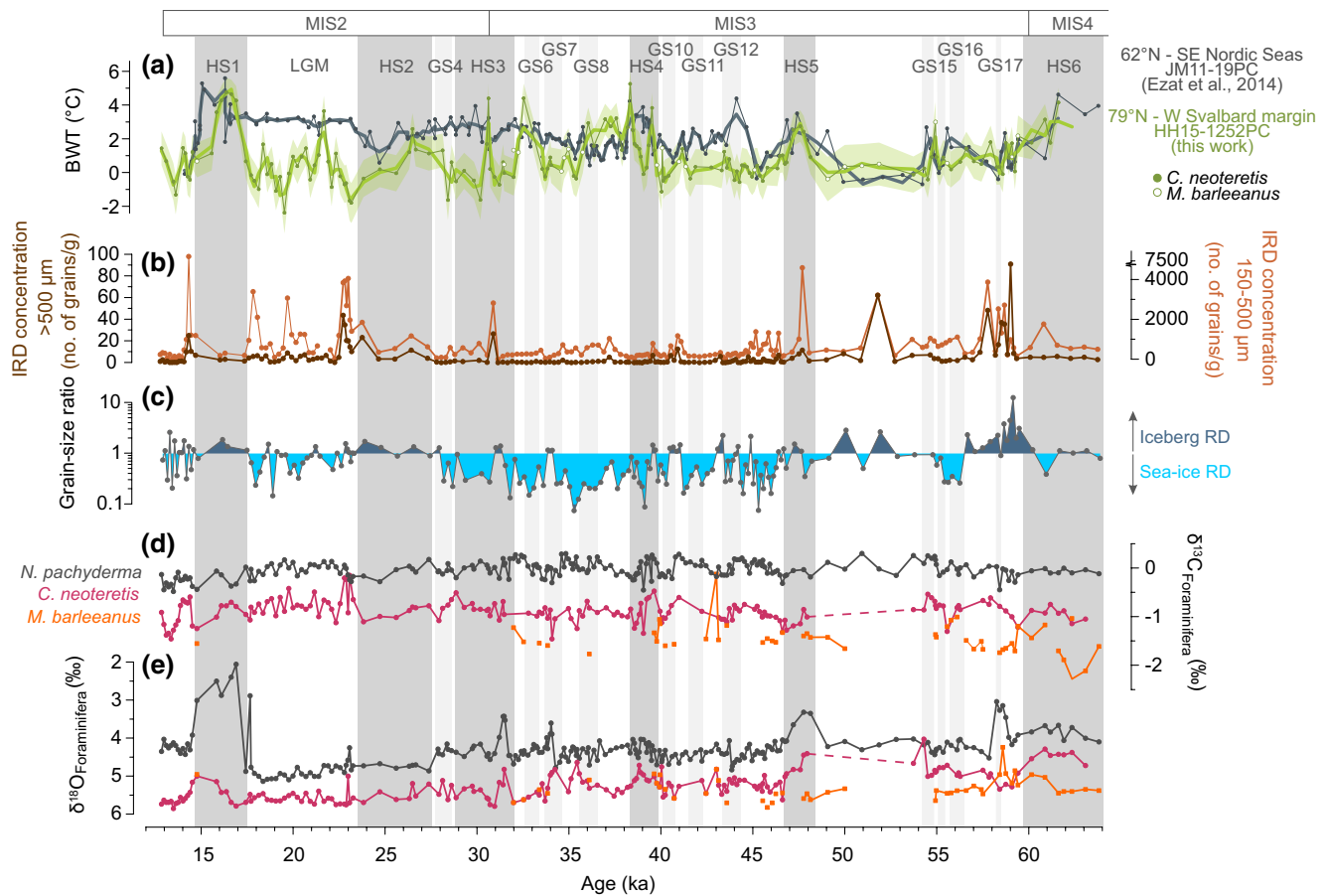
Figure 4. Records of core HH15-1252PC plotted versus with the GICC05modelext timescale (ka b2k; S.O. Rasmussen et al., 2014a; Svensson et al., 2008; Wolff et al., 2010). (a) Reconstructed bottom water temperature (BWT) (see text to Figure 3 for explanation). (b) Concentration of ice rafted debris (IRD) in number per gram dry weight sediment in 150–500 μm and >500 μm size fractions. (c) Grain-size ratio of IRD size fractions 150–500 μm/>500 μm; values > 1 indicate iceberg rafted debris and <1 indicate sea ice rafted debris (Jessen & Rasmussen, 2019). (d) δ¹³C measured in benthic foraminiferal species *Cassidulina neoteretis* and *Melonis barleeanus* and planktic species *Neogloboquadrina pachyderma*. (e) δ¹⁸O of the same species as in (d). Dark gray bands mark Heinrich Stadials (HS) and light gray bands Greenland Stadials (GS).

cies known to feed on phytodetritus (e.g., *Nonionella* spp., *Stainforthia* spp.) indicating presence of seasonal sea ice or the marginal ice zone (Figure 3 and Table 2).

During MIS 2 (30-11.7 ka), the concentration of coarse IRD is high compared to MIS 3 and planktic foraminiferal δ¹⁸O are also high (Figure 4). Jessen and Rasmussen (2019) suggested an extensive SBIS based on high planktic foraminiferal δ¹⁸O, presence of allochthonous coarse IRD and absence of local IRD. Although the origin of the IRD is not investigated in this work, the proximity of the two study areas and the increased presence of medium to coarse sandy materials together with the high planktic δ¹⁸O values during MIS 2 in core HH15-1252PC, also point to minimal local ice loss and an extensive SBIS. The BWT is variable throughout MIS 2, but remains within the limits of modern BWT at the study site, except for HS1, discussed further below. The dominance of *C. neoteretis* of high concentrations in MIS 2 indicates an amelioration of the oceanic conditions with an overall increased influence of AW in the study area and higher productivity (Seidenkrantz, 1995; Wollenburg et al., 2004) (Figure 3). This is further supported by the generally high concentrations of benthic foraminifera (up to ca. 300 tests/gram dry weight sediment during the LGM and late HS1).

During the last glacial maximum in MIS 2 (LGM; 24-19 ka) our core records variable BWT compared to the southern Nordic Seas (Ezat et al., 2014) (Figures 3, 4, and S4). The start of MIS 2, during HS2, in the western Svalbard margin is marked by a synchronous BWT decrease and high concentrations of coarse IRD indicating an increased production of icebergs related to the growth of the SBIS or a re-activation of

ice-streams (Jessen et al., 2010; Winsborrow et al., 2010) (Figure 4). This event also correlates to an event of anomalously low magnetic susceptibility around 24 ka BP (the "24-ka mass transport/IRD event" of Jessen & Rasmussen, 2019; see also above) and occurring at the end of HS2/beginning of GI2 (Jessen & Rasmussen, 2019; Jessen et al., 2010; T. L. Rasmussen et al., 2007). In core HH15-1252PC, the concentration of benthic foraminifera is low and species related to coarser sediments and stronger current activity such as *A. gallowayi* and *C. lobatulus* occur (Figure 3 and Table 2). Evidence of a similar mass transport event with similar timing is found all along the northwestern Barents Sea (Jessen & Rasmussen, 2019; Jessen et al., 2010; Laberg & Vorren, 1995; Vorren et al., 1998) and reaching to the Yermak Plateau (Chauhan et al., 2014; Howe et al., 2007). Jessen and Rasmussen (2019) interpret this event as increased slope instability and iceberg calving and thinning of the ice-sheet as it reached the shelf break.

Debris flow events could have entrained fresh cold shelf water via a hyperpycnal flow into the deepest basins (Stanford et al., 2011). The high benthic δ^{13}C (up to −0.15‰) observed contemporaneously with the debris flow event could reflect the input of well-ventilated shelf waters and the generally high benthic δ^{18}O (ca 5.7‰) are indicative of the cold BWT. Another hypothesis to explain the low temperatures during this interval involves dense cold brines (high benthic δ^{18}O and δ^{13}C; Mackensen et al., 2016; T. L. Rasmussen & Thomsen, 2009) formed on the shelf of Spitsbergen and reaching the study area. The low abundance of benthic foraminifera in this interval could be due to the corrosive nature of brines (e.g., Fossile et al., 2020) (Figure 3j). In addition, the increased relative abundances of the typical interstadial species *C. reniforme, C. lobatulus*, and *A. gallowayi* and decrease in % *C. neoteretis* (e.g., T. L. Rasmussen et al., 2014b; see also Section 5.2.1. below) confirm the presence of relatively cold saline waters (Steinsund, 1994) and precludes downtransportation of specimens. Knies et al. (2018) suggested the existence of a large polynya in front of the SBIS caused by strong easterly katabatic winds and a strong polar front pushing the sea ice eastwards during the LGM period (27-19.5 ka). This scenario could facilitate the formation of seasonal sea ice and brine rejection, and consequently the formation of a very dense cold, water mass formed in the coastal area and flowing downslope to our core site (Figure 5b).

5.2. Millennial-Scale Paleoceanographic Changes

5.2.1. Greenland Interstadials

In Greenland ice cores, interstadials are characterized by a short-lasting peak in maximum temperature followed by gradual cooling (Johnsen et al., 1992, 2001; Kindler et al., 2014). In core HH15-1252PC the end of stadials and beginning of interstadials, the % *Elphidium* spp. seems to increase followed by increase in % *C. reniforme* (most clearly seen in the transitions HS4–GI12, GS12–GI11, and GS7–GI6; Figure 3). In these environments, a replacement of *Elphidium* spp. by *C. reniforme* is interpreted as ameliorated conditions by increased primary production after a melting event (Korsun & Hald, 1998). Early during the GIs, the appearance and subsequent decrease of coarser IRD is also indicative of increased calving and melting due to the sea surface and atmospheric warming (Jessen & Rasmussen, 2019; T. L. Rasmussen & Thomsen, 2013) (Figures 3 and 5).

In the mid-late part of some interstadials, the phytodetritus species *Stainforthia* spp. and *Nonionella* spp. become dominant, particularly during MIS 3 (Figure 3). Their presence indicate that the core site must have been under the influence of the high-productivity zones of the marginal ice zone with increased seasonal sea-ice cover (Polyak et al., 2013; Figure 5). The relative dominance in the foraminiferal assemblages of *M. barleeanus* demonstrate the establishment of high and stable productivity during some of these interstadial periods (Wollenburg et al., 2001) (Table 2 and Figure 3). The intervals with dominance of *M. barleeanus, Nonionella* spp., and *Stainforthia* spp. are characterized by dissolution and a high degree of fragmentation and low concentrations and flux of faunas as recorded in nearby cores JM05-31GC, JM10-335GC, and JM10-333GC (T. L. Rasmussen et al., 2014b; Sztybor & Rasmussen, 2017) (Figure S1). The high productivity in late interstadials indicated by the composition of the benthic faunas, but with low concentrations is probably caused by the high accumulation rates of organic carbon that could cause dissolution of calcareous specimens (Wollenburg et al., 2004).

Our benthic foraminiferal data and succession of species in the GIs are supported by sea-ice studies in the southern Nordic Seas (Hoff et al., 2016; Wary et al., 2017). A high-resolution study of four D-O events in a
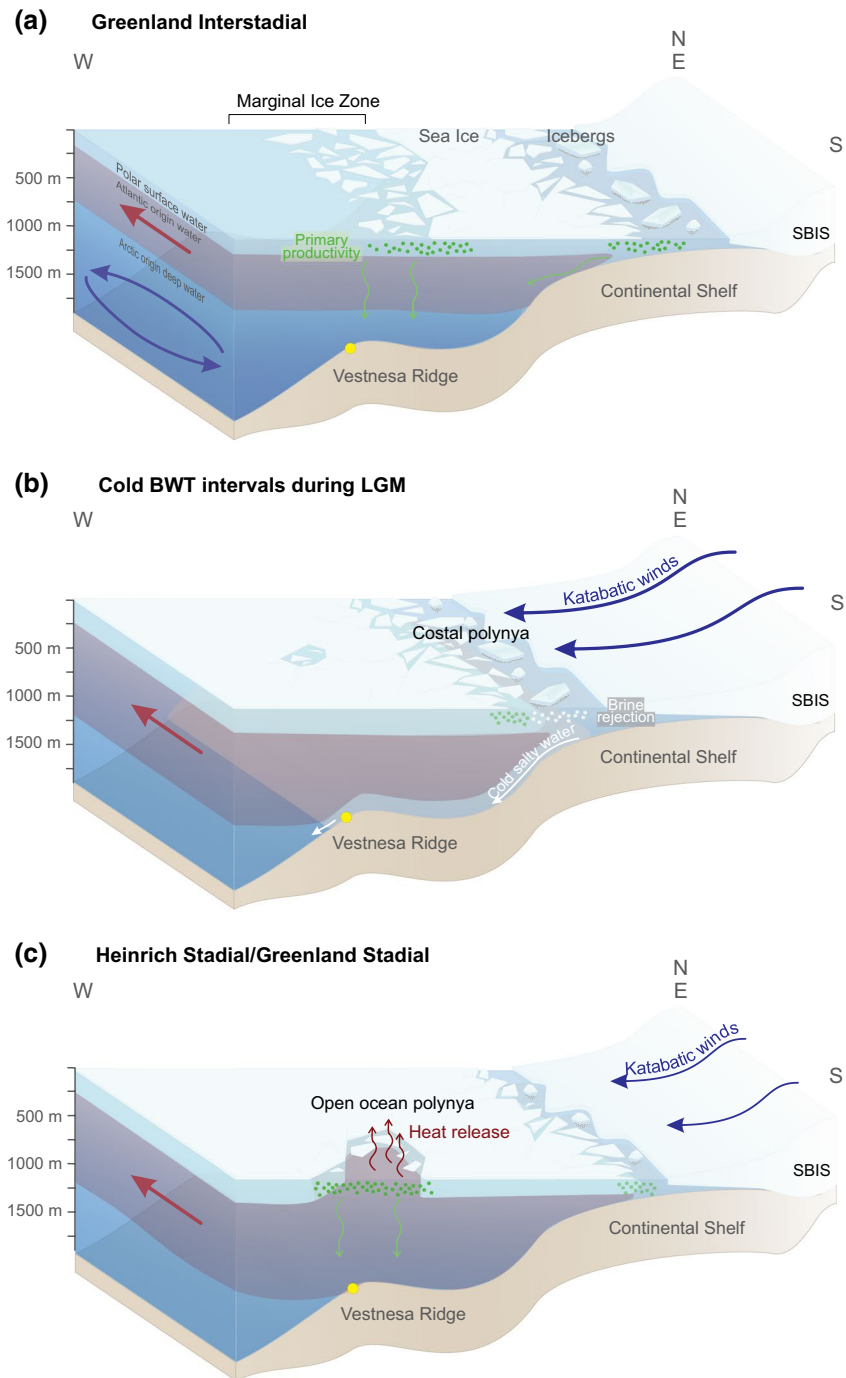
Figure 5. Schematic diagrams showing interpretations of paleoenvironments for (a) Greenland Interstadials, (b) last glacial maximum (LGM), and (c) Heinrich Stadials. Yellow dot shows location of core HH15-1252PC. Abbreviation: SBIS, Svalbard-Barents Sea Ice Sheet.

nearby core have confirmed this result (Sadatzki et al., 2019). Hoff et al. (2016) showed that sea-ice cover decreases abruptly at the start of GIs causing open ocean conditions and phytoplankton blooms. Sadatzki et al. (2019) also suggested that the most extensive open-ocean conditions coincided with the initial GI warming. Highest benthic foraminiferal concentrations occur late in the GS and at the beginning of GIs corresponding to the early GI phytoplankton blooms. By the mid-late GI, concentrations drop abruptly and species with an affinity to conditions at the sea-ice margin increase in relative abundance, as a sign of

the re-growth of sea ice during the interstadial cooling phase (Hoff et al., 2016; T. L. Rasmussen & Thomsen, 2004; Figures 3 and 5). Higher amounts of sea-ice related IRD support the presence of sea ice during these intervals (Figure 4).

Well within the GI, the lowest benthic foraminiferal concentrations coincide with the appearance of *C. lobatulus* and *A. gallowayi* and decrease/disappearance of the phytodetritus related species, indicating stronger bottom current activity (Figure 3). T. L. Rasmussen and Thomsen (2004) suggested that the interstadial oceanic setting was similar to modern conditions, with surface water of Atlantic origin flowing northwards in the Nordic Seas, overlaying a cold deep water created by winter convection. BWT seems to stabilize and be relatively lower than during the related stadial interval, confirming the presence of cooler waters in the area (Figures 3 and 4). In the southern Nordic Seas lower BWTs are also observed during interstadials (Ezat et al., 2014; Sessford et al., 2018, 2019). The strength of the convection decreases during the interstadial cold phase toward the onset of a GS (T. L. Rasmussen & Thomsen, 2004) (Figure 3).

5.2.2. Heinrich Stadials and Greenland Stadials

Both planktic and benthic foraminifera show low $\delta^{18}O$ values during stadials compared to the preceding interstadials (Figure 4). The most pronounced planktic $\delta^{18}O$ decreases occur during HSs in a time window of 1–2 Kyr (e.g., down to 2.06‰ and 3.35‰ during HS1 and HS5, respectively; Figure 3). Benthic $\delta^{18}O$ decreases within the intervals with the lowest planktic $\delta^{18}O$, together with the increase in BWT. Most of the decreases in benthic $\delta^{18}O$ can be explained by the increase in BWT (T. L. Rasmussen & Thomsen, 2004). This is indicated by calculation of local seawater $\delta^{18}O$ based on the combination of the stable isotope values and BWTs in core HH15-1252PC (Text S1 and Figure S5). The low planktic $\delta^{18}O$ has been attributed to low subsurface salinity due to the presence of polar meltwater from melting icebergs causing surface stratification (e.g., Bond et al., 1993) (here originating from the SBIS [e.g., Lekens et al., 2006]).

Environmental conditions with a persistent sea-ice cover, surface stratification due to presence of cold, polar meltwater insulating the AW from the atmosphere cause a decrease in paleoproductivity as seen in the Arctic Ocean today (Wollenburg et al., 2001). This is also indicated by the reduced concentration of the benthic foraminiferal faunas during HSs (Figures 3 and 5). Preservation of foraminifera in GS and HS events are excellent with low fragmentation (T. L. Rasmussen et al., 1996a, 1996b, 2014b). *Cassidulina neoteretis* is almost the only benthic foraminifera present (>70%), indicating at least temporarily ice-free conditions. Localized ice-free areas in a perennially sea-ice covered ocean can be explained by the development of polynyas (Figure 5). These could be caused by intermittent resurfacing of subsurface Atlantic warm and salty waters. Phytoplankton blooms in polynyas could allow the development of a benthic foraminiferal fauna, shown here by the gradually increasing benthic foraminiferal concentrations following BWT maxima (Figure 3).

The highest BWT occur during GSs, with maxima during most HSs, when temperature rises to between 2°C and 5°C (Figures 3 and 4). Greenland stadials GS6, GS8, and GS15 show similar trends, but the warming signals are most consistent during HSs. BWT increases related to HSs have been observed in the northwestern Atlantic and southern Nordic Seas (Ezat et al., 2014; Marcott et al., 2011; T. L. Rasmussen & Thomsen, 2004; T. L. Rasmussen et al., 1996b). At Vestnesa Ridge methane seep sites, the presence of vesicomyid/solemyid bivalves at HS1 has also been suggested as the result of higher BWT (Hansen et al., 2020; Sztybor & Rasmussen, 2017; Thomsen et al., 2019). In our core, the relative abundance of the "Atlantic species" group is high in HS1 (ca. 20% of the assemblage) indicating higher BWTs (Table 2), confirmed by our high Mg/Ca (BWT up to 5°C) (Figure 3). In other cores from the Nordic Seas and North Atlantic Ocean, the group occur during several HS and GS events indicting increased BWT (e.g., Chauhan et al., 2016; Danielsen, 2017; Ezat et al., 2014; Jansen et al., 1983; T. L. Rasmussen & Thomsen, 2004, 2017; T. L. Rasmussen et al., 1996a, 1996b, 2007, 2014b; Wollenburg et al., 2004) (Figure 6). Together with *C. neoteretis* that responds to a number of environmental parameters including higher temperatures, the benthic faunas together generally indicate warmer bottom waters during stadial events (see e.g., Jennings & Helgadottir, 1994; Jennings et al., 2004; Lubinski et al., 2001).

The warming during HSs in the Nordic Seas has previously been explained by the thickening and deepening of the AW down to at least 1,750 m in the absence/reduction of deep water formation (Ezat et al., 2014; T. L. Rasmussen & Thomsen, 2004; T. L. Rasmussen et al., 1996a, 1996b). During GSs and HSs the southeastern
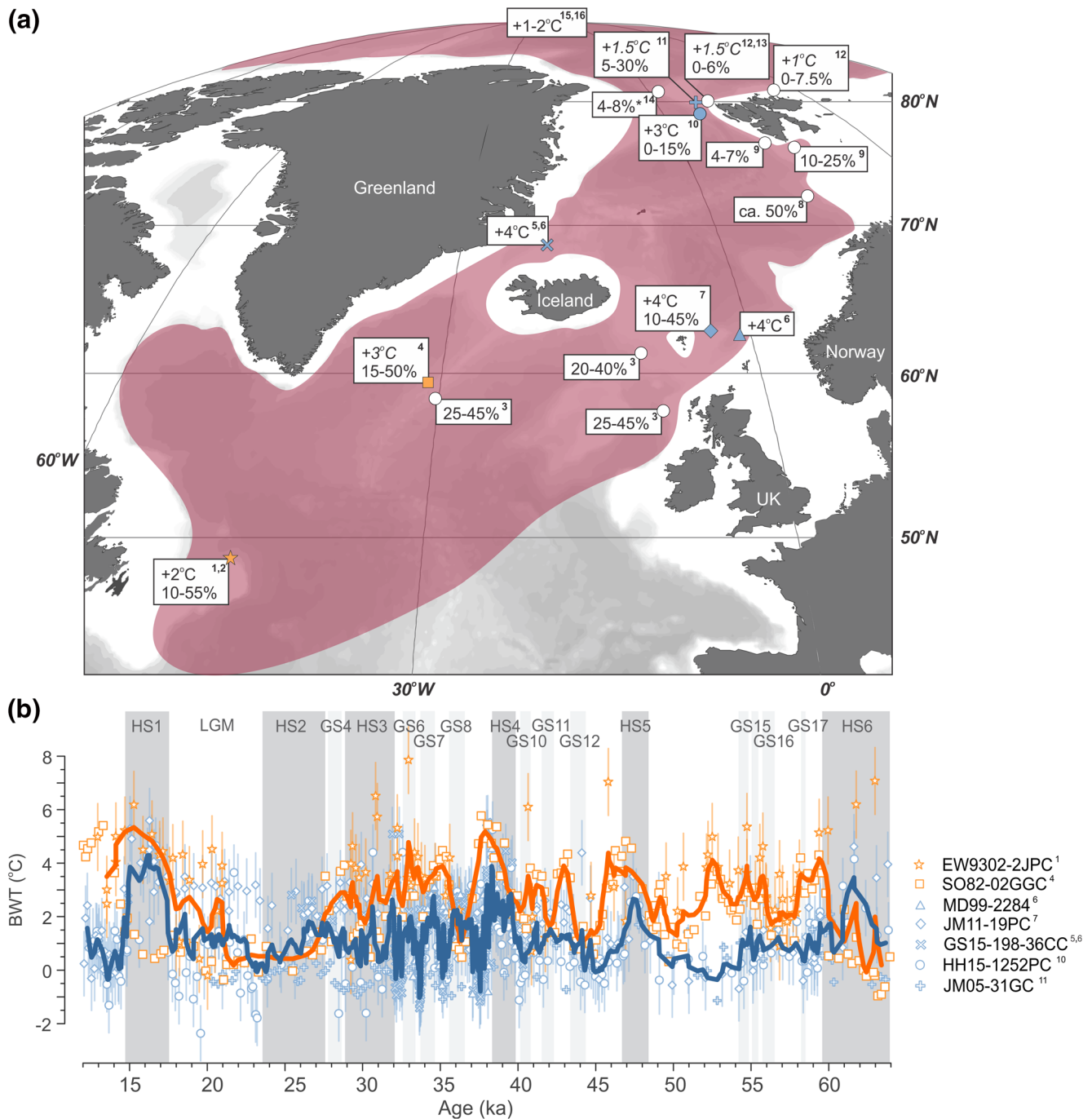
Figure 6. (a) Compilation of core records from the northern North Atlantic Ocean, Nordic Seas, and Arctic Ocean containing the "Atlantic species" group (in percentage; sensu Rasmussen et al. (1996a), except for core no. 13, where the Atlantic species group follows the definition of Wollenburg et al. [2004]) and absolute bottom water temperatures (BWT) (°C) increases during Heinrich Stadials and Greenland Stadials. BWT increases were calculated as difference to the previous interstadial period. BWT given in italics were obtained from benthic foraminiferal transfer functions. Colored area indicates northward Atlantic subsurface intermediate water flow. (b) BWT records compilation for the last 64 ka for water depths between 800 and 1,500 m. Smoothed lines were obtained with five point weighted average. Symbols (orange for the North Atlantic and blue for the Nordic Seas) are the same as in panel (a) to identify each specific core location. References: 1 = Marcott et al. (2011); 2 = T. L. Rasmussen et al. (2003); 3 = T. L. Rasmussen & Thomsen (2004); 4 = T. L. Rasmussen & Thomsen (2017); 5 = Sessford et al. (2018); 6 = Sessford et al. (2019); 7 = Ezat et al. (2014); 8 = Danielsen (2017); 9 = T. L. Rasmussen et al. (2007); 10 = This work; 11 = T. L. Rasmussen et al. (2014b); 12 = Chauhan et al. (2016); 13 = Chauhan et al. (2014); 14 = Wollenburg et al. (2004); 15 = Cronin et al. (2012); 16 = Cronin et al. (2017).

Nordic Seas were persistently covered by (nearly) perennial sea ice during GSs and HSs for the last 90 ka (Hoff et al., 2016). Results from the LGM of nearby core MSM5/5-712-2 from the eastern Fram Strait (Figure S1) showed almost full sea-ice cover (Müller & Stein, 2014) and therefore the Fram Strait probably also was sea-ice covered during earlier GS and HS. A strong halocline (T. L. Rasmussen & Thomsen, 2004; Wary et al., 2017), and extended sea-ice cover would permit the subduction and advection of warm subsurface AWs without losing heat. The stratification would be more pronounced during HSs than during GSs as indicated by the low planktic foraminiferal $\delta^{18}O$, and leading to warmer BWT during HSs than during GS. Another potential cause of the warming of the intermediate water depths are the lower sea level and smaller continental shelf during these periods (Cronin et al., 2012). The subduction of the AW below a stronger halocline occurs today in the northern Fram Strait. There the AW becomes an intermediate water mass, being insulated from the atmosphere below the cold, low-saline polar surface water and cooling only ca. 2°C from the moment it enters the Arctic Ocean through the Fram Strait until it reaches the Chuckchi Sea (Rudels et al., 2004).

A previous reconstruction of BWT based on transfer functions of benthic foraminiferal faunas (i.e., based on an average of the whole assemblage) records a BWT increase of up to 3°C during HSs in the southern Yermak Plateau at ca. 800 m water depth (T. L. Rasmussen et al.,2014b). In the central-northwestern Barents Sea between 448 and 785 m water depth, BWT up to 1.5°C were reconstructed using benthic foraminiferal transfer functions (Chauhan et al., 2014, 2016). During HSs in the North Atlantic and SE Nordic Seas at water depths between 1,200 and 1,500 m, BWT increased to 5.5°C (Ezat et al., 2014; Marcott et al., 2011; Sessford et al., 2018, 2019) and in the Fram Strait our results show a temperature increase to 5°C, based on benthic foraminiferal Mg/Ca (Figure 6). This indicates a minimal heat loss in the Nordic Seas, probably due to the insulation of the subsurface below the strong halocline. In the Arctic Ocean, between 800 and 1,500 m water depth the benthic ostracod Mg/Ca indicated a temperature increase between 1°C and 2°C during the same periods (Cronin et al., 2012, 2017).

The warming at intermediate water depths is therefore consistent from the North Atlantic Ocean from 45°N (Marcott et al., 2011) into the Nordic Seas at 62°N (Ezat et al., 2014) and through the Fram Strait at 79°N (this study) to the Chukchi Sea (Cronin et al., 2012) (Figure 6). Such an extensive heat reservoir would have contributed significantly to the melting of the sea ice and atmospheric heating at the end of the GS and HS events and beginning of GI events. Toward the end of this long period of stratification, the supply of icebergs and meltwater probably declined, leading to increased density in the surface waters until surface and subsurface water densities were similar enough to allow for mixing. This is supported by the model experiment performed by Jensen et al. (2016), who showed that both the decrease of freshwater input and the increase of subsurface temperatures could trigger instability and disappearance of sea ice. According to Cronin et al. (2012) in the Arctic Ocean during stadial conditions, the reduced hydrological cycle and subsequent decrease in river discharge could have major effects in shallowing of the halocline and increase in surface salinity. In a sea-ice free ocean the AW could resurface releasing the accumulated heat from the ocean to the atmosphere. Due to its high salinity, the cooling of this water mass at its contact with the atmosphere could also reactivate the convection in the Nordic Seas, contributing to the formation of NADW, as in the modern Nordic Seas. With a strengthened thermohaline circulation heat would be transported back to northern latitudes at the surface. Although the onset of the abrupt interstadial warming must have involved complex atmosphere-cryosphere-ocean-se- ice interactions (e.g., Li & Born, 2019; Sheriff-Tadano & Abe-Ouchi, 2020), our compilation of BWT records (Figure 6) highlights the importance of a vast subsurface heat reservoir from 45°N to the Chuckchi Sea in driving these rapid events.

6. Summary and Conclusions

We have studied piston core HH15-1252PC from 1,273 m water depth north of Vestnesa Ridge at 79°N in the eastern Fram Strait for the reconstruction of water mass exchange through the Fram Strait and the evolution of convection in the Nordic Seas in relation to abrupt climate oscillations. Combined Mg/Ca measurements, stable isotopes, benthic foraminiferal fauna analysis and grain-size distribution and deposition of IRD, showed distinct paleoceanographic patterns that align with GI and GS (particularly HSs) in the northern Nordic Seas during the last glacial period.

GIs followed the previously suggested evolution, with oceanographic settings similar to modern with the presence of cold bottom water and deep convection. The occurrence of phytodetritus species suggest seasonal or temporary sea-ice cover in the area, leading to high productivity. The last glacial maximum (24-19 ka) showed large variations in BWT, probably related to the dynamics of the SBIS during that period.

HSs showed increases in BWT of up to 5°C due to the subduction of the AW masses beneath a fresh surface water layer and a strong halocline and stop or near-stop in deep convection. The development of *Cassidulina neoteretis* during these intervals with extensive sea-ice cover could be the result of open ocean polynyas caused by short episodes of resurfacing of the warm Atlantic origin waters, which would allow some food supply to the deep ocean.

Our results are in agreement with previously published work in the northern North Atlantic, southern Nordic Seas and Arctic Ocean, where a warm AW mass occupied the intermediate water depths below a strong halocline during HSs stretching from 45°N in the North Atlantic Ocean into the Nordic Seas to 79°N and to the Chukchi Sea in the Arctic Ocean. The resurfacing of this vast heat reservoir of AW during HSs caused release of heat to the atmosphere that preconditioned the ocean to the onset of convection and a new GI. This work highlights the important role of the oceanographic changes in the high latitude North Atlantic for the development of GI-GS cycles.

Data Availability Statement

The data from this paper is available at PANGAEA database: https://doi.pangaea.de/10.1594/PANGAEA.925428.

References

Aagaard, K., & Coachman, L. K. (1968). The East Greenland Current north of Denmark Strait: Part I. *Arctic*, *21*, 181–200. https://doi.org/10.14430/arctic3262

Aagaard, K., Coachman, L. K., & Carmack, E. (1981). On the halocline of the Arctic Ocean. *Deep Sea Research Part A. Oceanographic Research Papers*, *28*(6), 529–545. https://doi.org/10.1016/0198-0149(81)90115-1

Alve, E. (1995). Benthic foraminiferal distribution and recolonization of formerly anoxic environments in Drammensfjord, southern Norway. *Marine Micropaleontology*, *25*(2–3), 169–186. https://doi.org/10.1016/0377-8398(95)00007-n

Alve, E. (2003). A common opportunistic foraminiferal species as an indicator of rapidly changing conditions in a range of environments. *Estuarine, Coastal and Shelf Science*, *57*(3), 501–514. https://doi.org/10.1016/s0272-7714(02)00383-9

Barrientos, N., Lear, C. H., Jakobsson, M., Stranne, C., O'Regan, M., Cronin, T. M., et al. (2018). Arctic Ocean benthic foraminifera Mg/Ca ratios and global Mg/Ca-temperature calibrations: New constraints at low temperatures. *Geochimica et Cosmochimica Acta*, *236*, 240–259. https://doi.org/10.1016/j.gca.2018.02.036

Batchelor, C. L., Margold, M., Krapp, M., Murton, D. K., Dalton, A. S., Gibbard, P. L., et al. (2019). The configuration of Northern Hemisphere ice sheets through the Quaternary. *Nature Communications*, *10*(1), 3713. https://doi.org/10.1038/s41467-019-11601-2

Belanger, P. E., & Streeter, S. S. (1980). Distribution and ecology of benthic foraminifera in the Norwegian-Greenland Sea. *Marine Micropaleontology*, *5*, 401–428. https://doi.org/10.1016/0377-8398(80)90020-1

Blaauw, M. (2010). Methods and code for 'classical' age-modelling of radiocarbon sequences. *Quaternary Geochronology*, *5*(5), 512–518. https://doi.org/10.1016/j.quageo.2010.01.002

Bond, G. C., Broecker, W., Johnsen, S., McManus, J., Labeyrie, L., Jouzel, J., & Bonani, G. (1993). Correlations between climate records from North Atlantic sediments and Greenland ice. *Nature*, *365*(6442), 143–147. https://doi.org/10.1038/365143a0

Bond, G. C., & Lotti, R. (1995). Iceberg discharges into the North Atlantic on millennial time scales during the last glaciation. *Science*, *267*(5200), 1005–1010. https://doi.org/10.1126/science.267.5200.1005

Boyle, E. A., & Keigwin, L. D. (1985). Comparison of Atlantic and Pacific paleochemical records for the last 215,000 years: Changes in deep ocean circulation and chemical inventories. *Earth and Planetary Science Letters*, *76*(1–2), 135–150. https://doi.org/10.1016/0012-821x(85)90154-2

Brady, E. C., & Otto-Bliesner, B. L. (2011). The role of meltwater-induced subsurface ocean warming in regulating the Atlantic meridional overturning in glacial climate simulations. *Climate Dynamics*, *37*(7–8), 1517–1532. https://doi.org/10.1007/s00382-010-0925-9

Bünz, S., Polyanov, S., Vadakkepuliyambatta, S., Consolaro, C., & Mienert, J. (2012). Active gas venting through hydrate-bearing sediments on the Vestnesa Ridge, offshore W-Svalbard. *Marine Geology*, *332*, 189–197. https://doi.org/10.1016/j.margeo.2012.09.012

Caralp, M. H. (1989). Abundance of *Bulimina exilis* and *Melonis barleeanum*: Relationship to the quality of marine organic matter. *Geo-Marine Letters*, *9*(1), 37–43. https://doi.org/10.1007/bf02262816

Cedhagen, T. (1991). Retention of chloroplasts and bathymetric distribution in the sublittoral foraminiferan *Nonionellina labradorica*. *Ophelia*, *33*(1), 17–30. https://doi.org/10.1080/00785326.1991.10429739

Chauhan, T., Rasmussen, T. L., & Noormets, R. (2016). Palaeoceanography of the Barents Sea continental margin, north of Nordaustlandet, Svalbard, during the last 74 ka. *Boreas*, *45*(1), 76–99. https://doi.org/10.1111/bor.12135

Chauhan, T., Rasmussen, T. L., Noormets, R., Jakobsson, M., & Hogan, K. A. (2014). Glacial history and paleoceanography of the southern Yermak Plateau since 132 ka BP. *Quaternary Science Reviews*, *92*, 155–169. https://doi.org/10.1016/j.quascirev.2013.10.023

Corliss, B. H. (1985). Microhabitats of benthic foraminifera within deep-sea sediments. *Nature*, *314*(6010), 435–438. https://doi.org/10.1038/314435a0

Cronin, T. M., Dwyer, G. S., Caverly, E. K., Farmer, J., DeNinno, L. H., Rodriguez-Lazaro, J., & Gemery, L. (2017). Enhanced Arctic amplification began at the Mid-Brunhes Event~ 400,000 years ago. *Scientific Reports*, *7*(1), 1–7. https://doi.org/10.1038/s41598-017-13821-2

Cronin, T. M., Dwyer, G. S., Farmer, J., Bauch, H. A., Spielhagen, R. F., Jakobsson, M., et al. (2012). Deep Arctic Ocean warming during the last glacial cycle. *Nature Geoscience*, *5*(9), 631–634. https://doi.org/10.1038/ngeo1557

Danielsen, I. K. (2017). *Paleoceanographic development during the last deglaciation and Holocene, over the Bear Island slide scar, SW Barents Sea* (Master's thesis). UiT Norges arktiske universitet. Retrieved from https://munin.uit.no/bitstream/handle/10037/10615/thesis.pdf?sequence=2isAllowed=y

Dansgaard, W., Clausen, H. B., Gundestrup, N., Hammer, C. U., Johnsen, S. F., Kristinsdottir, P. M., & Reeh, N. (1982). A new Greenland deep ice core. *Science*, *218*(4579), 1273–1277. https://doi.org/10.1126/science.218.4579.1273

Dansgaard, W., Johnsen, S. J., Clausen, H. B., Dahl-Jensen, D., Gundestrup, N. S., Hammer, C. U., et al. (1993). Evidence for general instability of past climate from a 250-kyr ice-core record. *Nature*, *364*(6434), 218–220. https://doi.org/10.1038/364218a0

Davies, S. M., Wastegård, S., Abbott, P. M., Barbante, C., Bigler, M., Johnsen, S. J., et al. (2010). Tracing volcanic events in the NGRIP ice-core and synchronising North Atlantic marine records during the last glacial period. *Earth and Planetary Science Letters*, *294*(1–2), 69–79. https://doi.org/10.1016/j.epsl.2010.03.004

Davies, S. M., Wastegård, S., Rasmussen, T. L., Svensson, A., Johnsen, S. J., Steffensen, J. P., & Andersen, K. K. (2008). Identification of the Fugloyarbanki tephra in the NGRIP ice core: A key tie-point for marine and ice-core sequences during the last glacial period. *Journal of Quaternary Science*, *23*(5), 409–414. https://doi.org/10.1002/jqs.1182

de Villiers, S., Greaves, M., & Elderfield, H. (2002). An intensity ratio calibration method for the accurate determination of Mg/Ca and Sr/Ca of marine carbonates by ICP-AES. *Geochemistry, Geophysics, Geosystems*, *3*, 623–634. https://doi.org/10.1029/2001GC000169

Dokken, T. M., & Hald, M. (1996). Rapid climatic shifts during isotope stages 2–4 in the Polar North Atlantic. *Geology*, *24*(7), 599–602. https://doi.org/10.1130/0091-7613(1996)024%3C0599:RCSDIS%3E2.3.CO;2

Dowdeswell, J. A., & Dowdeswell, E. K. (1989). Debris in icebergs and rates of glaci-marine sedimentation: Observations from Spitsbergen and a simple model. *The Journal of Geology*, *97*(2), 221–231. https://doi.org/10.1086/629296

Duplessy, J. C., Moyes, J., & Pujol, C. (1980). Deep water formation in the North Atlantic Ocean during the last ice age. *Nature*, *286*(5772), 479–482. https://doi.org/10.1038/286479a0

Eidvin, T., Jansen, E., & Riis, F. (1993). Chronology of Tertiary fan deposits off the western Barents Sea: Implications for the uplift and erosion history of the Barents Shelf. *Marine Geology*, *112*(1–4), 109–131. https://doi.org/10.1016/0025-3227(93)90164-q

Eiken, O., & Hinz, K. (1993). Contourites in the Fram Strait. *Sedimentary Geology*, *82*(1–4), 15–32. https://doi.org/10.1016/0037-0738(93)90110-q

Elliot, M., Labeyrie, L., Dokken, T., & Manthé, S. (2001). Coherent patterns of ice-rafted debris deposits in the Nordic regions during the last glacial (10–60 ka). *Earth and Planetary Science Letters*, *194*(1–2), 151–163. https://doi.org/10.1016/s0012-821x(01)00561-1

Ezat, M. M., Rasmussen, T. L., & Groeneveld, J. (2014). Persistent intermediate water warming during cold stadials in the southeastern Nordic seas during the past 65 ky. *Geology*, *42*(8), 663–666. https://doi.org/10.1130/g35579.1

Ezat, M. M., Rasmussen, T. L., & Groeneveld, J. (2016). Reconstruction of hydrographic changes in the southern Norwegian Sea during the past 135 kyr and the impact of different foraminiferal Mg/Ca cleaning protocols. *Geochemistry, Geophysics, Geosystems*, *17*(8), 3420–3436. https://doi.org/10.1002/2016gc006325

Ezat, M. M., Rasmussen, T. L., Hönisch, B., Groeneveld, J., & Demenocal, P. (2017). Episodic release of CO_2 from the high-latitude North Atlantic Ocean during the last 135 kyr. *Nature Communications*, *8*(1), 1–10. https://doi.org/10.1038/ncomms14498

Ezat, M. M., Rasmussen, T. L., Skinner, L. C., & Zamelczyk, K. (2019). Deep ocean 14C ventilation age reconstructions from the Arctic Mediterranean reassessed. *Earth and Planetary Science Letters*, *518*, 67–75. https://doi.org/10.1016/j.epsl.2019.04.027

Ezat, M. M., Rasmussen, T. L., Thornalley, D. J., Olsen, J., Skinner, L. C., Hönisch, B., & Groeneveld, J. (2017b). Ventilation history of Nordic Seas overflows during the last (de)glacial period revealed by species-specific benthic foraminiferal ^{14}C dates. *Paleoceanography*, *32*(2), 172–181. https://doi.org/10.1002/2016pa003053

Fatela, F., & Taborda, R. (2002). Confidence limits of species proportions in microfossil assemblages. *Marine Micropaleontology*, *45*(2), 169–174. https://doi.org/10.1016/s0377-8398(02)00021-x

Fossile, E., Nardelli, M. P., Jouini, A., Lansard, B., Pusceddu, A., Moccia, D., et al. (2020). Benthic foraminifera as tracers of brine production in the Storfjorden "sea ice factory". *Biogeosciences*, *17*(7), 1933–1953. https://doi.org/10.5194/bg-17-1933-2020

Ganopolski, A., & Rahmstorf, S. (2001). Rapid changes of glacial climate simulated in a coupled climate model. *Nature*, *409*(6817), 153–158. https://doi.org/10.1038/35051500

Gooday, A. J., & Hughes, J. A. (2002). Foraminifera associated with phytodetritus deposits at a bathyal site in the northern Rockall Trough (NE Atlantic): Seasonal contrasts and a comparison of stained and dead assemblages. *Marine Micropaleontology*, *46*(1–2), 83–110. https://doi.org/10.1016/s0377-8398(02)00050-6

Gooday, A. J., & Lambshead, P. J. D. (1989). Influence of seasonally deposited phytodetritus on benthic foraminiferal populations in the bathyal northeast Atlantic: The species response. *Marine Ecology Progress Series*, *58*, 53–67. https://doi.org/10.3354/meps058053

Gottschalk, J., Szidat, S., Michel, E., Mazaud, A., Salazar, G., Battaglia, M., et al. (2018). Radiocarbon measurements of small-size foraminiferal samples with the Mini Carbon Dating System (MICADAS) at the University of Bern: Implications for paleoclimate reconstructions. *Radiocarbon*, *60*(2), 469–491. https://doi.org/10.1017/rdc.2018.3

Griggs, A. J., Davies, S. M., Abbott, P. M., Rasmussen, T. L., & Palmer, A. P. (2014). Optimising the use of marine tephrochronology in the North Atlantic: A detailed investigation of the Faroe Marine Ash Zones II, III and IV. *Quaternary Science Reviews*, *106*, 122–139. https://doi.org/10.1016/j.quascirev.2014.04.031

Hald, M., & Korsun, S. (1997). Distribution of modern benthic foraminifera from fjords of Svalbard, European Arctic. *The Journal of Foraminiferal Research*, *27*(2), 101–122. https://doi.org/10.2113/gsjfr.27.2.101

Hansen, J., Ezat, M. M., Åström, E. K., & Rasmussen, T. L. (2020). New late Pleistocene species of Acharax from Arctic methane seeps off Svalbard. *Journal of Systematic Palaeontology*, *18*(2), 197–212. https://doi.org/10.1080/14772019.2019.1594420

Hasenfratz, A. P., Schiebel, R., Thornalley, D. J., Schönfeld, J., Jaccard, S. L., Martínez-García, A., et al. (2017). Mg/Ca-temperature calibration for the benthic foraminifera *Melonis barleeanum* and *Melonis pompilioides*. *Geochimica et Cosmochimica Acta*, *217*, 365–383. https://doi.org/10.1016/j.gca.2017.08.038

Heaton, T. J., Köhler, P., Butzin, M., Bard, E., Reimer, R. W., Austin, W. E., et al. (2020). Marine20 – The marine radiocarbon age calibration curve (0–55,000 cal BP). *Radiocarbon*, *62*, 1–42. https://doi.org/10.1017/rdc.2020.68

Heinrich, H. (1988). Origin and consequences of cyclic ice rafting in the northeast Atlantic Ocean during the past 130,000 years. *Quaternary Research*, *29*(2), 142–152. https://doi.org/10.1016/0033-5894(88)90057-9

Hemming, S. R. (2004). Heinrich events: Massive late Pleistocene detritus layers of the North Atlantic and their global climate imprint. *Reviews of Geophysics*, *42*, RG1005. https://doi.org/10.1029/2003rg000128

Hoff, U., Rasmussen, T. L., Stein, R., Ezat, M. M., & Fahl, K. (2016). Sea ice and millennial-scale climate variability in the Nordic seas 90 kyr ago to present. *Nature Communications*, *7*(1), 1–10. https://doi.org/10.1038/ncomms12247

Hopkins, T. S. (1991). The GIN Sea – A synthesis of its physical oceanography and literature review 1972–1985. *Earth-Science Reviews*, *30*(3–4), 175–318. https://doi.org/10.1016/0012-8252(91)90001-v

Howe, J. A., Shimmield, T. M., Harland, R. E. X., & Eyles, N. (2007). Late Quaternary contourites and glaciomarine sedimentation in the Fram Strait. *Sedimentology*, *55*(1), 179–200. https://doi.org/10.1111/j.1365-3091.2007.00897.x

Huber, C., Leuenberger, M., Spahni, R., Flückiger, J., Schwander, J., Stocker, T. F., et al. (2006). Isotope calibrated Greenland temperature record over Marine Isotope Stage 3 and its relation to CH_4. *Earth and Planetary Science Letters*, *243*(3–4), 504–519. https://doi.org/10.1016/j.epsl.2006.01.002

Hughes, A. L., Gyllencreutz, R., Lohne, Ø. S., Mangerud, J., & Svendsen, J. I. (2016). The last Eurasian ice sheets – A chronological database and time-slice reconstruction, DATED-1. *Boreas*, *45*(1), 1–45. https://doi.org/10.1111/bor.12142

Jansen, E., Sejrup, H.-P., Fjæran, T., Hald, M., Holtedahl, H., & Skarbø, O. (1983). Late Weichselian paleoceanography of the southeastern Norwegian Sea. *Norsk Geologisl Tidsskrift*, *63*, 117–146.

Jennings, A. E., & Helgadottir, G. (1994). Foraminiferal assemblages from the fjords and shelf of eastern Greenland. *The Journal of Foraminiferal Research*, *24*(2), 123–144. https://doi.org/10.2113/gsjfr.24.2.123

Jennings, A. E., Weiner, N. J., Helgadottir, G., & Andrews, J. T. (2004). Modern foraminiferal faunas of the southwestern to northern Iceland shelf: Oceanographic and environmental controls. *The Journal of Foraminiferal Research*, *34*(3), 180–207. https://doi.org/10.2113/34.3.180

Jensen, M. F., Nilsson, J., & Nisancioglu, K. H. (2016). The interaction between sea ice and salinity-dominated ocean circulation: Implications for halocline stability and rapid changes of sea ice cover. *Climate Dynamics*, *47*(9–10), 3301–3317. https://doi.org/10.1007/s00382-016-3027-5

Jernas, P., Klitgaard-Kristensen, D., Husum, K., Koç, N., Tverberg, V., Loubere, P., et al. (2018). Annual changes in Arctic fjord environment and modern benthic foraminiferal fauna: Evidence from Kongsfjorden, Svalbard. *Global and Planetary Change*, *163*, 119–140. https://doi.org/10.1016/j.gloplacha.2017.11.013

Jessen, S. P., & Rasmussen, T. L. (2019). Ice-rafting patterns on the western Svalbard slope 74–0 ka: Interplay between ice-sheet activity, climate and ocean circulation. *Boreas*, *48*(1), 236–256. https://doi.org/10.1111/bor.12358

Jessen, S. P., Rasmussen, T. L., Nielsen, T., & Solheim, A. (2010). A new Late Weichselian and Holocene marine chronology for the western Svalbard slope 30,000–0 cal years BP. *Quaternary Science Reviews*, *29*(9–10), 1301–1312. https://doi.org/10.1016/j.quascirev.2010.02.020

Johnsen, S. J., Clausen, H. B., Dansgaard, W., Fuhrer, K., Gundestrup, N., Hammer, C. U., et al. (1992). Irregular glacial interstadials recorded in a new Greenland ice core. *Nature*, *359*(6393), 311–313. https://doi.org/10.1038/359311a0

Johnsen, S. J., Dahl-Jensen, D., Gundestrup, N., Steffensen, J. P., Clausen, H. B., Miller, H., et al. (2001). Oxygen isotope and palaeotemperature records from six Greenland ice-core stations: Camp Century, Dye-3, GRIP, GISP2, Renland and NorthGRIP. *Journal of Quaternary Science*, *16*(4), 299–307. https://doi.org/10.1002/jqs.622

Kindler, P., Guillevic, M., Baumgartner, M. F., Schwander, J., Landais, A., & Leuenberger, M. (2014). Temperature reconstruction from 10 to 120 kyr b2k from the NGRIP ice core. *Climate of the Past*, *10*(2), 887–902. https://doi.org/10.5194/cp-10-887-2014

Knies, J., Köseoğlu, D., Rise, L., Baeten, N., Bellec, V. K., Bøe, R., et al. (2018). Nordic Seas polynyas and their role in preconditioning marine productivity during the Last Glacial Maximum. *Nature Communications*, *9*(1), 1–10. https://doi.org/10.1038/s41467-018-06252-8

Knutti, R., Flückiger, J., Stocker, T. F., & Timmermann, A. (2004). Strong hemispheric coupling of glacial climate through freshwater discharge and ocean circulation. *Nature*, *430*(7002), 851–856. https://doi.org/10.1038/nature02786

Korsun, S., & Hald, M. (1998). Modern benthic foraminifera off Novaya Zemlya tidewater glaciers, Russian Arctic. *Arctic and Alpine Research*, *30*(1), 61–77. https://doi.org/10.2307/1551746

Korsun, S., & Hald, M. (2000). Seasonal dynamics of benthic foraminifera in a glacially fed fjord of Svalbard, European Arctic. *The Journal of Foraminiferal Research*, *30*(4), 251–271. https://doi.org/10.2113/0300251

Kristjánsdóttir, G. B., Lea, D. W., Jennings, A. E., Pak, D. K., & Belanger, C. (2007). New spatial Mg/Ca-temperature calibrations for three Arctic, benthic foraminifera and reconstruction of north Iceland shelf temperature for the past 4000 years. *Geochemistry, Geophysics, Geosystems*, *8*, Q03P21. https://doi.org/10.1029/2006gc001425

Laberg, J. S., & Vorren, T. O. (1995). Late Weichselian submarine debris flow deposits on the Bear Island Trough mouth fan. *Marine Geology*, *127*(1–4), 45–72. https://doi.org/10.1016/0025-3227(95)00055-4

Landais, A., Masson-Delmotte, V., Jouzel, J., Raynaud, D., Johnsen, S., Huber, C., et al. (2006). The glacial inception as recorded in the NorthGRIP Greenland ice core: Timing, structure and associated abrupt temperature changes. *Climate Dynamics*, *26*(2–3), 273–284. https://doi.org/10.1007/s00382-005-0063-y

Lekens, W. A., Sejrup, H. P., Haflidason, H., Knies, J., & Richter, T. (2006). Meltwater and ice rafting in the southern Norwegian Sea between 20 and 40 calendar kyr B.P.: Implications for Fennoscandian Heinrich events. *Paleoceanography*, *21*, PA3013. https://doi.org/10.1029/2005pa001228

Li, C., & Born, A. (2019). Coupled atmosphere-ice-ocean dynamics in Dansgaard-Oeschger events. *Quaternary Science Reviews*, *203*, 1–20. https://doi.org/10.1016/j.quascirev.2018.10.031

Linke, P., & Lutze, G. F. (1993). Microhabitat preferences of benthic foraminifera – A static concept or a dynamic adaptation to optimize food acquisition? *Marine Micropaleontology*, *20*(3–4), 215–234. https://doi.org/10.1016/0377-8398(93)90034-u

Locarnini, R. A., Mishonov, A. V., Baranova, O. K., Boyer, T. P., Zweng, M. M., Garcia, H. E., et al. (2018). World Ocean Atlas 2018. In A. Mishonov Technical (Ed.), *NOAA Atlas NESDIS 81*(Volume 1: Temperature, p. 52).

Lubinski, D. J., Polyak, L., & Forman, S. L. (2001). Freshwater and Atlantic water inflows to the deep northern Barents and Kara seas since ca 13 ^{14}C ka: Foraminifera and stable isotopes. *Quaternary Science Reviews*, *20*(18), 1851–1879. https://doi.org/10.1016/s0277-3791(01)00016-6

Mackensen, A., & Hald, M. (1988). *Cassidulina teretis* Tappan and *C. laevigata* d'Orbigny; their modern and late Quaternary distribution in northern seas. *The Journal of Foraminiferal Research*, *18*(1), 16–24. https://doi.org/10.2113/gsjfr.18.1.16

Mackensen, A., & Schmiedl, G. (2016). Brine formation recorded by stable isotopes of recent benthic foraminifera in Storfjorden, Svalbard: Palaeoceanographical implications. *Boreas*, *45*(3), 552–566. https://doi.org/10.1111/bor.12174

Mackensen, A., & Schmiedl, G. (2019). Stable carbon isotopes in paleoceanography: Atmosphere, oceans, and sediments. *Earth-Science Reviews*, *197*, 102893. https://doi.org/10.1016/j.earscirev.2019.102893

Mackensen, A., Schumacher, S., Radke, J., & Schmidt, D. N. (2000). Microhabitat preferences and stable carbon isotopes of endobenthic foraminifera: Clue to quantitative reconstruction of oceanic new production? *Marine Micropaleontology*, *40*(3), 233–258. https://doi.org/10.1016/s0377-8398(00)00040-2

Mackensen, A., Sejrup, H. P., & Jansen, E. (1985). The distribution of living benthic foraminifera on the continental slope and rise off southwest Norway. *Marine Micropaleontology*, *9*(4), 275–306. https://doi.org/10.1016/0377-8398(85)90001-5

Marcott, S. A., Clark, P. U., Padman, L., Klinkhammer, G. P., Springer, S. R., Liu, Z., et al. (2011). Ice-shelf collapse from subsurface warming as a trigger for Heinrich events. *Proceedings of the National Academy of Sciences of the United States of America*, *108*(33), 13415–13419. https://doi.org/10.1073/pnas.1104772108

McCorkle, D. C., Keigwin, L. D., Corliss, B. H., & Emerson, S. R. (1990). The influence of microhabitats on the carbon isotopic composition of deep-sea benthic foraminifera. *Paleoceanography*, *5*(2), 161–185. https://doi.org/10.1029/pa005i002p00161

Mudie, P. J., Keen, C. E., Hardy, I. A., & Vilks, G. (1984). Multivariate analysis and quantitative paleoecology of benthic foraminifera in surface and Late Quaternary shelf sediments, northern Canada. *Marine Micropaleontology*, *8*(4), 283–313. https://doi.org/10.1016/0377-8398(84)90018-5

Müller, J., & Stein, R. (2014). High-resolution record of late glacial and deglacial sea ice changes in Fram Strait corroborates ice-ocean interactions during abrupt climate shifts. *Earth and Planetary Science Letters*, *403*, 446–455. https://doi.org/10.1016/j.epsl.2014.07.016

Ottesen, D., Dowdeswell, J. A., & Rise, L. (2005). Submarine landforms and the reconstruction of fast-flowing ice streams within a large Quaternary ice sheet: The 2500-km-long Norwegian-Svalbard margin (57°–80°N). *Geological Society of America Bulletin*, *117*(7–8), 1033–1050. https://doi.org/10.1130/b25577.1

Pena, L. D., Calvo, E., Cacho, I., Eggins, S., & Pelejero, C. (2005). Identification and removal of Mn-Mg-rich contaminant phases on foraminiferal tests: Implications for Mg/Ca past temperature reconstructions. *Geochemistry, Geophysics, Geosystems*, *6*, Q09P02. https://doi.org/10.1029/2005gc000930

Polyak, L., Best, K. M., Crawford, K. A., Council, E. A., & St-Onge, G. (2013). Quaternary history of sea ice in the western Arctic Ocean based on foraminifera. *Quaternary Science Reviews*, *79*, 145–156. https://doi.org/10.1016/j.quascirev.2012.12.018

Polyak, L., Korsun, S., Febo, L. A., Stanovoy, V., Khusid, T., Hald, M., et al. (2002). Benthic foraminiferal assemblages from the southern Kara Sea, a river-influenced Arctic marine environment. *The Journal of Foraminiferal Research*, *32*(3), 252–273. https://doi.org/10.2113/32.3.252

Polyak, L., & Mikhailov, V. (1996). Post-glacial environments of the southeastern Barents Sea: Foraminiferal evidence. *Geological Society, London, Special Publications*, *111*(1), 323–337. https://doi.org/10.1144/gsl.sp.1996.111.01.21

Rasmussen, S. O., Bigler, M., Blockley, S. P., Blunier, T., Buchardt, S. L., Clausen, H. B., et al. (2014a). A stratigraphic framework for abrupt climatic changes during the Last Glacial period based on three synchronized Greenland ice-core records: Refining and extending the INTIMATE event stratigraphy. *Quaternary Science Reviews*, *106*, 14–28. https://doi.org/10.1016/j.quascirev.2014.09.007

Rasmussen, T. L., Oppo, D. W., Thomsen, E., & Lehman, S. J. (2003). Deep sea records from the southeast Labrador Sea: Ocean circulation changes and ice-rafting events during the last 160,000 years. *Paleoceanography*, *18*, 10181. https://doi.org/10.1029/2001pa000736

Rasmussen, T. L., & Thomsen, E. (2004). The role of the North Atlantic Drift in the millennial timescale glacial climate fluctuations. *Palaeogeography, Palaeoclimatology, Palaeoecology*, *210*(1), 101–116. https://doi.org/10.1016/j.palaeo.2004.04.005

Rasmussen, T. L., & Thomsen, E. (2009). Stable isotope signals from brines in the Barents Sea: Implications for brine formation during the last glaciation. *Geology*, *37*(10), 903–906. https://doi.org/10.1130/g25543a.1

Rasmussen, T. L., & Thomsen, E. (2013). Pink marine sediments reveal rapid ice melt and Arctic meltwater discharge during Dansgaard–Oeschger warmings. *Nature Communications*, *4*(1), 1–8. https://doi.org/10.1038/ncomms3849

Rasmussen, T. L., & Thomsen, E. (2017). Ecology of deep-sea benthic foraminifera in the North Atlantic during the last glaciation: Food or temperature control. *Palaeogeography, Palaeoclimatology, Palaeoecology*, *472*, 15–32. https://doi.org/10.1016/j.palaeo.2017.02.012

Rasmussen, T. L., Thomsen, E., Labeyrie, L., & van Weering, T. C. (1996a). Circulation changes in the Faeroe-Shetland Channel correlating with cold events during the last glacial period (58–10 ka). *Geology*, *24*(10), 937–940. https://doi.org/10.1130/0091-7613(1996)024%3C0937:ccitfs%3E2.3.co;2

Rasmussen, T. L., Thomsen, E., van Weering, T. C., & Labeyrie, L. (1996b). Rapid changes in surface and deep water conditions at the Faeroe Margin during the last 58,000 years. *Paleoceanography*, *11*(6), 757–771. https://doi.org/10.1029/96pa02618

Rasmussen, T. L., Thomsen, E., & Nielsen, T. (2014b). Water mass exchange between the Nordic seas and the Arctic Ocean on millennial timescale during MIS 4–MIS 2. *Geochemistry, Geophysics, Geosystems*, *15*(3), 530–544. https://doi.org/10.1002/2013gc005020

Rasmussen, T. L., Thomsen, E., Ślubowska, M. A., Jessen, S., Solheim, A., & Koç, N. (2007). Paleoceanographic evolution of the SW Svalbard margin (76°N) since 20,000 ^{14}C yr BP. *Quaternary Research*, *67*(1), 100–114. https://doi.org/10.1016/j.yqres.2006.07.002

Rudels, B. (1987). On the mass balance of the Polar Ocean, with special emphasis on the Fram Strait. *Norsk Polarinstitutt Skrifter, No. 188*. Retrieved from http://hdl.handle.net/11250/173528

Rudels, B., Jones, E. P., Schauer, U., & Eriksson, P. (2004). Atlantic sources of the Arctic Ocean surface and halocline waters. *Polar Research*, *23*(2), 181–208. https://doi.org/10.3402/polar.v23i2.6278

Ruff, M., Szidat, S., Gäggeler, H. W., Suter, M., Synal, H. A., & Wacker, L. (2010). Gaseous radiocarbon measurements of small samples. *Nuclear Instruments and Methods in Physics Research Section B: Beam Interactions with Materials and Atoms*, *268*(7–8), 790–794. https://doi.org/10.1016/j.nimb.2009.10.032

Sadatzki, H., Dokken, T. M., Berben, S. M., Muschitiello, F., Stein, R., Fahl, K., et al. (2019). Sea ice variability in the southern Norwegian Sea during glacial Dansgaard-Oeschger climate cycles. *Science Advances*, *5*(3), eaau6174. https://doi.org/10.1126/sciadv.aau6174

Sarnthein, M., Stattegger, K., Dreger, D., Erlenkeuser, H., Grootes, P., Haupt, B. J., et al. (2001). Fundamental modes and abrupt changes in North Atlantic circulation and climate over the last 60 ky – Concepts, reconstruction and numerical modeling. In P. Schäfer W. Ritzrau M. Schlüter & J. Thiede (Eds.), *The Northern North Atlantic* (pp. 365–410). Berlin, Heidelberg: Springer. https://doi.org/10.1007/978-3-642-56876-3_21

Schönfeld, J. (2001). Benthic foraminifera and pore-water oxygen profiles: A re-assessment of species boundary conditions at the western Iberian margin. *The Journal of Foraminiferal Research*, *31*(2), 86–107. https://doi.org/10.2113/0310086

Seidenkrantz, M. S. (1995). *Cassidulina teretis* Tappan and *Cassidulina neoteretis* new species (Foraminifera): Stratigraphic markers for deep sea and outer shelf areas. *Journal of Micropalaeontology*, *14*(2), 145–157. https://doi.org/10.1144/jm.14.2.145

Seidenkrantz, M. S. (2013). Benthic foraminifera as palaeo sea-ice indicators in the subarctic realm-examples from the Labrador Sea-Baffin Bay region. *Quaternary Science Reviews*, *79*, 135–144. https://doi.org/10.1016/j.quascirev.2013.03.014

Sejrup, H. P., Fjaeran, T., Hald, M., Beck, L., Hagen, J., Miljeteig, I., et al. (1981). Benthonic foraminifera in surface samples from the Norwegian continental margin between 62 degrees N and 65 degrees N. *The Journal of Foraminiferal Research*, *11*(4), 277–295. https://doi.org/10.2113/gsjfr.11.4.277

Sessford, E. G., Jensen, M. F., Tisserand, A. A., Muschitiello, F., Dokken, T., Nisancioglu, K. H., & Jansen, E. (2019). Consistent fluctuations in intermediate water temperature off the coast of Greenland and Norway during Dansgaard-Oeschger events. *Quaternary Science Reviews*, *223*, 105887. https://doi.org/10.1016/j.quascirev.2019.105887

Sessford, E. G., Tisserand, A. A., Risebrobakken, B., Andersson, C., Dokken, T., & Jansen, E. (2018). High-resolution Benthic Mg/Ca temperature record of the intermediate water in the Denmark Strait Across D-O stadial-interstadial cycles. *Paleoceanography and Paleoclimatology*, *33*(11), 1169–1185. https://doi.org/10.1029/2018pa003370

Sherriff-Tadano, S., Abe-Ouchi, A., & Oka, A. (2020). Impact of mid-glacial ice sheets on deep ocean circulation and global climate: Role of surface cooling on the AMOC. *Climate of the Past Discussions*, *17*, 1–28. https://doi.org/10.5194/cp-2020-75

Stanford, J. D., Rohling, E. J., Bacon, S., Roberts, A. P., Grousset, F. E., & Bolshaw, M. (2011). A new concept for the paleoceanographic evolution of Heinrich event 1 in the North Atlantic. *Quaternary Science Reviews*, *30*(9–10), 1047–1066. https://doi.org/10.1016/j.quascirev.2011.02.003

Steinsund, P. I. (1994). *Benthic foraminifera in surface sediments of the Barents and Kara seas: Modern and late Quaternary applications* (Unpublished PhD thesis). Norway: University of Tromsø.

Svensson, A., Andersen, K. K., Bigler, M., Clausen, H. B., Dahl-Jensen, D., Davies, S. M., et al. (2008). A 60 000 year Greenland stratigraphic ice core chronology. *Climate of the Past*, *4*(1), 47–57. https://doi.org/10.5194/cp-4-47-2008

Sztybor, K., & Rasmussen, T. L. (2017). Late glacial and deglacial palaeoceanographic changes at Vestnesa Ridge, Fram Strait: Methane seep versus non-seep environments. *Palaeogeography, Palaeoclimatology, Palaeoecology*, *476*, 77–89. https://doi.org/10.1016/j.palaeo.2017.04.001

Thomsen, E., Rasmussen, T. L., Sztybor, K., Hanken, N. M., Tendal, O. S., & Uchman, A. (2019). Cold-seep fossil macrofaunal assemblages from Vestnesa Ridge, eastern Fram Strait, during the past 45 000 years. *Polar Research*, *38*, 3310. https://doi.org/10.33265/polar.v38.3310

Thornalley, D. J., Bauch, H. A., Gebbie, G., Guo, W., Ziegler, M., Bernasconi, S. M., et al. (2015). A warm and poorly ventilated deep Arctic Mediterranean during the last glacial period. *Science*, *349*(6249), 706–710. https://doi.org/10.1126/science.aaa9554

Vogt, P. R., Crane, K., Sundvor, E., Max, M. D., & Pfirman, S. L. (1994). Methane-generated (?) pockmarks on young, thickly sedimented oceanic crust in the Arctic: Vestnesa ridge, Fram strait. *Geology*, *22*(3), 255–258. https://doi.org/10.1130/0091-7613(1994)022%3C0255:mgpoyt%3E2.3.co;2

Vorren, T. O., Laberg, J. S., Blaume, F., Dowdeswell, J. A., Kenyon, N. H., Mienert, J., et al. (1998). The Norwegian–Greenland Sea continental margins: Morphology and late Quaternary sedimentary processes and environment. *Quaternary Science Reviews*, *17*(1–3), 273–302. https://doi.org/10.1016/s0277-3791(97)00072-3

Wary, M., Eynaud, F., Rossignol, L., Zaragosi, S., Sabine, M., Castera, M. H., & Billy, I. (2017). The southern Norwegian Sea during the last 45 ka: Hydrographical reorganizations under changing ice-sheet dynamics. *Journal of Quaternary Science*, *32*(7), 908–922. https://doi.org/10.1002/jqs.2965

Wastegård, S., & Rasmussen, T. L. (2014). Faroe Marine Ash Zone IV: A new MIS 3 ash zone on the Faroe Islands margin. *Geological Society, London, Special Publications*, *398*(1), 81–93. https://doi.org/10.1144/sp398.3

Wefer, G., Heinze, P. M., & Berger, W. H. (1994). Clues to ancient methane release. *Nature*, *369*(6478), 282. https://doi.org/10.1038/369282a0

Winsborrow, M. C., Andreassen, K., Corner, G. D., & Laberg, J. S. (2010). Deglaciation of a marine-based ice sheet: Late Weichselian palaeo-ice dynamics and retreat in the southern Barents Sea reconstructed from onshore and offshore glacial geomorphology. *Quaternary Science Reviews*, *29*(3–4), 424–442. https://doi.org/10.1016/j.quascirev.2009.10.001

Wolff, E. W., Chappellaz, J., Blunier, T., Rasmussen, S. O., & Svensson, A. (2010). Millennial-scale variability during the last glacial: The ice core record. *Quaternary Science Reviews*, *29*(21–22), 2828–2838. https://doi.org/10.1016/j.quascirev.2009.10.013

Wollenburg, J. E., Knies, J., & Mackensen, A. (2004). High-resolution paleoproductivity fluctuations during the past 24 kyr as indicated by benthic foraminifera in the marginal Arctic Ocean. *Palaeogeography, Palaeoclimatology, Palaeoecology*, *204*(3–4), 209–238. https://doi.org/10.1016/s0031-0182(03)00726-0

Wollenburg, J. E., & Kuhnt, W. (2000). The response of benthic foraminifers to carbon flux and primary production in the Arctic Ocean. *Marine Micropaleontology*, *40*(3), 189–231. https://doi.org/10.1016/s0377-8398(00)00039-6

Wollenburg, J. E., Kuhnt, W., & Mackensen, A. (2001). Changes in Arctic Ocean paleoproductivity and hydrography during the last 145 kyr: The benthic foraminiferal record. *Paleoceanography*, *16*(1), 65–77. https://doi.org/10.1029/1999pa000454

Wollenburg, J. E., & Mackensen, A. (1998). Living benthic foraminifers from the central Arctic Ocean: Faunal composition, standing stock and diversity. *Marine Micropaleontology*, *34*(3–4), 153–185. https://doi.org/10.1016/s0377-8398(98)00007-3

References From the Supporting Information

GEOSECS Executive Committee. (1987). GEOSECS Atlantic, Pacific, and Indian Ocean Expeditions, vol. 7, Shorebased Data and Graphics, p. 100. Washington, DC: National Science Foundation.

O'Neil, J. R., Clayton, R. N., & Mayeda, T. K. (1969). Oxygen isotope fractionation in divalent metal carbonates. *The Journal of Chemical Physics*, *51*(12), 5547–5558. https://doi.org/10.1063/1.1671982

Shackleton, N. J. (1974). Attainment of isotopic equilibrium between ocean water and the benthonic foraminifera genus *Uvigerina*: Isotopic changes in the ocean during the last glacial. *Colloques Internationaux du CNRS*. (219).

Spratt, R. M., & Lisiecki, L. E. (2016). A Late Pleistocene sea level stack. *Climate of the Past*, *12*(4), 1079–1092. https://doi.org/10.5194/cpd-11-3699-2015

Paper II

1 **Deglacial bottom water warming intensified Arctic methane seepage, Northwestern**

2 **Barents Sea**

3 N. El bani Altuna,[1*] T. L. Rasmussen,[1] M. M. Ezat,[1,2] S. Vadakkepuliyambatta,[1] J. Groeneveld,[3,]

4 [4] M. Greaves[5]

5

6 [1]CAGE-Centre for Arctic Gas Hydrate, Environment and Climate, Department of Geosciences,

7 UiT-The Arctic University of Norway, Tromsø, Norway

8 [2]Department of Geology, Faculty of Science, Beni-Suef University, Beni-Suef, Egypt

9 [3]Alfred Wegener Institute, Helmholtz Center for Polar and Marine Research, Bremerhaven,

10 Germany

11 [4]MARUM-Center for Marine Environmental Sciences, University of Bremen, Bremen,

12 Germany

13 [5]Godwin Laboratory for Palaeoclimate Research, Department of Earth Sciences, University of

14 Cambridge, Cambridge, UK

15

16 *Corresponding author: naima.e.altuna@uit.no

17

18

19

20

21

22

23

24

25

26

27

28

29

30

31

32

33

Abstract

Changes in the Arctic climate-ocean system can rapidly impact carbon cycling and cryosphere. Methane release from the seafloor has been widespread in the Barents Sea since the last deglaciation, being closely linked to changes in pressure and bottom water temperature (BWT). Here, we present the first post-glacial BWT record (18,000–0 years before present) based on Mg/Ca in benthic foraminifera from an area where methane seepage occurs and proximal to a former Arctic ice-sheet grounding zone. Coupled ice sheet-hydrate stability modeling shows that phases of extreme BWT up to 6°C and associated with inflow of Atlantic Water repeatedly destabilized subsurface hydrates, facilitating the release of greenhouse gasses from the seabed. Furthermore, these warming events played an important role in triggering multiple collapses of the marine-based Svalbard-Barents Sea Ice Sheet. Future warming of the Atlantic Water could lead to widespread disappearance of gas hydrates and melting of the remaining marine-terminating glaciers.

Introduction

The Arctic has experienced dramatic changes during recent decades in response to climate warming. In particular, the Barents Sea has shown signs of an ongoing "Atlantification", with increased inflow of warm Atlantic Water (AW) and a significant loss of sea ice[1]. The incursion of warm AW onto the Barents Shelf can also destabilize buried gas hydrates – frozen compounds of water and methane – releasing greenhouse gases into the water column[2–4]. Although methane released from the seafloor is microbially consumed in the sediment by anaerobic oxidation of methane[5,6] or dissolved/consumed by aerobic methane oxidation in the water column[7,8], a major methane venting event induced by dissociation of gas hydrates could amplify the effects of the current ocean acidification[9] and, if escaping to the atmosphere could lead to further warming.

Past periods with subsurface inflow of warm AW have been recorded in sediment cores from the Nordic Seas during Heinrich Stadials (HS)[10–12]. These are millennial-scale events related to extensive discharge of icebergs and meltwater into the North Atlantic that occurred in the last glacial period[13]. During the Last Glacial Maximum (ca. 26,000–19,000 calendar (cal) years before present (BP)), the Svalbard-Barents Sea Ice Sheet (SBIS) reached its maximum extent, covering the entire Barents Sea shelf[14]. Paleoceanographic studies[15,16] and ice-ocean modelling[17,18] have suggested that subsurface warming was a major factor in driving the collapse of the marine-based SBIS. The western Barents Sea margin during the last deglaciation is thus a highly relevant analogue for the ongoing subsurface warming-induced retreat of the Western Antarctic Ice Sheet (WAIS)[19] and marine terminating glaciers in Greenland[20].

We have reconstructed bottom water temperatures by the study of core HH18-1059GC (hereafter core 1059), recovered from Storfjordrenna (Storfjorden Trough) in the northwestern Barents Sea at a water depth of 382 m (Fig. 1). Warm Atlantic water derived from the North Atlantic Current flows from the southern Nordic Seas to the Fram Strait along the western Svalbard margin as the West Spitsbergen Current[21] (Fig. 1). A branch of the Atlantic Water enters Storfjordrenna and Storfjorden in the eastern part. The East Spitsbergen Current, a cold polar current, enters Storfjordrenna from the Arctic Ocean and northeast Barents Sea and flows in the western part of Storfjorden and along the inner Spitsbergen shelf (Fig. 1). During the late winter-spring season, the AW generally flows above 200 m in the upper part of water column with a temperature ca. 3°C and a salinity above 34.95 psu, below a polar, low-salinity, surface water layer[21]. This is because (depending on the prevailing wind directions and sea-ice conditions), a polynya may form in late winter and spring in Storfjorden resulting in the formation of brine-enriched shelf water (-1.9°C, >34.8 psu) that flows along the bottom of Storfjordrenna on its way to the shelf edge[21]. In summer-autumn, the AW occupies the entire

water column. In July 2018, when core 1059 was retrieved, the AW reached the seafloor with a temperature of 2.5°C (Fig. 1C).

Previous attempts to estimate paleo-BWT in Storfjordrenna have involved converting benthic foraminiferal $\delta^{18}O$[15] into BWT by assuming constant seawater $\delta^{18}O$ similar to modern values[22] or calculating BWT using benthic foraminiferal transfer functions[16] (Fig. S2). The latter method quantifies BWT as an average of the whole foraminiferal assemblage and might therefore be biased towards species-specific ecological preferences other than temperature (e.g., food and oxygen availability, salinity, and water depth). Here, we present the first BWT record based on Mg/Ca, measured in the benthic foraminiferal species *Cassidulina neoteretis,* in order to more accurately quantify and constrain past temperature changes in the western Barents Sea.

Our record spans the early deglaciation (since the Late Glacial 18,000 cal years BP) to the late Holocene, including the cold atmospheric periods Heinrich Stadial 1 (HS1; 17,500–14,600 cal years BP) and Younger Dryas (YD; 12,800–11,700 cal years BP) and the warm interstadial phases Bølling-Allerød (14,600–12,800 cal years BP) and the Holocene (since 11,700 cal years BP)[23] (Fig. 2). The core site is located close to an area of methane release from gas hydrate mounds ("Pingo area") in the northwestern Barents Sea[22], allowing correlation and comparison between methane-influenced records[24] and records from unaffected areas (e.g., core 1059; see Methods). The gas hydrate stability zone outcrops at this water depth in the outer Storfjordrenna[25], in an area also strongly affected by the inflow of the warm Atlantic Water (Fig. 1) .

Results and discussion
Bottom water temperatures during the last 17,500 cal years

The BWT in Storfjordrenna varied between 1.5 to 5.5°C since the start of HS1 at 17,500 cal years BP (Fig. 3a). The warmest BWT occurred during HS1 and the following deglaciation

107   (Bølling-Allerød interstadials, 14,600–12,800 cal years BP), with an average of 4.4±1°C (Fig.

108   3a). Our results generally agree with previous BWT estimates by transfer functions from this

109   area[16] (Fig. S2). Quantifications of BWT based on benthic foraminiferal Mg/Ca from

110   intermediate water depth (down to at least 1,273 m water depth) in the southern Nordic Seas[11]

111   and the western Svalbard margin[12] show similar trends with a warming of the bottom water of

112   up to 5.5°C during HS1. During HS1 and older HS events during the last glacial period, the

113   AW could flow northwards beneath a polar meltwater layer with an extended sea-ice cover and

114   a strong halocline preserving most of its heat[10,11]. The meltwater came from the melting of

115   icebergs released from the Northern hemisphere ice sheets and the formation of cold deep water

116   stopped or became very weak due to reduced oceanic convection in the Nordic Seas.

117   The end of HS1 is marked by a progressive increase in BWT up to 5.3±1°C, shortly before

118   the beginning of the Bølling-Allerød interstadials (Fig. 3a). The transition to a warmer climate

119   is characterized by laminated fine clays deposited from meltwater plumes[26] (Fig. 2). The

120   benthic foraminiferal fauna is dominated by *Elphidium excavatum*[15], a benthic foraminifera that

121   tolerates turbid meltwater, highly variable environmental conditions, and low salinities[27,28]

122   indicating rapid ice retreat and melt-back of the SBIS[16,29].

123   During the YD, the BWT was relatively low (2.5±1°C) and was closer to modern values

124   (Fig. 2). The YD was linked to a slow-down of the Atlantic Meridional Overturning (AMOC)[30]

125   but differs from other HS events as it occurred during warm conditions[10]. The YD cold spell

126   coincided with the deglaciation of the Arctic Ocean sending sea-ice loaded cold water into the

127   Nordic Seas and North Atlantic[31]. Seasonal sea-ice cover and an increased seasonal brine

128   formation throughout most of the YD[32], probably kept the seafloor relatively cool as today (Fig.

129   3a).

130   Bottom water temperature progressively increased up to ca. 5°C by the early Holocene

131   between 11,700 and 9,000 cal years (Fig. 3a). During this period, benthic foraminiferal

132 assemblages show an increase in relative abundances of *Cibicides lobatulus* and *Melonis*

133 *barleeanus* supporting the presence of stronger advection of AW and a reduced cover of sea

134 ice[15]. During the Mid-Late Holocene, the BWT stabilized with an average of 3.3±1°C, except

135 for a short warming event around 6,000 years.

136

137 **Bottom water temperature and gas-hydrate dissociation**

138 Bottom water temperature is an effective regulator of the stability of sub-seafloor gas

139 hydrates, with minor fluctuations on a seasonal basis directly impacting the flow of greenhouse

140 gases from the seabed to the water column[22]. Using our BWT time-series, we reconstruct the

141 dynamic evolution of the gas hydrate stability zone (GHSZ) by performing modeling of the

142 thickness of the GHSZ to provide the first oceanographically constrained history of methane-

143 venting from the northwestern Barents Sea area (see Methods). The measured benthic

144 foraminiferal species, *C. neoteretis,* thrives under the influence of AW[27,28], and therefore, the

145 thickness of the GHSZ presented in this work should be considered as a narrowest limit (see

146 Methods).

147 During the late glacial from 18,000–17,500 cal years BP, the rapid removal of the glacial

148 overburden from the presence of a thick ice sheet followed by the initial intrusion of the warm

149 AW caused the ca. 200 m thick GHSZ to disappear entirely within ca. 1,000 years (Fig. 3b, Fig.

150 4a,b and Fig. S4). The GHSZ continued to outcrop at the sediment surface in the area during

151 the HS1 and warm Bølling and Allerød interstadials with high BWT. The GHSZ reappeared

152 and thickened at the Allerød-YD transition following a decrease in BWT (Fig. 3b). The

153 climatically unstable periods of the YD and earliest Holocene with highly variable BWT

154 resulted in rapid fluctuations in thickness of the GHSZ (0 to between 50 and 80 m) (Fig. 3b).

155 Thereafter, it disappeared again during the Holocene Thermal Maximum, before increasing to

156 a thickness of 60–75 m beginning from 4,500 cal years BP in the late Holocene, when BWT

157   stabilized to modern values (Fig. 1c and Fig. 3a). Seismic data from the area shows that the

158   base of the modern GHSZ (i.e. the bottom-simulating reflector) occurs today between 85 and

159   150 m below the seafloor[25], validating the results of our model.

160   We have correlated nearby core CAGE15-2-920GC (hereafter core 920) from a hydrate

161   pingo to our core 1059 (Fig. 1 and Fig. S3). Core 920, analyzed for its content of archaeobacteria

162   and their ^{13}C signals, indicates three major episodes of methane venting[24]. Based on our

163   correlation and placing core 920 into our age model (see Methods), increased release of gas

164   occurs in the late HS1, during the Bølling interstadial and Allerød interstadial.

165   In the "Pingo area" methane is released through several gas hydrate mounds connected to

166   the Hornsund fault system in Storfjordrenna[25]. The record from core 920 shows when the

167   methane flux in Storfjordrenna increased during the deglaciation. There is no signal in core 920

168   for most of HS1, which would have been expected given the rapid disappearance of the GHSZ

169   and the following high BWT (Fig. 3b,c). Data from the SW Barents Sea indicated a maximum

170   in seepage right after the retreat of the SBIS 18,000–16,000 cal years BP[33]. The venting right

171   after depressurizing from the ice-burden might not be recorded perhaps because (1) it was a

172   very rapid and violent event, (2) the gas escaped through cracks in the gas phase or (3) it escaped

173   through cracks and faults elsewhere. Indeed, studies from the SW Barents Sea[33,34] also indicated

174   increase in methane venting during the Bølling and Allerød intervals supporting the hypothesis

175   of the protracted nature of methane release from gas hydrate dissociation during the

176   deglaciation over millennial timescales, where high flux of methane follows the phase of

177   maximum high BWT and decreases during the cold YD (Fig. 3a,b,c and Fig. 4c,d).

178

179   **Significance of bottom water temperature changes for methane release and ice retreat**

180   Our BWT record for the western Barents Sea provides the first quantifiable evidence for

181   bottom warming events in the northwestern Barents Sea since the Last Glacial Maximum,

182 providing a direct means of comparison of its impact on the ice sheet and hydrate dissociation.

183 The core site in Storfjordrenna is located in front of a former major ice stream of the SBIS[35],

184 which had retreated to the central part of the shelf at least before 18,150 cal years BP

185 (16,750±110 ^{14}C years[15] calibrated with Normarine18[29]) (see Methods). The collapse and

186 retreat of this ice stream from the shelf edge has been linked to oceanographic forcing[36],

187 enhanced by the seafloor geometry and substrate[37,38]. The three major periods of high BWT

188 (with temperatures ca. 4–5°C) identified after 18,000 cal years BP correlate closely with major

189 postglacial retreat phases of the SBIS in Storfjordrenna and Storfjorden[16,38] (Fig. S4).

190 The early retreat of the SBIS from the outer part of Storfjordrenna, was probably accelerated

191 by the presence of warm (4.4±1°C) AW flowing eastwards during the late glacial and HS1[15]

192 (Fig. 3a and Fig. S4) followed by an increased release of methane from the seafloor[24] (Fig. 3c).

193 The contemporaneous and rapid reduction in thickness of the GHSZ in Storfjordrenna has

194 previously been attributed to decompression associated with deglaciation of the SBIS[39]. Our

195 data suggest that the high BWT most likely also played an important role, driving the retreat of

196 the SBIS, and preconditioning and accelerating the postglacial thinning of the GHSZ much

197 faster than previously suggested[22].

198 We observe a decrease in seawater δ^{18}O following the peak in BWT during HS1, potentially

199 indicating a freshening of the bottom waters (Fig. 3a,e). This indicates that the advection of

200 warm AW into the western Barents Sea probably resulted in basal melting of the SBIS, forcing

201 a rapid retreat of the ice stream in Storfjordrenna and a significant supply of freshwater (Fig.

202 4b)[15,16]. Similar chronologies of the retreat patterns of the Storfjordrenna Ice Stream and north

203 Norwegian Ice Streams likely suggest that the retreat was controlled by a common forcing (i.e.

204 atmosphere and/or oceanic control) rather than by local factors only[16] (Fig. 4a–d). Subsurface

205 melting has been suggested by model studies to be the major control on the retreat of the marine-

206 based SBIS[17], in contrast to the minor role played by atmospheric forcing and sea level rise[18].

207   Our BWT, with three main phases of AW warm pulses, agrees with the stepwise retreat pattern

208   of the SBIS previously documented in Storfjordrenna[37] and the SW Barents Sea[40].

209   The BWT increase at the beginning of the Holocene between 11,300 and 9,000 cal years

210   BP, may have driven the final retreat of the SBIS in Storfjorden[16] and disappearance of the

211   GHSZ (Fig. 3b). By the Mid-Late Holocene, modern BWT values were reached (Fig. 3a). The

212   lower summer BWT and the increased pressure related to sea-level rise during the Holocene

213   probably thickened the GHSZ again (Fig. 3b and Fig. 4f). Seasonal variations in bottom water

214   temperature today and during the late Holocene[32,41] were pronounced due to increased brine

215   formation in Storfjorden creating dense, cold outflow water via Storfjordrenna (winter with

216   strong brine formation: T= -1.3°C, S= 35.3 psu[15]; summer T= 2.5–3°C, S= 34.9–35 psu; Fig.

217   1c). This strong seasonal variability is likely to accelerate the destabilization of the GHSZ and

218   cause variable seasonal patterns of methane seepage on Arctic continental shelves[2–4] (Fig. 4f).

219   A modelling exercise on the fate of the GHSZ in the southwestern Barents Sea, under

220   warming ocean conditions since 1960, indicates that the inflow of Atlantic water played a major

221   role in the thinning of the GHSZ between 1985 and 2010[42]. Furthermore, a linear increase of

222   1°C of BWT from 2010 to 2060 would cause a further thinning of the GHSZ, allowing shallow

223   (<80 mbsf) methane hydrates to dissociate and release between 1 and 8 Gt of carbon into the

224   ocean[42]. Under a very high baseline scenario of greenhouse gas emissions (RCP8.5)[43], CMIP5

225   climate predictions[44] of BWT show that the temperature could increase up to 5°C by the end

226   of the 21st century in the western Barents Sea at water depths of 390 m[45], similar to the estimated

227   BWT in Storfjordrenna during HS1 and the Bølling-Allerød interstadials (Fig. 3).

228   The mechanisms underlying the intrusion of warm AW into the western Barents Sea were

229   different in the past (i.e. when AW could flow with minimal heat loss beneath a thick

230   halocline[10,11]). However, our study shows that the rate of thinning of the GHSZ in

231   Storfjordrenna was at least six times faster than previously estimated, occurring over a period

232 of 1,000 years compared to the suggested 6,000 years[22]. The high BWT during HS1 (Fig. 4b)

233 drove the rapid thinning of the GHSZ, and probably the enhanced gas hydrate dissociation and

234 methane seepage reconstructed for the Bølling-Allerød interstadials (Fig. 3a,b,c, and Fig. 4c,d).

235 These results highlight the important role of BWT changes in gas hydrate systems in shallow

236 water at millennial time scales. At human time-scales, the migration of the GHSZ occurs in

237 response to seasonal variations in BWT in shallow waters when gas hydrates form in the near-

238 surface sediments[46]. Records of past BWT at different time scales underline the risk that the

239 current "Altantification" process in the Arctic bears in triggering an increase in seepage of

240 methane into the ocean, causing increase in ocean acidification and potentially amplifying the

241 effects of current climate change if reaching the atmosphere.

242

243 **Methods**

244 **Core handling**

245 Core HH18-1059GC (core 1059) (76°06.117'N; 15°58.077'E, 382 m water depth) was

246 retrieved from the southwestern Barents Sea during a cruise in July 2018 with R/V Helmer

247 Hanssen (Fig. 1). The 4.15 m long core was split into 1-m sections, capped and taped at both

248 ends and stored at 4°C right after retrieval. Prior to opening, the core sections were X-rayed,

249 and logged with a GEOTEK 7.9 Multi Sensor Logger. The core was split longitudinally into

250 two halves. The work half was color imaged with a Jai L-107CC 3 CCD RGB line scan camera

251 installed on an Avaatech XRF. The archive half was scanned at 10 and 30 kV on an Avaatech

252 XRF for bulk element ratios.

253 Thereafter, the work half was sampled in 1-cm thick slices. Samples were weighed, freeze-

254 dried and weighed again. Samples were selected following the main focus of our study: (a) from

255 3.9 to 2.9 m samples were selected every 2 cm, except at 3.66–3.64 m and 3.83–3.80 m where

256 every cm was selected; (b) from 2.9 to 0.1 m samples were selected every 10 cm; (c) from 0.1

257   to 0 m, every 2 cm was selected. The samples were wet-sieved over 63 μm, 100 μm and 500

258   μm mesh-sizes. The residues were dried at 40°C, weighed and the weight percent of each grain

259   size was calculated.

260

261   **Lithology, radiocarbon dating and construction of the age model**

262   The lithological log is based on visual examination, together with the records of X-ray

263   scanning, grain-size distribution and magnetic susceptibility (Fig. 2).

264   Nine AMS-^{14}C dates were acquired on samples of the planktic foraminiferal species

265   *Neogloboquadrina pachyderma* and bivalve samples at the ^{14}Chrono Centre, Queens

266   University, Northern Ireland (Table S1 and Fig. 2). Two additional dates from the upper and

267   lower boundaries of the laminated layer with a low concentration of foraminifera in core 1059

268   were added from correlation to dates of the same laminated layer from the well-dated nearby

269   located cores JM02-460[15] and HH15-1282GC[16] . Dates older than 12,436 ± 66 ^{14}C years were

270   calibrated using the Normarine18 calibration curve which uses variable reservoir ages ranging

271   from 420 ^{14}C years to 1,620 ^{14}C years prior to the Bølling-Allerød warming[29]. Dates younger

272   than 10,827 ^{14}C years were calibrated using the Marine20 calibration curve[47]. Individual

273   samples were calibrated using the CLAM 2.3.5 package[48] (Table S1). The age model was built

274   using the BACON 2.4.3 package[49] in R software. Core 1059 covers the early deglaciation (since

275   18,000 cal years BP) to the late Holocene (Fig. 2 and Fig. 3).

276

277   **Stable isotope analyses**

278   Oxygen and carbon isotopes were analyzed on pristine tests of the planktic foraminiferal

279   species *Neogloboquadrina pachyderma* and on the benthic foraminiferal species *Cassidulina*

280   *neoteretis,* in the size fraction 150 to 250 μm. The measurements were performed on 10 to 20

281   specimens (only 8 samples out of 117 samples contained less than 10 specimens) of each

282   species using a Thermo Scientific MAT253 IRMS and Gasbench II at the Department of

283   Geosciences, UiT The Arctic University of Norway, Tromsø. The precision of the instrument

284   is 0.1‰ for oxygen and carbon isotopes and the results are reported versus the in-house Vienna

285   Pee Dee Belemnite standard.

286   The measured $\delta^{13}C$ values of *C. neoteretis* range from -1.77‰ to -0.51‰ (Fig. 3f). These

287   values are within the expected range of $\delta^{13}C$ values for *C. neoteretis*[50] indicating that core 1059

288   has not been affected by methane seepage and any associated diagenetic coatings. We therefore

289   concluded that core 1059 was suitable for benthic foraminiferal Mg/Ca-based reconstructions

290   of BWT.

291

292   **Mg/Ca analysis and bottom water temperature calculation**

293   A total of 15 to 30 pristine tests of the dominant benthic foraminiferal species in the core

294   *Cassidulina neoteretis*, were picked for Mg/Ca analyses from the 150 to 250 μm size fraction.

295   The oxidative-reductive approach was used to clean the samples prior to the analysis[51–53]. This

296   cleaning approach includes clay removal, reductive cleaning with hydrous hydrazine, oxidative

297   cleaning with oxygen peroxide and weak acid leach. After cleaning the samples were dissolved

298   in HNO_3 (0.1M) and the $[Ca^{2+}]$ was measured in an inductively coupled plasma-optical

299   emission spectrometer (Agilent 5100 ICP-OES) at the Department of Earth Sciences at the

300   University of Cambridge. Due to the small amount of material, samples were analyzed again at

301   fixed $[Ca^{2+}]$ concentration[54] of ca. 20 ppm in order to determine the trace element content.

302   Instrumental precision of the ICP-OES was monitored using an in-house standard solution with

303   a Mg/Ca 1.474 mmol/mol. The average Mg/Ca on repeated measurements (n=14) of the in-

304   house standard solution at $[Ca^{2+}]$ of 20 ppm during this work was 1.476 mmol/mol (std. dev. =

305   0.009 mmol/mol, r.s.d. = 0.58%). Elemental ratios Mn/Ca, Fe/Ca and Al/Ca were used in

306   combination to evaluate contamination and two samples indicating potential contamination

307   were excluded (Table S2). Thereafter, we applied Grubb's test to identify any outlier in the

308   Mg/Ca data and two samples were excluded (Table S2). The remaining samples showed low

309   correlation between Mn/Ca, Fe/Ca, and Mg/Ca (r^2=0.14 for Mn/Ca-Mg/Ca; r^2=0.06 for Fe/Ca-

310   Mg/Ca; aluminum concentrations were below the detection limit indicating no clay

311   contamination; Fig. S5 and Fig. S6).

312   Mg/Ca values were converted into temperature using the calibration equation for *C.*

313   *neoteretis* from Kristjánsdóttir et al.[55]:

314    $$Mg/Ca = 0.864 \pm 0.07 \times \exp (0.082 \pm 0.020 \times BWT)$$

315   The calibration error ($\pm 0.62°C^{55}$), the analytical error (± 0.017 mmol/mol equivalent to

316   0.18°C using Kristjánsdóttir et al.'s calibration) and the standard deviation of the replicates of

317   four samples (± 0.078 mmol/mol equivalent to 0.78°C) were used to calculate the error, that is

318   the result of the squared root of the sum of the squared individual errors. The analytical error

319   was calculated as two times the mean standard deviation of the repeated measurements on the

320   inhouse standard solution. This gave an estimated propagation error of $\pm 1.01°C$ for *C.*

321   *neoteretis.* When an average BWT was presented in the main text, the error was calculated

322   taking into account the propagation error of the measurement ($\pm 1.01°C$) and the standard

323   deviation of the mean and the higher "error" value was chosen.

324   Considering the affinity of *C. neoteretis* for Atlantic Water (AW)[27,28] and the hydrography

325   of Storfjordrenna, our BWT record probably represents the temperature range of this water

326   mass. Today, the AW has a temperature of ca. 3 °C in Storfjordrenna and is representative of

327   years with low brine production (in years with strong brine formation temperature may reach

328   down to -1.3°C and salinity increase to 35.3)[21]. We therefore speculate that in the past, during

329   periods with strong stratification, such as the early deglaciation, with low seasonality and no or

330   low brine flow[32], the AW reached the deepest part of Storfjordrenna almost all year and

331   therefore that our BWT represents an annual mean. During periods of strong seasonality (e.g.

332   Late Holocene[15]), our BWT would represent seasons of AW inflow (i.e., modern summer-

333   autumn conditions).

334

335   **Ice volume correction for stable isotopes**

336   We used *Cassidulina neoteretis* ($\delta^{18}O_{calcite}$) and BWT to calculate seawater $\delta^{18}O$ ($\delta^{18}O_{sw}$)

337   using the equation of Lubinski et al.[56] with a slight modification:

338    $$\delta^{18}O_{calcite} - 0.27 - ((-16.9 + BWT) / -4) = \delta^{18}O_{sw}$$

339   In addition, we attempted to remove the ice volume component in our $\delta^{18}O_{sw}$ record (i.e., to

340   calculate $\delta^{18}O_{local\ sw}$) using the relative sea level record of Spratt and Lisiecki[57] and a conversion

341   factor of 0.009‰ of $\delta^{18}O$ per meter of sea level change[57].

342

343   **Transient modeling of the thickness of the gas hydrate stability zone (GHSZ)**

344   Variations in the thickness of gas hydrate stability within the sediments over the last 35,000

345   years were estimated by employing a diffusive heat transport model, in combination with

346   theoretical hydrate stability estimates[58]. The diffusive heat flow model was designed in 1D with

347   2,000 cells at a resolution of 1m with upper boundary at the seafloor and basal boundary 2,000

348   meters below the seafloor. Initial boundary conditions at 35,000 years were set assuming

349   average present-day BWT of 2°C ([22], this study), sediment thermal diffusivity of 3.71×10^{-7} m^2s^{-1}

350   [1] (derived using a thermal conductivity of 1.41 $Wm^{-1}K^{-1}$ [59], bulk sediment density of 1,900 kgm^{-3}

351   [3], and specific heat capacity of 2,000 $Jkg^{-1}K^{-1}$ [3], and a linear thermal gradient of 0.035°Cm^{-1} [25].

352   Ice sheet was assumed to be present at the study area from 35,000 to 18,500 years BP[15,22].

353   During this period, a constant ice sheet thickness of 900 m and a constant basal ice temperature

354   of -2°C[22] was used to determine pressure and temperature conditions within the sediments.

355   After the ice sheet retreat at 18,500 years BP, the reconstructed BWT presented in this study

356   was used as the upper boundary condition until the present day. The transient diffusive heat

357 transport in sediments was then estimated using an explicit finite-difference numerical solution

358 of the Fourier heat equation[60].

359   The subsurface thermal profile over the past 35,000 years generated by the heat flow model

360 was then integrated with pressure changes resulting from variations in sea level[61] and

361 topographic changes due to glacial isostatic effects. The maximum subsidence generated by the

362 ice loading during the period 35,000 to 18,500 years BP was ca. 85 m[22]. The subsidence and the

363 subsequent uplift were linearly distributed over the modeled period with peak subsidence

364 reaching at 18,500 years BP and uplift reaching zero by the present day. The pressure and

365 temperature conditions were then compared with the theoretical hydrate stability phase

366 diagrams generated with the CSMHYD program[58] to estimate the thickness of gas hydrate

367 stability zone at any time step. The gas hydrate phase boundary was generated for a feed gas

368 composition containing 99.54% methane, 0.41% ethane, and 0.05% propane[22] as well as an

369 assumed pore-water salinity of 35 psu. The sensitivity of GHSZ to the input parameters of the

370 model was analyzed assuming a plausible range of values (see Fig. S7 and Table S3 for details).

371

372 **Correlation of cores**

373   Sediment core 1059 was taken from a non-methane affected area close to core CAGE 15-2

374 920GC (core 920) taken from a methane hydrate mound (termed "pingo")[24]. The two cores

375 were correlated using minima and maxima in Zr/Rb and Fe/Ca ratios (Fig. S3). In Yao et al.[24]

376 the age-depth model of core 920 is established by correlation to the reference core CAGE 15-

377 2 921GC, with one radiocarbon date and three tie-points to other cores in the region. In order

378 to allow a direct comparison between core 920 and our core 1059, a new and improved age-

379 depth model of core 920 was established using our much more detailed chronology.

380   The concentration in $\mu g\ g^{-1}$ of Archaea and bacterial lipids indicating anaerobic oxidation of

381 methane are presented in Yao et al.[24]. However, with the new age model that takes the highly

382   variable sedimentation rates in the area into consideration[15,16], we calculated the flux of

383   bacterial lipids to indicate the productivity (cm µg g^{-1} ky^{-1}) using the archaeol concentrations[24]

384   and the sedimentation rate. Only flux and δ^{13}C of archaeols are shown in Fig. 3 (see Yao et al.[24]

385   for more data).

386

387   **Supplementary Materials**

388   **Fig. S1**
389   **Fig. S2**
390   **Fig. S3**
391   **Fig. S4**
392   **Fig. S5**
393   **Fig. S6**
394   **Fig. S7**
395   **Table S1**
396   **Table S2**
397   **Table S3**
398

References

400 1. Asbjørnsen, H., Årthun, M., Skagseth, Ø. & Eldevik, T. Mechanisms Underlying Recent
401   Arctic Atlantification. *Geophys. Res. Lett.* **47**, (2020).
402 2. Kretschmer, K., Biastoch, A., Rüpke, L. & Burwicz, E. Modeling the fate of methane
403   hydrates under global warming. *Glob. Biogeochem. Cycles* **29**, 610–625 (2015).
404 3. Berndt, C. *et al.* Temporal Constraints on Hydrate-Controlled Methane Seepage off
405   Svalbard. *Science* **343**, 284–287 (2014).
406 4. Ferré, B. *et al.* Reduced methane seepage from Arctic sediments during cold bottom-water
407   conditions. *Nat. Geosci.* **13**, 144–148 (2020).
408 5. Reeburgh, W. S. Oceanic Methane Biogeochemistry. *Chem. Rev.* **107**, 486–513 (2007).
409 6. Hinrichs, K.-U. & Boetius, A. The Anaerobic Oxidation of Methane: New Insights in
410   Microbial Ecology and Biogeochemistry. in *Ocean Margin Systems* (eds. Wefer, G. et al.)
411   457–477 (Springer Berlin Heidelberg, 2002).
412 7. McGinnis, D. F., Greinert, J., Artemov, Y., Beaubien, S. E. & Wüest, A. Fate of rising
413   methane bubbles in stratified waters: How much methane reaches the atmosphere? *J.*
414   *Geophys. Res.* **111**, C09007 (2006).
415 8. Boetius, A. & Wenzhöfer, F. Seafloor oxygen consumption fuelled by methane from cold
416   seeps. *Nat. Geosci.* **6**, 725–734 (2013).
417 9. Biastoch, A. *et al.* Rising Arctic Ocean temperatures cause gas hydrate destabilization and
418   ocean acidification. *Geophys. Res. Lett.* **38**, (2011).
419 10. Rasmussen, T. L. & Thomsen, E. The role of the North Atlantic Drift in the millennial
420   timescale glacial climate fluctuations. *Palaeogeogr. Palaeoclimatol. Palaeoecol.* **210**, 101–
421   116 (2004).
422 11. Ezat, M. M., Rasmussen, T. L. & Groeneveld, J. Persistent intermediate water warming
423   during cold stadials in the southeastern Nordic seas during the past 65 k.y. *Geology* **42**,
424   663–666 (2014).
425 12. El bani Altuna, N., Ezat, M. M., Greaves, M. & Rasmussen, T. L. Millennial-scale changes
426   in bottom water temperature and water mass exchange through the Fram Strait 79ºN, 63–
427   13 ka. *Paleoceanogr. Paleoclimatology* (2021).
428 13. Bond, G. C. & Lotti, R. Iceberg Discharges Into the North Atlantic on Millennial Time
429   Scales During the Last Glaciation. *Science* **267**, 1005–1010 (1995).
430 14. Hughes, A. L. C., Gyllencreutz, R., Lohne, Ø. S., Mangerud, J. & Svendsen, J. I. The last
431   Eurasian ice sheets - a chronological database and time-slice reconstruction, DATED-1.
432   *Boreas* **45**, 1–45 (2016).
433 15. Rasmussen, T. L. *et al.* Paleoceanographic evolution of the SW Svalbard margin (76°N)
434   since 20,000 ^{14}C yr BP. *Quat. Res.* **67**, 100–114 (2007).
435 16. Rasmussen, T. L. & Thomsen, E. Climate and ocean forcing of ice-sheet dynamics along
436   the Svalbard-Barents Sea ice sheet during the deglaciation ~20,000–10,000 years BP. *Quat.*
437   *Sci. Adv.* **3**, 100019 (2021).
438 17. Petrini, M. *et al.* Simulated last deglaciation of the Barents Sea Ice Sheet primarily driven
439   by oceanic conditions. *Quat. Sci. Rev.* **238**, 106314 (2020).

18. Alvarez-Solas, J., Banderas, R., Robinson, A. & Montoya, M. Ocean-driven millennial-scale variability of the Eurasian ice sheet during the last glacial period simulated with a hybrid ice-sheet–shelf model. *Clim. Past* **15**, 957–979 (2019).

19. Khazendar, A. *et al.* Rapid submarine ice melting in the grounding zones of ice shelves in West Antarctica. *Nat. Commun.* **7**, 13243 (2016).

20. Straneo, F. & Heimbach, P. North Atlantic warming and the retreat of Greenland's outlet glaciers. *Nature* **504**, 36–43 (2013).

21. Skogseth, R., Haugan, P. M. & Jakobsson, M. Watermass transformations in Storfjorden. *Cont. Shelf Res.* **25**, 667–695 (2005).

22. Serov, P. *et al.* Postglacial response of Arctic Ocean gas hydrates to climatic amelioration. *Proc. Natl. Acad. Sci.* **114**, 6215–6220 (2017).

23. Rasmussen, S. O. *et al.* A stratigraphic framework for abrupt climatic changes during the Last Glacial period based on three synchronized Greenland ice-core records: refining and extending the INTIMATE event stratigraphy. *Quat. Sci. Rev.* **106**, 14–28 (2014).

24. Yao, H., Niemann, H. & Panieri, G. Multi-proxy approach to unravel methane emission history of an Arctic cold seep. *Quat. Sci. Rev.* **244**, 106490 (2020).

25. Waage, M. *et al.* Geological controls on fluid flow and gas hydrate pingo development on the Barents Sea margin. *Geochem. Geophys. Geosystems* **20**, 630–650 (2019).

26. Jessen, S. P., Rasmussen, T. L., Nielsen, T. & Solheim, A. A new Late Weichselian and Holocene marine chronology for the western Svalbard slope 30,000–0 cal years BP. *Quat. Sci. Rev.* **29**, 1301–1312 (2010).

27. Hald, M. & Korsun, S. Distribution of modern benthic foraminifera from fjords of Svalbard, European Arctic. *J. Foraminifer. Res.* **27**, 101–122 (1997).

28. Korsun, S. & Hald, M. Seasonal dynamics of benthic foraminifera in a glacially fed fjord of Svalbard, European Arctic. *J. Foraminifer. Res.* **30**, 251–271 (2000).

29. Brendryen, J., Haflidason, H., Yokoyama, Y., Haaga, K. A. & Hannisdal, B. Eurasian Ice Sheet collapse was a major source of Meltwater Pulse 1A 14,600 years ago. *Nat. Geosci.* **13**, 363–368 (2020).

30. Carlson, A. E. What Caused the Younger Dryas Cold Event? *Geology* **38**, 383–384 (2010).

31. Keigwin, L. D. *et al.* Deglacial floods in the Beaufort Sea preceded Younger Dryas cooling. *Nat. Geosci.* **11**, 599–604 (2018).

32. Rasmussen, T. L. & Thomsen, E. Brine formation in relation to climate changes and ice retreat during the last 15,000 years in Storfjorden, Svalbard, 76-78°N. *Paleoceanography* **29**, 911–929 (2014).

33. Crémière, A. *et al.* Timescales of methane seepage on the Norwegian margin following collapse of the Scandinavian Ice Sheet. *Nat. Commun.* **7**, 11509 (2016).

34. Argentino, C. *et al.* Dynamic and history of methane seepage in the SW Barents Sea: new insights from Leirdjupet Fault Complex. *Sci. Rep.* **11**, 4373 (2021).

35. Pedrosa, M. T. *et al.* Seabed morphology and shallow sedimentary structure of the Storfjorden and Kveithola trough-mouth fans (North West Barents Sea). *Mar. Geol.* **286**, 65–81 (2011).

36. Patton, H. *et al.* Deglaciation of the Eurasian ice sheet complex. *Quat. Sci. Rev.* **169**, 148–172 (2017).

483   37. Shackleton, C. S., Winsborrow, M. C. M., Andreassen, K., Lucchi, R. G. & Bjarnadóttir,
484   L. R. Ice-margin retreat and grounding-zone dynamics during initial deglaciation of the
485   Storfjordrenna Ice Stream, western Barents Sea. *Boreas* **49**, 38–51 (2020).

486   38. Nielsen, T. & Rasmussen, T. L. Reconstruction of ice sheet retreat after the Last Glacial
487   maximum in Storfjorden, southern Svalbard. *Mar. Geol.* **402**, 228–243 (2018).

488   39. Andreassen, K. *et al.* Massive blow-out craters formed by hydrate-controlled methane
489   expulsion from the Arctic seafloor. *Science* **356**, 948–953 (2017).

490   40. Andreassen, K., Winsborrow, M., Bjarnadóttir, L. R. & Rüther, D. C. Ice stream retreat
491   dynamics inferred from an assemblage of landforms in the northern Barents Sea. *Quat. Sci.*
492   *Rev.* 246–257 (2014).

493   41. Knies, J. *et al.* Sea-ice dynamics in an Arctic coastal polynya during the past 6500 years.
494   *arktos* **3**, 1 (2017).

495   42. Vadakkepuliyambatta, S., Chand, S. & Bünz, S. The history and future trends of ocean
496   warming-induced gas hydrate dissociation in the SW Barents Sea. *Geophys. Res. Lett.* **44**,
497   835–844 (2017).

498   43. Riahi, K. *et al.* RCP 8.5—A scenario of comparatively high greenhouse gas emissions.
499   *Clim. Change* **109**, 33–57 (2011).

500   44. Taylor, K. E., Stouffer, R. J. & Meehl, G. A. An Overview of CMIP5 and the Experiment
501   Design. *Bull. Am. Meteorol. Soc.* **93**, 485–498 (2012).

502   45. Vadakkepuliyambatta, S. *et al.* Climatic impact of Arctic Ocean methane hydrate
503   dissociation in the 21st-century. 27 (2017).

504   46. Ferré, B., Mienert, J. & Feseker, T. Ocean temperature variability for the past 60 years on
505   the Norwegian-Svalbard margin influences gas hydrate stability on human time scales. *J.*
506   *Geophys. Res. Oceans* **117**, C10017 (2012).

507   47. Heaton, T. J. *et al.* Marine20–The marine radiocarbon age calibration curve (0–55,000 cal
508   BP). *Radiocarbon* **62**, 779–820 (2020).

509   48. Blaauw, M. Methods and code for 'classical' age-modelling of radiocarbon sequences.
510   *Quat. Geochronol.* **5**, 512–518 (2010).

511   49. Blaauw, M. & Christen, J. A. Flexible paleoclimate age-depth models using an
512   autoregressive gamma process. *Bayesian Anal.* **6**, 457–474 (2011).

513   50. McCorkle, D. C., Keigwin, L. D., Corliss, B. H. & Emerson, S. R. The influence of
514   microhabitats on the carbon isotopic composition of deep-sea benthic foraminifera.
515   *Paleoceanography* **5**, 161–185 (1990).

516   51. Boyle, E. A. & Keigwin, L. D. Comparison of Atlantic and Pacific paleochemical records
517   for the last 215,000 years: changes in deep ocean circulation and chemical inventories.
518   *Earth Planet. Sci. Lett.* **76**, 135–150 (1985).

519   52. Pena, L. D., Calvo, E., Cacho, I., Eggins, S. & Pelejero, C. Identification and removal of
520   Mn-Mg-rich contaminant phases on foraminiferal tests: Implications for Mg/Ca past
521   temperature reconstructions. *Geochem. Geophys. Geosystems* **6** (2005).

522   53. Ezat, M. M., Rasmussen, T. L. & Groeneveld, J. Reconstruction of hydrographic changes
523   in the southern Norwegian Sea during the past 135 kyr and the impact of different
524   foraminiferal Mg/Ca cleaning protocols. *Geochem. Geophys. Geosystems* **17**, 3420–3436
525   (2016).

54. de Villiers, S., Greaves, M. & Elderfield, H. An intensity ratio calibration method for the accurate determination of Mg/Ca and Sr/Ca of marine carbonates by ICP-AES. *Geochem. Geophys. Geosystems* **3** (2002).

55. Kristjánsdóttir, G. B., Lea, D. W., Jennings, A. E., Pak, D. K. & Belanger, C. New spatial Mg/Ca-temperature calibrations for three Arctic, benthic foraminifera and reconstruction of north Iceland shelf temperature for the past 4000 years. *Geochem. Geophys. Geosystems* **8**, Q03P21 (2007).

56. Lubinski, D. J., Polyak, L. & Forman, S. L. Freshwater and Atlantic water inflows to the deep northern Barents and Kara seas since ca 13 14C ka: foraminifera and stable isotopes. *Quat. Sci. Rev.* **20**, 1851–1879 (2001).

57. Spratt, R. M. & Lisiecki, L. E. A Late Pleistocene sea level stack. *Clim. Past* **12**, 1079–1092 (2016).

58. Sloan, E. D. & Koh, C. *Clathrate Hydrates of Natural Gases, Third Edition*. (CRC Press, 2007).

59. Crane, K. *et al.* Thermal evolution of the western Svalbard margin. *Mar. Geophys. Res.* **9**, 165–194 (1988).

60. Phrampus, B. J. & Hornbach, M. J. Recent changes to the Gulf Stream causing widespread gas hydrate destabilization. *Nature* **490**, 527–530 (2012).

61. Grant, K. M. *et al.* Rapid coupling between ice volume and polar temperature over the past 150,000 years. *Nature* **491**, 744–747 (2012).

62. Svensson, A. *et al.* A 60 000 year Greenland stratigraphic ice core chronology. *Clim. Past* **4**, 47–57 (2008).

Fig. 1. Physical oceanography and bathymetry of the study area. (**A**) Map showing major surface currents (based on ref. 10) and maximum extent of Svalbard-Barents Sea Ice Sheet (SBIS) during the Late Glacial Maximum (LGM) according to ref. 9 (dashed white line). (**B**) Bathymetric map of the "Pingo area" of methane hydrate mounds in the northwestern Barents Sea, where gas seepage occurs (Fig. S1). (**C**) Conductivity-Temperature-Depth (CTD) profiles (July 2014 and April 2015 from core site of JM02-460; July 2018 from core site of HH18-1059GC). The right columns in panel (**C**) indicate the two different hydrographic scenarios: 1 = when the Atlantic Water occupies the entire water column and 2 = when a winter polynya and winter conditions allow the formation of brine (Br in figure) enriched shelf waters. Star shows location of core HH18-1059GC (1059 in text). Location of core JM02-460[15] is indicated with white circle (**A**) and core CAGE 15-2 920GC (920 in text)[24] is shown with white pentagon (**B**). Abbreviations: WSC: West Spitsbergen Current; ESC: East Spitsbergen Current.
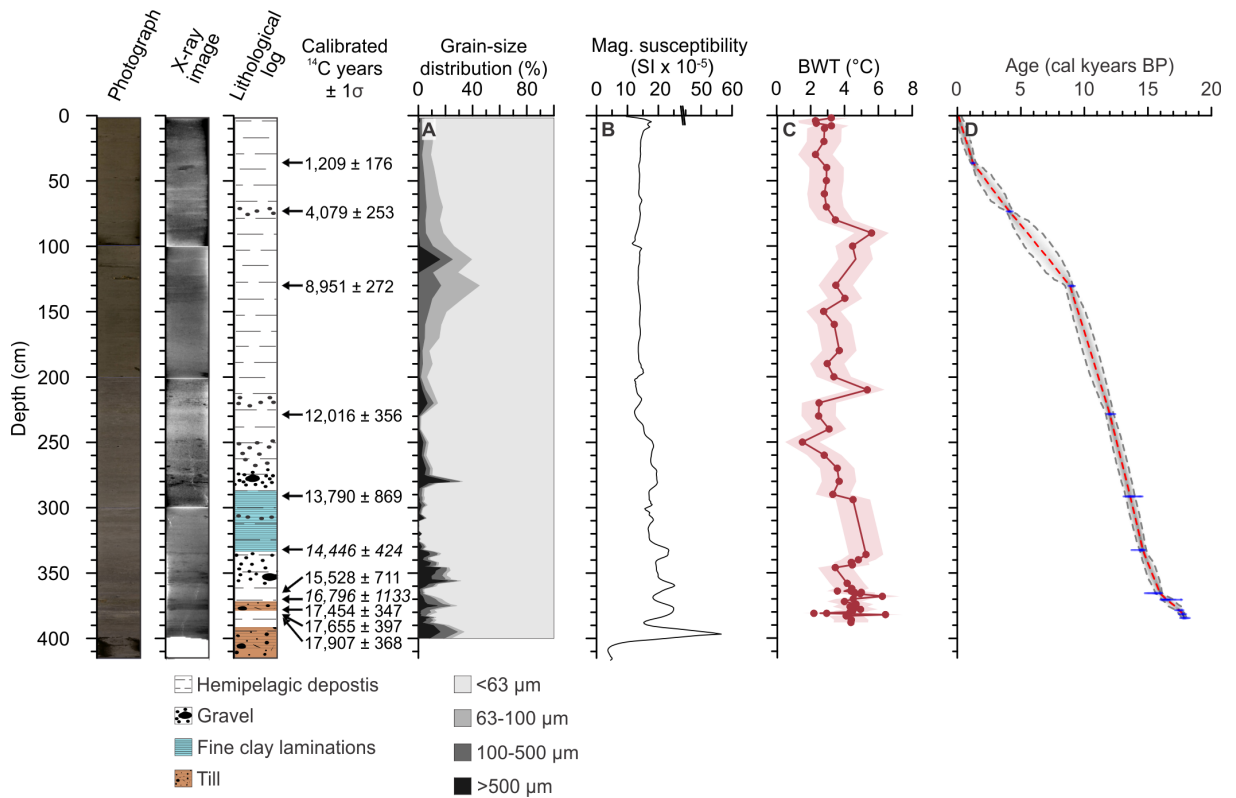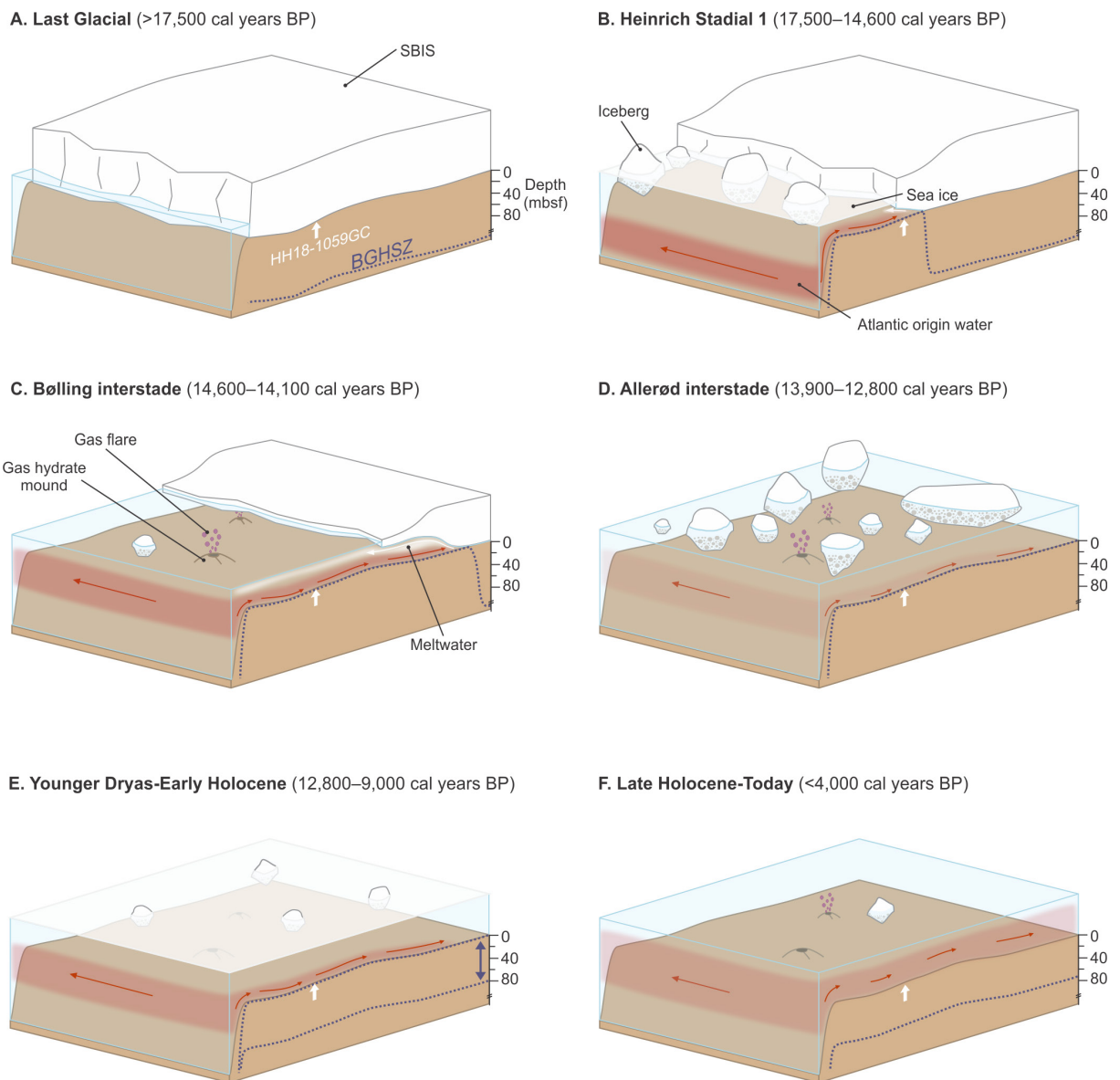
Fig. 2. Lithology, calibrated ages, sedimentological and physical properties of core 1059. (**A**) Weight percentages of the different grain-size fractions. (**B**) Magnetic susceptibility. (**C**) Reconstructed bottom water temperature (BWT). (**D**) Age-depth model. Left columns: XRF-Image scan, X-ray images and lithological log with cal ages indicated of core 1059. Ages in italics are transferred ages from two nearby cores (see text for explanation).
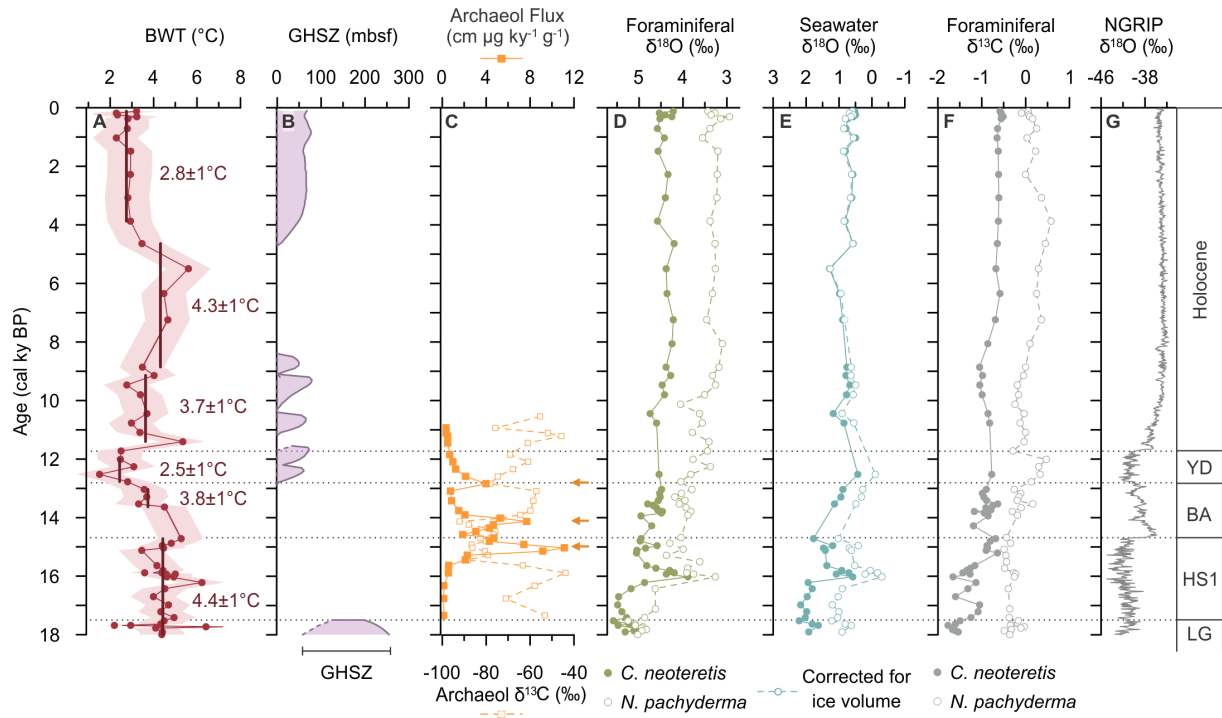
Fig. 3. Bottom water temperature in Storfjordrenna, stable isotopes, methane seepage and evolution of the gas hydrate stability zone (GHSZ). (**A**) Reconstructed bottom water temperature (BWT) derived from benthic foraminiferal Mg/Ca. Shaded area indicates the uncertainty interval calculated with error propagation. Thick vertical lines represent the average BWT for each interval. For the Bølling-Allerød interval the average only represents the Allerød interstade due to the lack of datapoints during Bølling. (**B**) Top (dashed line) and base (solid line) of the gas hydrate stability zone (GHSZ), which is represented by the colored area. (**C**) Archaeol flux and archaeol carbon isotopes from core 920[24] (see Methods). Methane seepage events shown by these data are indicated with the dark orange arrows. (**D**) Benthic (*Cassidulina neoteretis*) and planktic (*Neogloboquadrina pachyderma*; dashed lines) foraminiferal oxygen isotopes. (**E**) Seawater oxygen isotopes calculated using bottom water temperature and benthic δ18O_calcite (continuous line) and corrected for ice volume (dashed line). (**F**) Benthic (*C. neoteretis*) and planktic (*N. pachyderma*; dashed lines) carbon isotopes. (**G**) NGRIP ice core δ18O record in the GICC05modelext timescale[23,62]. Abbreviations: LG: Late Glacial; HS1: Heinrich Stadial 1; BA: Bølling-Allerød interstadials; YD: Younger Dryas stadial.

24

A. Last Glacial (>17,500 cal years BP)

SBIS

0
40 Depth
80 (mbsf)

HH18-1059GC

BGHSZ

B. Heinrich Stadial 1 (17,500–14,600 cal years BP)

Iceberg

Sea ice

0
40
80

Atlantic origin water

C. Bølling interstade (14,600–14,100 cal years BP)

Gas flare

Gas hydrate
mound

0
40
80

Meltwater

D. Allerød interstade (13,900–12,800 cal years BP)

0
40
80

E. Younger Dryas-Early Holocene (12,800–9,000 cal years BP)

0
40
80

F. Late Holocene-Today (<4,000 cal years BP)

0
40
80

Fig. 4. Paleoenvironmental evolution of Storfjordrenna and the Svalbard-Barents Sea Ice Sheet (SBIS) since the early deglaciation to the late Holocene. Gas hydrate stability zone (GHSZ) thickness changes in meters below seafloor (mbsf) in relation to bottom water temperatures and ice retreat patterns are shown. The dark purple dotted line indicates the base of the gas hydrate stability zone (BGHSZ), which corresponds to lower limit of the GHSZ. The uppermost limit (top of gas hydrate occurrence zone) is at the seafloor[22]. Inflow and relative temperature of the Atlantic water are shown in red, where stronger red indicates relatively higher temperature. Thick white arrow marks the position of core 1059. Age for each interval is shown as calibrated ages before present (BP).
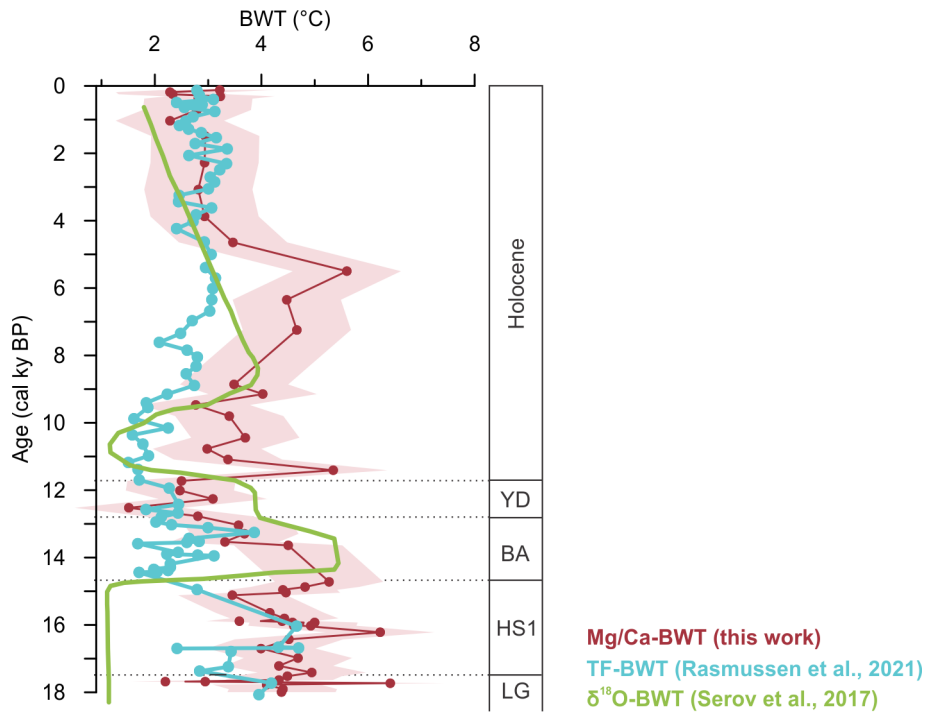
Supplementary Materials

2
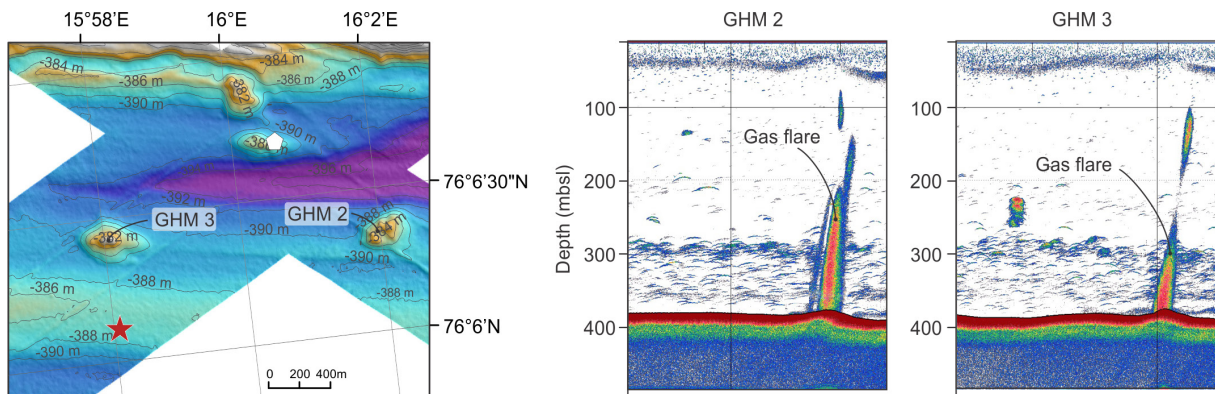
3

4 **Fig. S1. Methane seepage from the seafloor in Storfjordrenna.** Bathymetric map (left) and

5 echosounder images of Gas Hydrate Mounds (GHM) 2 and 3. The red star indicates the location

6 of core 1059. The location of core CAGE 15-2 920GC (920 in text)[1] is shown with white

7 pentagon.
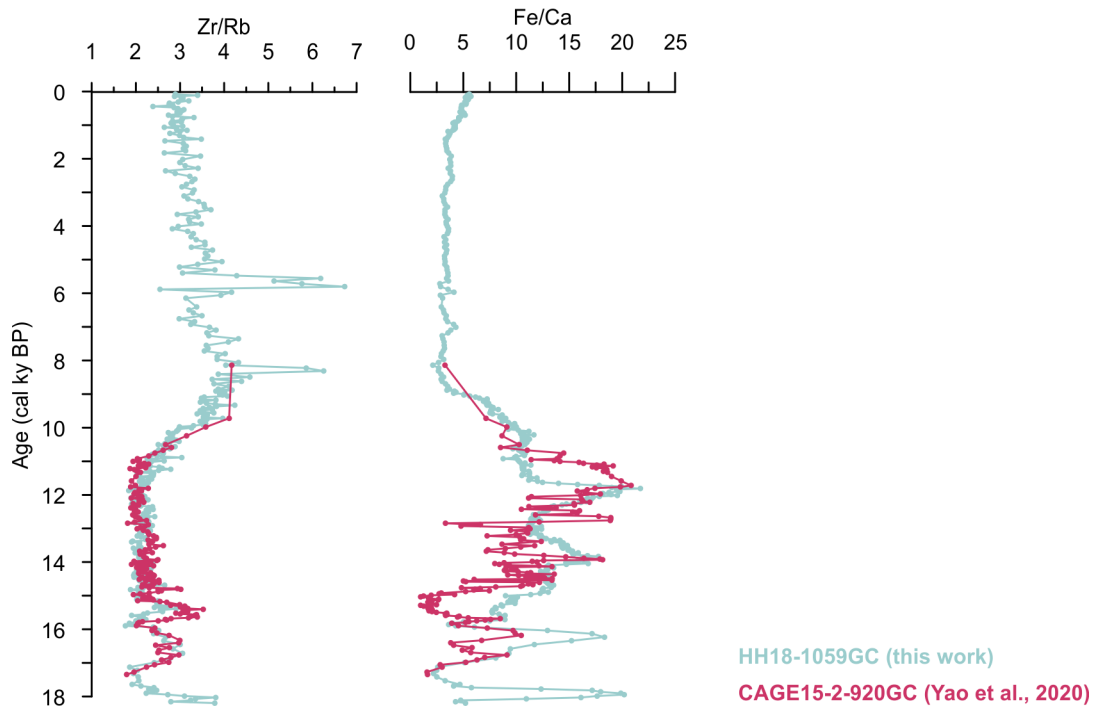
8

Fig. S2. Bottom water temperature (BWT) records in Storfjordrenna. In core JM02-460PC BWT was calculated using benthic foraminiferal transfer functions (TF)[2] or estimated using benthic foraminiferal $\delta^{18}O$ [3], whereas in this work we used benthic foraminiferal Mg/Ca measured on *Cassidulina neoteretis* (see Methods). For location see Fig. S1.

Fig. S3. Correlation of cores 1059 and 920. Core 920 was studied for archaeol and bacterial lipids related to the presence of methane[1]. The cores were correlated based on XRF data (Zr/Rb and Fe/Ca). For location see Fig. S1.
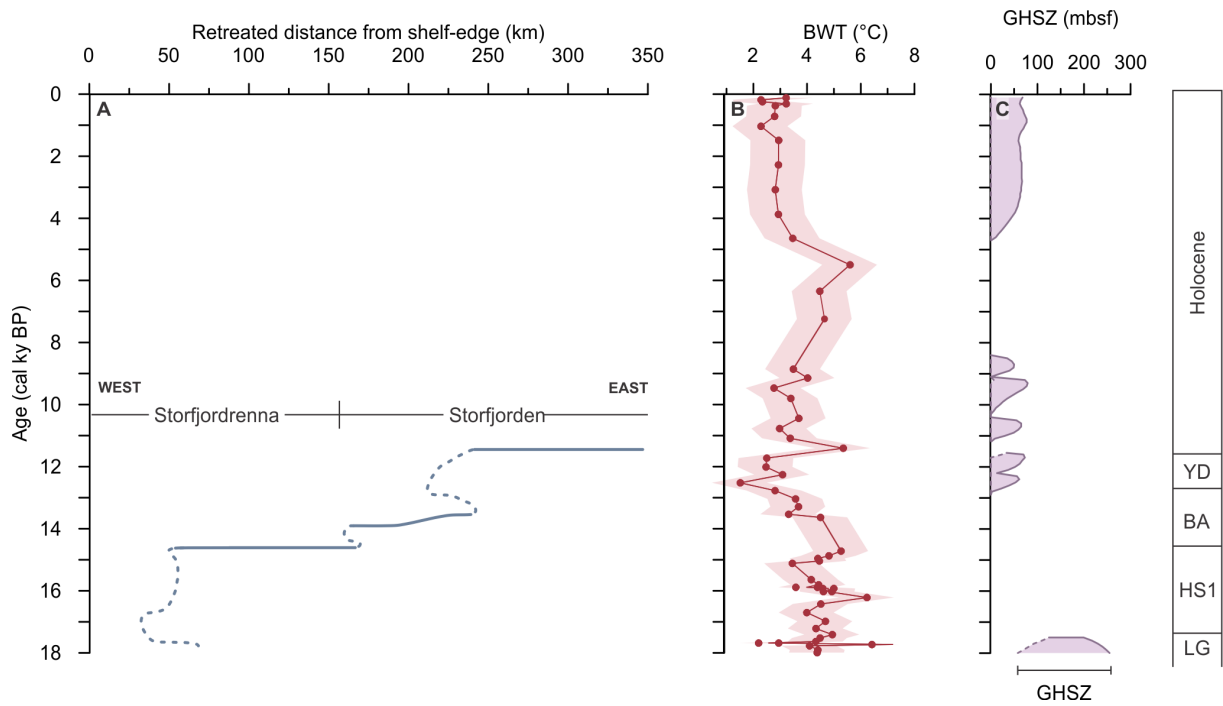
Fig. S4. Bottom water temperature affect ice-sheet retreat and GHSZ thickness. (**A**) Time-distance diagram of Svalbard Barents Sea Ice sheet from shelf-edge to inner Storfjorden[2]. (**B**) Bottom water temperature (BWT). (**C**) Top (dashed line) and base (solid line) of the gas hydrate stability zone (GHSZ), which is represented by the colored area.

26
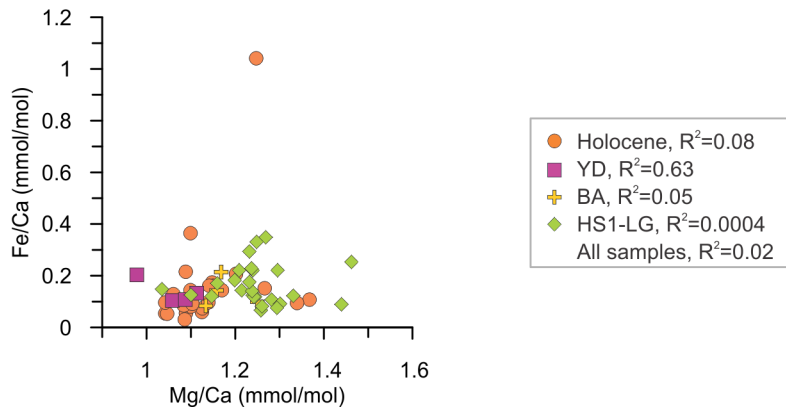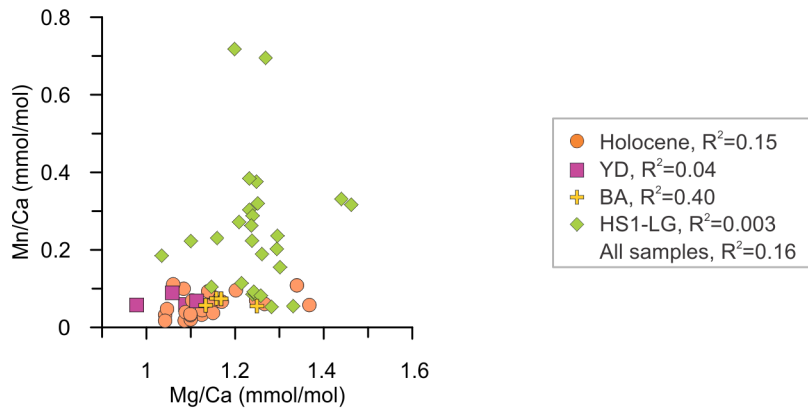
Fig. S5. Mn/Ca-Mg/Ca and Fe/Ca-Mg/Ca values for used samples. Aluminum concentrations were below detection limits and are not shown.

29

30
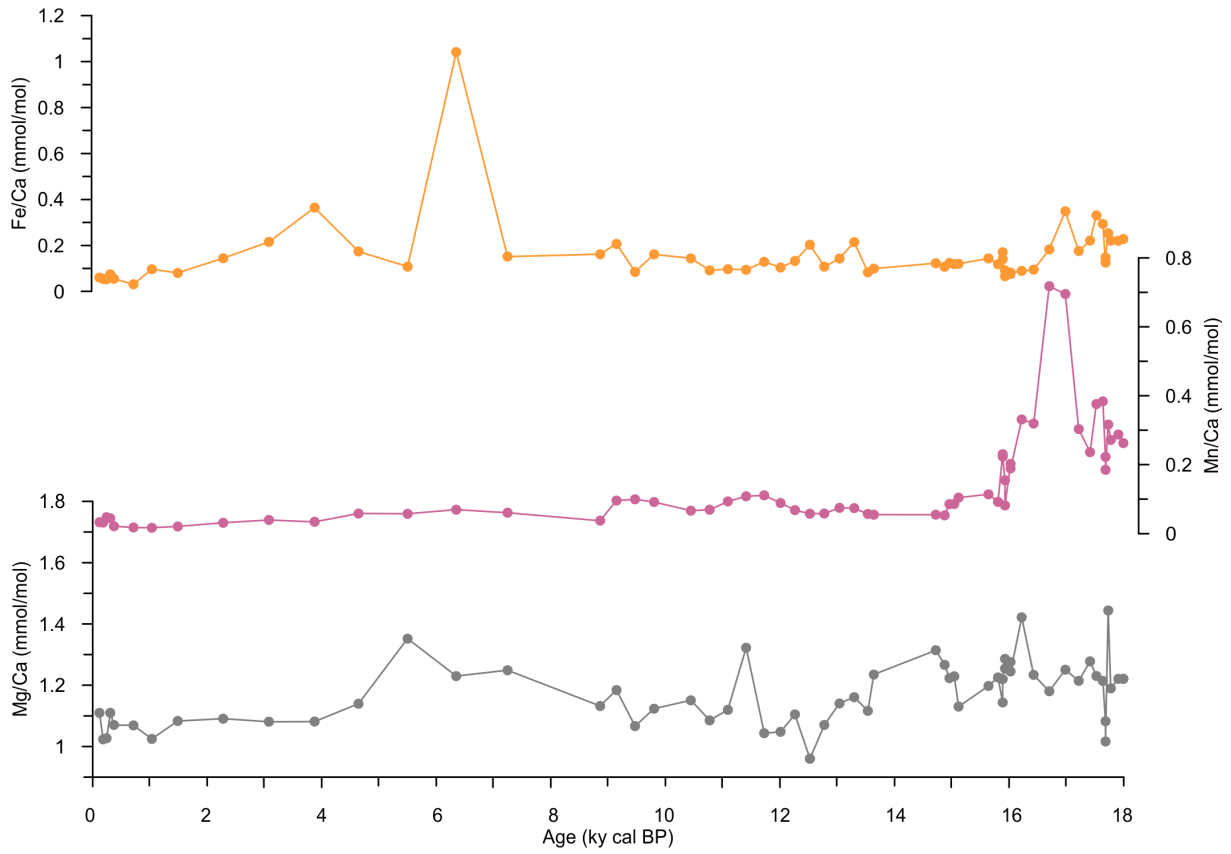
Fig. S6. Downcore Mg/Ca, Mn/Ca- and Fe/Ca for samples used. Aluminum concentrations were below detection limits and are not shown.

33

34

Fig. S7. Impact of input parameters on the modeled gas hydrate stability zone (GHSZ).
Minimum and maximum variation in the GHSZ, due to uncertainties in bottom water
temperature, thermal gradient, porewater salinity, and thermal properties listed in Table S3.

38

39   **Table S1. Radiocarbon dates and calibrated ages in core HH18-1059GC.**
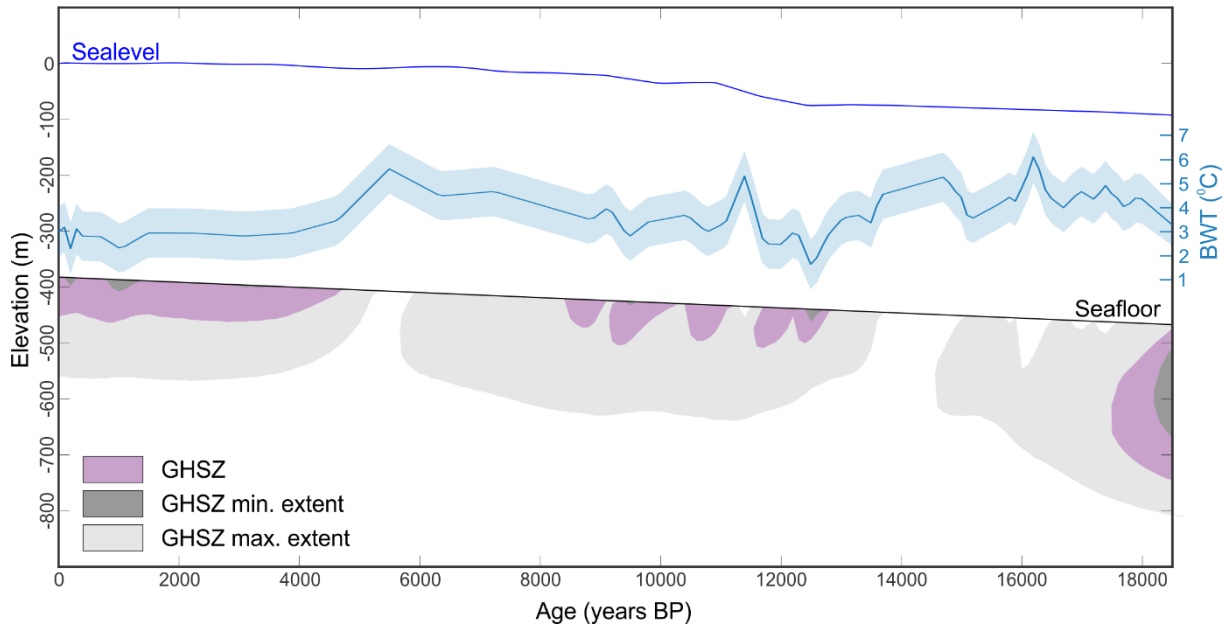
Core Depth (cm)	Lab code	Material	Sample mass (mg)	^{14}C age (years ± 1σ)	Mid-point of calibrated age 2σ (years ± 1σ)	Reference
36	UBA-42727	Bivalve	6.1	1,821 ± 25	1,209 ± 176	This work
73	UBA-42728	Bivalve	13.2	4,190 ± 33	4,079 ± 253	This work
130	UBA-42481	*N. pachyderma* (foraminifera)	6.8	8,537 ± 36	8,951 ± 272	This work
228	UBA-43810	*Astarte* sp. (bivalve)	14.4	10,776 ± 40	12,016 ± 356	This work
291	UBA-42482	*N. pachyderma* (foraminifera)	4.4	12,436 ± 66	13,790 ± 869	This work
332	UB-31784	*Nuculana* spp. (bivalve)	-	13,042 ± 47	14,446 ± 424	Rasmussen et al.[2]
365	UBA-42483	*N. pachyderma* (foraminifera)	6.4	14,595 ± 64	15,528 ± 711	This work
370	AAR-9448	*N. pachyderma* (foraminifera)	-	15,250 ± 130	16,796 ± 1,133	Rasmussen et al.[4]
378	UBA-42484	*N. pachyderma* (foraminifera)	6	15,956 ± 59	17,454 ± 347	This work
381	UBA-42485	*N. pachyderma* (foraminifera)	6.3	16,281 ± 72	17,655 ± 397	This work
384	UBA-42486	*N. pachyderma* (foraminifera)	6.2	16,458 ± 96	17,907 ± 368	This work

40

41

42 **Table S2. Trace element ratios.** Excluded samples showing clear signs of contamination

43 (highlighted in bold) or identified as outliers by the Grubb's test are marked in italics.

Depth (cm)	Age (cal years BP)	Al/Ca (mmol/mol)	Fe/Ca (mmol/mol)	Mn/Ca (mmol/mol)	Mg/Ca (mmol/mol)
2	12	-	0.06	0.03	1.12
4	183	-	0.05	0.03	1.04
6	244	-	0.05	0.05	1.05
8	309	-	0.07	0.04	1.13
10	374	-	0.05	0.02	1.09
20	713	-	0.03	0.02	1.09
30	1,033	-	0.10	0.02	1.04
40	1,486	-	0.08	0.02	1.10
50	2,279	-	0.14	0.03	1.10
60	3,077	-	0.22	0.04	1.09
70	3,875	-	0.36	0.03	1.10
80	4,642	-	0.17	0.06	1.15
90	5,498	-	0.11	0.06	1.37
100	6,348	-	1.04	0.07	1.25
110	7,243	-	0.15	0.06	1.27
130	8,860	-	0.16	0.04	1.15
140	9,146	-	0.21	0.10	1.20
150	9,470	-	0.09	0.10	1.08
160	9,802	-	0.16	0.09	1.14
180	10,445	-	0.14	0.07	1.17
190	10,772	-	0.09	0.07	1.10
200	11,089	-	0.10	0.09	1.14
210	11,409	-	0.09	0.11	1.34
220	11,725	-	0.13	0.11	1.06
230	12,011	-	0.10	0.09	1.06
240	12,261	-	0.13	0.07	1.11
250	12,523	-	0.20	0.06	0.98
260	12,774	-	0.11	0.06	1.09
270	13,039	-	0.14	0.07	1.16
280	13,295	-	0.21	0.07	1.17
290	13,535	-	0.08	0.06	1.13
292	*13,585*	***1.83***	*0.12*	*0.06*	*1.12*
294	13,638	-	0.10	0.06	1.25
296	*13,689*	-	***9.73***	*0.17*	*8.21*
336	14,720	-	0.12	0.05	1.33
340	14,874	-	0.11	0.05	1.28
342	14,958	-	0.12	0.09	1.24
344	15,042	-	0.12	0.09	1.25
346	15,118	-	0.12	0.10	1.15
358	15,639	-	0.14	0.11	1.21
360	15,730	0.57	0.08	0.08	1.25

362	15,806	-	0.12	0.09	1.24
364	15,887	-	0.14	0.22	1.24
364	15,887	-	0.17	0.23	1.16
365	15,928	-	*0.07*	*0.17*	*1.75*
365	15,928	-	0.09	0.16	1.30
365	15,928	-	0.07	0.08	1.26
366	16,026	-	0.08	0.20	1.29
366	16,026	-	0.08	0.19	1.26
368	16,219	-	0.09	0.33	1.44
370	16,428	-	0.09	0.32	1.25
372	16,701	-	0.18	0.72	1.20
374	16,982	-	0.35	0.69	1.27
376	17,215	-	0.18	0.30	1.23
378	17,413	-	0.22	0.24	1.30
379	17,523	-	0.33	0.38	1.25
380	17,636	-	0.29	0.38	1.23
381	17,683	-	0.13	0.22	1.10
381	17,683	-	0.15	0.19	1.03
382	17,730	-	0.25	0.32	1.46
382	17,730	-	*0.64*	*0.34*	*1.66*
383	17,774	-	0.22	0.27	1.21
386	17,906	-	0.22	0.29	1.24
388	17,994	-	0.23	0.26	1.24

44

45

46　**Table S3. Uncertainty range of input parameters on the modeled gas hydrate stability**

47　**zone (GHSZ).** We use the following uncertainties in input parameters to estimate the variations

48　in GHSZ arising from them.

Parameter	Uncertainty / Range
Bottom water temperature	$\pm$ 1.01°C (this study)
Thermal gradient	$\pm$ 0.0028°C m^{-1} (based on Yamano et al.[5] for the BSR estimated value of 0.035°C m^{-1} by Waage et al.[6])
Pore-water salinity	34–36 PSU [7]
Bulk sediment thermal conductivity	1–2.44 Wm^{-1}K^{-1} [8,9]
Bulk sediment density	1727–2100 kgm^{-3} [8,9]
Bulk sediment specific heat capacity	1614–2505 Jkg^{-1}K^{-1} [8,9]

49

50

References in supplementary material

1. Yao, H., Niemann, H. & Panieri, G. Multi-proxy approach to unravel methane emission history of an Arctic cold seep. *Quat. Sci. Rev.* **244**, 106490 (2020).
2. Rasmussen, T. L. & Thomsen, E. Climate and ocean forcing of ice-sheet dynamics along the Svalbard-Barents Sea ice sheet during the deglaciation ~20,000–10,000 years BP. *QSA* **3**, 100019 (2021).
3. Serov, P. *et al.* Postglacial response of Arctic Ocean gas hydrates to climatic amelioration. *Proc Natl Acad Sci USA* **114**, 6215–6220 (2017).
4. Rasmussen, T. L. *et al.* Paleoceanographic evolution of the SW Svalbard margin (76°N) since 20,000 ^{14}C yr BP. *Quaternary Research* **67**, 100–114 (2007).
5. Yamano, M., Uyeda, S., Aoki, Y. & Shipley, T. H. Estimates of heat flow derived from gas hydrates. *Geology* **10**, 339–343 (1982).
6. Waage, M. *et al.* Geological controls on fluid flow and gas hydrate pingo development on the Barents Sea margin. *Geochem. Geophys. Geosyst.* **20**, 630–650 (2019).
7. Skogseth, R., Haugan, P. M. & Jakobsson, M. Watermass transformations in Storfjorden. *Cont. Shelf Res.* **25**, 667–695 (2005).
8. Crane, K. *et al.* Thermal evolution of the western Svalbard margin. *Mar Geophys Res* **9**, 165–194 (1988).
9. Berndt, C. *et al.* Temporal Constraints on Hydrate-Controlled Methane Seepage off Svalbard. *Science* **343**, 284–287 (2014).

Paper III

Appendix A. Summary in Basque – Laburpena euskaraz

Azken bi hamarkadetan, berotegi-efektuko gas-isuri antropogenikoen ondorioz Lurraren tenperatura igo egin da (IPCC, 2014). Prozesu hau are nabariagoa da Artikoan; han, tenperatura-igoera munduko batezbestekoa baino bi aldiz handiagoa izaten ari da (Najafi et al., 2015; Meredith et al., 2019). Fenomeno horri "Artikoko anplifikazioa" deritzo, eta atzeraelikadura-mekanismo positiboen emaitza da; besteak beste, itsas izotzaren galeraren ondoriozko albedo-efektuaren murrizketaren eta iparralderanzko beroaren garraioan gertatzen ari diren aldaketen ondorio (Serreze & Barry, 2011).

Atlantikoko ur bero eta gaziak Ozeano Artikora Fram Itsasertzetik eta Barents Itsasotik sartzen dira batik bat. Barents Itsasoak azken hamarkadetan bero-fluxuaren igoera nabaria jasan du, Atlantikoko uren sarrera handitzearen eta itsas-izotzaren estalkia murriztearen ondorioz (Årthun et al., 2012; Polyakov et al., 2017). Artikoko sedimentuek gas-hidratozko erreserba handiak dituzte, bereziki Barents Itsasoa bezalako plataforma kontinentaletan. Gas-hidratoak gasa (gehienetan metanoa, CH_4) ur solidoaren kristal-egituran harrapatuta duten konposatuak dira, eta egonkorrak dira presio altuan eta tenperatura baxuan (Sloan & Koh, 2007). Hidratoak ez egonkortu ezkero (presioa jaitsita edo tenperatura igota), disoziatu, eta gasa isuri dezakete itsas-hondoko sedimentuetatik ur-zutabera. Bada, itsas-hondora iritsi daitezkeen Atlantikoko ur beroek itsas hondoan egonkor dauden gas-hidratoen disoziazioa abiarazi dezakete; horrek aldaketa klimatikoaren efektuak areagotuko lituzke (e.g., Westbrook et al., 2009; Maslin et al., 2010; Biastoch et al., 2011; Kretschmer et al., 2015; Ruppel & Kessler, 2017).

Itsas hondotik isurtzen den gasak ur-zutabea zeharkatu eta atmosferara iritsi daiteke, bereziki arro ez oso sakonetan. Ur-zutabean disolbatutako metanoak ozeanoen azidifikazioa eta uretan disolbatutako oxigenoaren murrizketa eragin badezake ere (Biastoch et al., 2011), badirudi gaur egun Artikoko plataforma kontinentalean itsas hondoko sedimentuetatik askatzen den metanoa ez dela atmosferara iristen eta, beraz, honek ez luke atmosferaren berotegi-efektua areagotuko (Myhre et al., 2016). Hala ere, proiekzio klimatikoek Artikoa are gehiago berotzea aurreikusten dute (Overland et al., 2019), eta horregatik da garrantzitsua ikertzea zer gertatuko liteke metano-hidratoekin, itsasoa nabarmen berotzen bada.

Etorkizuneko proiekzio-klimatikoetan ziurgabetasunak handiak dira oraindik, eta horiek hobetzeko beharrezkoa da, besteak beste, epe luzeko iraganeko egoera klimatikoei buruzko ezagutza areagotzea. Izan ere, Lurraren historian badira gaur egungoaren antzekoak diren

berotze-aldiak, adibidez Dansgaard-Oescgher gertakariak azken Izotz Aroan. Milaka urte gutxi batzuk irauten zuten gertakari horietan, Ipar Atlantikoren klimak hotzaldi egonkorren eta bat-bateko beroaldien artean oszilatzen zuen, eta hamarkada gutxi batzuetan ematen ziren trantsizio horietan tenperatura-igoera 5ºC-tik 16,5 ºC-ra izan zitekeen (Dansgaard et al., 1993; Bond et al., 1993; Kindler et al., 2014). Trantsizio horietako eta gaur egungo atmosferaren berotze-tasak Artikoan antzekoak edo handiagoak dira (Jansen et al., 2020).

Ez dago argi oraindik zein prozesuk eragin zezakeen bat-bateko berotze hori, baina badirudi egile gehienak ados daudela itsas izotzaren estalkiak eta ozeanoen zirkulazioaren berrantolaketak Ipar Atlantikoan garrantzi handia izan zutela (Broecker et al., 1985; Ganopolski & Rahmstorf, 2001; Rahmstorf, 2002; Gildor & Tziperman, 2003; Knutti et al., 2004; T. L. Rasmussen & Thomsen, 2004; Li et al., 2010; Petersen et al., 2013; Sadatzki et al., 2019; Jansen et al., 2020). Premisa hau da: zirkulazio ozeanikoa zenbat eta indartsuagoa izan Atlantikoan, orduan eta bero gehiago garraiatuko da iparralderantz (Rahmstorf, 2002). Gaur egun, Atlantikoko ur bero eta gaziak Ipar Atlantikotik Itsaso Nordikoetara sartzen dira Svalbard mendebaldetik Ozeano Artikoan sartzeko (1. irudia). Bide horretan, Atlantikoko urek beroa galtzen dute atmosferara; horrek epel mantentzen du Europa iparraldeko klima, besteak beste. Fram Itsasertzean, berriz, Groenlandia ekialdetik ur polarra (hotza eta gazitasun txikikoa) sartzen da Itsaso Nordikoetara. Bertan, bi ur-masak nahastu egiten dira, eta hondoratuko den dentsitate altuko (hotza eta gazia) ur-masa sortzen dute (1. irudia). Ur-masa hotz eta gazi hori itsas hondotik hegoaldera garraitzen da, Ipar Atlantikoko itsas hondoko ur-masaren osagaia izateko.

Dansgaard-Oeschger beroaldietan ozeanoen zirkulazioa gaur egungoaren antzekoa zen, baina hotzaldietan zirkulazioa ahulagoa izan ohi zen eta itsas hondoko ur hotz gutxiago sortzen zen (T. L. Rasmussen et al., 1996a,b; T. L. Rasmussen & Thomsen, 2004; Ezat et al., 2014; Lynch-Stieglitz et al., 2007). Hotzaldietan, itsas izotzak eta gazitasun txikiko ur-masa polar zabal batek Itsaso Nordikoen gainazala estaltzen zuen (T. L. Rasmussen & Thomsen, 2004; Hoff et al., 2016; Sadatzki et al., 2019, 2020). Atlantikoko urek Itsaso Nordikoetara sartzen jarraitzen zuten, baina azalean egon beharrean (gaur egun bezala), dentsitate altuagoa izanik, hondoratu egiten ziren gazitasun txikiko ur-masaren azpian (T. L. Rasmussen & Thomsen, 2004; Ezat et al., 2014). Itsas hondoko ur hotz gutxiago sortzen zenez, Atlantikoko urak hondoratu, hedatu eta itsas hondoa okupatu zezaketen ia berorik galdu gabe (Ezat et al., 2014; Sessford et al., 2019). Iraganeko Atlantikoko zirkulazio ozeanikoaren indarra ikertzeko,

itsas hondoko uren tenperatura erabili daiteke zeharkako adierazle gisa, tenperatura altuak (>1°C) Atlantikoko uren adierazle izanik.

Tesi honen interesa Dansgaard-Oescgher gertakarietan eta azken Izotz Aroaren ostean milurtetan gertatu ziren aldaketa paleozeanografikoak ulertzean datza, baita aldaketa paleozenografiko horiek itsas-hondoko metano-isurien historiarekin duten erlazioa aztertzean ere. Orain arte honen inguruan egin diren ikerketa gehienak Itsaso Nordikoen hegoaldean ardaztu dira eta tesi honetan iparraldeko laginak ikertu ditugu. Horretarako, Fram Itsasartean eta Barents Itsaso ipar-mendebaldean Atlantikoko ur beroaren sarrerak izan duen eboluzioa aztertu dugu, itsas hondoko uren tenperatura eta itsas izotzaren historia berreraikiz. Ikertutako bi eskualdeetan itsas hondoko sedimentuetan gas-hidratoak daude eta sedimentu horietatik metano-jarioak gertatzen dira. Tesi honetan ondorengo hiru artikulu zientifikoak aurkezten dira:

I. Artikuluan, Vestnesa Ridgen (Fram Itsasertzaren ekialdean) itsas hondoko tenperaturak Dasngaard-Oeschger gertakarietan berreraiki ditugu, azken Izotz Aroan, duela 63000 eta 13000 urte bitartean. Vestnesa Ridge 1273 m-ko sakoneran dagoen konturita bat da, eta handik metano-jarioak gertatzen dira gaur egun. Itsas hondoko tenperaturak berreraikitzeko foraminifero bentonikoen Mg/Ca teknika erabili dugu. Horrez gain, foraminifero bentoniko eta plantonikoen oxigeno- eta karbono-isotopo egonkorren neurketak, foraminifero bentonikoen espezien identifikazioak eta populazioaren ikerketak, eta izotzak garraiatutako detrituaren kontaketak eskualde horretako eboluzio paleoazenografikoa ulertzea ahalbidetu digu. Milurteko beroaldietan itsas hondoko tenperatura baxuak izan ohi ziren, gaur egungoen antzekoak. Hotzaldietan berriz, itsas-hondoko tenperatura altua izan ohi zen, tarte batzuetan 5°C-koa izanik. Garai horietan, Atlantikoko urekiko afinitatea duten foraminifero bentonikoak ziren nagusi, eta beroaldietan, aldiz, materia organiko ugari dagoenean hazten diren foraminiferoak nabarmentzen ziren, sasoiko itsas izotzaren presentziak sortzen duen "elikagai" ugaritasunaren ondorio bezala seguruenik.

Aurretiaz, Ipar Atlantikoan, Itsaso Nordikoetan eta Ozeano Artikoko itsas-hondoko tenperaturen bilketa ere egin dugu. Konpilazio horrek erakusten du milurteko hotzaldietan bero-metaketa handi bat eman zela Ipar Atlantikotik Ozeano Artikora, gainazalean kokatzen ziren dentsitate baxuko ur hotz eta freskoen azpian. Bero-metaketa handi horren liberazioak bat-bateko Dansgaard-Oescgher beroaldietan rol garrantzitsua jokatu zuela proposatzen dugu.

II. Artikulua, Storfjordrennan (Barents Itsasoaren ipar-mendebaldean) kokatuta dago. Bertan azken Izotz Aro ostetik, itsas-hondotik metano-isuriak gertatzen dira gas-hidratoen disoziazioaren ondorioz. Azken Izotz Aroan Barents Itsasoa izotz-geruza lodi batez estalita zegoen, eta izotz-geruza atzeratzearen ondoriozko presio jaitsierak sedimentuetan metatu ziren gas-hidratoak ezegonkortu zituen. Artikulu honetarako itsas hondoko tenperaturak berreraiki ditugu foraminifero bentonikoen Mg/Ca teknika erabiliz, 382 sakoneran 'Pingo area' deritzon lekuan, azken 18000 urteetan. Sedimentuan gas-hidratoak egonkorrak diren eremuaren lodiera modelizatu dugu, berreraikitako itsas hondoko tenperaturak erabilita, besteak beste. Itsas hondoko tenperatura beroenek hotzaldiekin bat egiteaz gain, izotz-geruzaren atzeratze fase ezberdinekin ere bat datoz. Hasiera batean, izotz-geruzaren desagerpenak (Atlantikoko ur-beroen sarrerak baldintzatuta) gas-hidratoen egonkortasun-eremua desagerrarazi zuen, gas-hidratoen disoziazioa erraztuz. Gerora itsas hondoko tenperaturaren eboluzioak erabat baldintzatu zuen gas-hidratoen egonkortasun-eremua, tenperatura altuenek egonkortasun-eremua desagerrarazi zutelarik. Lan honetan itsas hondoko uren tenperaturaren igoerak gas-hidrato sistema ez-sakonetan izan dezakeen efektua azpimarratu dugu, baita ur beroen infiltrazioak eragin dezakeen izotz-geruzen atzeratzea ere.

III. Artikuluaren helburua itsas hondoko tenperaturaren eta itsas izotzaren eboluzioaren arteko erlazioa aztertzea da, Dansgaard-Oeschger gertakarietan. Horretarako, Vestnesa Ridgeko laginetan itsas izotzaren nolakotasunaren adierazgarriak diren biomarkatzaileak neurtu ditugu (IP25, HBI III eta kalkulatutako indizeak). Beroaldietan, sasoiko itsas izotz a edota ozeanoa ia irekia zegoen. Hotzaldietan, berriz, itsas izotz estaldura zabala zen, aurretiaz beste egile batzuek Itsaso Nordikoen hegoaldean proposatu duten bezala. Horrek itsas hondoko uren beroaren galera saihesten zuen, eta Atlantikoko urek itsas hondoan tenperatura altuak izatea ahalbidetu. Itsas izotzaren biomarkatzaileak, I. Artikulurako berreraikitako itsas hondoko tenperaturekin konparatuz, bien arteen lotura estua dagoela ikus daiteke, batez ere, hotzaldietan: itsas hondoko tenperatura jaistearekin batera, itsas izotzaren ezaugarriak aldatu egiten dira, udaberriko itsas izotzaren estalkia murriztu egiten da, eta ozeanoaren azala ireki. Itsas izotzaren eta itsas hondoko tenperaturen akoplamendu horrek agerian uzten du ozeanoaren zirkulazioaren eta izotz estalkiaren arteko erlazio estua Dansgaard-Oescgher gertakarietan.

Tesi honen berritasun nagusia goi-latitudeetan itsas hondoko bi tenperatura erregistroen

ekoizpena da, Atlantikoko uren eboluzioa eta, ondorioz, ozeanoen zirkulazioaren ebazteko aukera ematen dutenak. Bi erregistroak arro eta sakonera ezberdinetan egon arren, elkarren artean koherenteak dira, eta aurretiaz hegoaldean eraikitako erregistroekin (Ezat et al., 2014; Sessford et al., 2019) bat egiten dute, eta Itsaso Nordikoen irudia osatzen dute, Dansgaard-Oeschger gertakarietan. Emaitzek erakusten dute azken Izotz Aroan ozeanoen zirkulazioaren erregimen-aldaketen eta itsas izotzaren arteko lotura (kausal?) estua dela, baita itsas-hondoko uren tenperaturaren igoerak gas-hidratoen sistemetan duen funtsezko eragina ere. Tesi honetan aurkeztutako ikerketen emaitzak baliagarriak dira komunitate paleozeanografikoarentzat, eta ozeano, itsas kriosfera eta karbonoaren zikloaren arteko atzeraelikadura-mekanismoak ikertzen dituen ororentzat.